# High frequency and nonlinear phenomena in thin active ferromagnetic planar structures

Yury Ignatov

**N° d'ordre : 191**

**ECOLE CENTRALE DE LILLE**

# THÈSE

présentée en vue
d'obtenir le grade de

# DOCTEUR

En
Spécialité : Micro et Nano Technologies, Acoustique et Télécommunications
Par


## Yury Ignatov


**DOCTORAT DELIVRE CONJOINTEMENT PAR L'ECOLE CENTRALE DE LILLE ET L'INSTITUT DE PHYSIQUE ET DE TECHNOLOGIE DE MOSCOU**

Titre de la thèse:

# Phénomènes hyperfréquences et nonlinéaires dans les structures actives ferromagnétiques planaires

Soutenue le 29 juin 2012 devant le jury d'examen composé de :

| | | |
|---|---|---|
| **Président** | Mr. Olivier BOU MATAR-LACAZE | Professeur à l'Ecole Centrale de Lille |
| **Rapporteur** | Mr. Jean-Claude LEVY | Professeur à l'Université Paris-Diderot |
| **Rapporteur** | Mr. Mikhail LOGUNOV | Professeur à Ogarev Université d'Etat de Mordovia |
| **Examinateur** | Mr. Yuri PYL'NOV | Professeur à l'Institut Radiotechnique, electronique et Automation de Moscou |
| **Examinateur** | Mr. Jean JURASZEK | Maitre de conferences à l'Université de Rouen |
| **Examinateur** | Mr. Alexey KLIMOV | Professeur à l'Institut Radiotechnique, electronique et Automation de Moscou |
| ***Directeur de Thèse*** | Mr. Vladimir PREOBRAZHENSKY | Professeur à l'Ecole Centrale de Lille<br>Directeur de recherche à l'Académie des Sciences de Russie |
| ***Directeur de Thèse*** | Mr. Sergey NIKITOV | Professeur à l'Institut de Physique et de Technologie de Moscou |
| **Invités** | Mr. Philippe PERNOD | Professeur à l'Ecole Centrale de Lille |
| | Mr. Nicolas TIERCELIN | Chargé de recherche CNRS à l'IEMN |
| | Mr. Andrei BRYSEV | Chef du laboratoire à Physics Institute Wave Phenomena de Moscou |


Thèse préparée dans le Laboratoire International Associé LEMAC à l'Institut d'Electronique, de Microélectronique et de Nanotechnologie (IEMN, UMR CNRS 8520) (France) et à l'Institut de Physique et de Technologie de Moscou (MIPT) (Russie) dans le cadre d'une cotutelle

Ecole Doctorale SPI 072 (Lille I, Lille III, Artois, ULCO, UVHC, EC Lille)
PRES Université Lille Nord-de-France

# Acknowledgement

This work was carried out in the International Associated Laboratory on Nonlinear Magnetoacoustics of the condensed matter (LEMAC), in the Institute of Electronics, Microelectronics and Nanotechnologies (IEMN, CNRS/UMR 8520, France) in cooperation with Moscow Institute of Physics and Technologies (MIPT, State University, Russia).

First, I would like to sincerely thank the directors of my thesis in France Pr. Philippe Pernod and Pr. Vladimir Preobrazhensky from Ecole Centrale de Lille who invited me to work with IEMN-LEMAC, for the guidance and confidence, for the care and support that they provided me all through the three years of work.

I would like also to especially thank the director of the thesis from the russian side of Moscow Institute of Physics and Technologies, Pr. Sergey Nikitov. I am extremely thankful for the comfortable and friendly ambience that he provided me with during all my studies in Moscow, for his benevolence and willigness to help me with any difficulty that I had, for those kind and sympathetic words that I heard from him at each of our meetings.

My sincere thanks are due to the official referees, Messrs. Jean-Claude Levi and Mikhail Logunov, for their detailed review, constructive criticism and excellent advice during the preparation of this thesis. I warmly thank the other members of thesis committee, Nicolas Tiercelin and Yury Pyl'nov, for their valuable advice. Their extensive suggestions and discussions around my work have been of great value in this study.

I thank the French Embassy in Moscow and the French Ministry of Foreign Affairs that provided me with this unique chance to receive the PhD scholarship that allowed me to come to France.

Of course, I am very thankful to research team of IEMN-LEMAC. It was an absolute pleasure to work with such professionals and great people including Alexey Klimov, Yannick Dusch, Olexandr Yevstafiev, Pavel Shirkovsky, etc.

I would also thank Mairead Butler and Emma McLaughlin, whose help with spelling mistakes corrections can scarcely be overestimated.

For the financial part, this work was mainly supported by RFBR Grants No. 09-02-93107-NCNIL_a, 08-02-00785-a, 09_02_12455_ofi_m, 09_02_12433_OFI_M, the ANR project No. ANR-08-NANO-035-01, The CNRS grant to the Joint international Laboratory LIA LEMAC, and by the French Embassy in Moscow (French Ministery of Foreing Affairs). I would also like to thank Dr. G. A. Ovsyannikov for providing perovskite samples and discussions.

# Table of figures

*4 - noise signal from the microwave detector that is not involved in the experiment;*

*5 - tools for the formatting of graphic representation.*

*Fig. 9.* *Magnetic field dependence of the HF reflection coefficient R expressed in arbitrary units at different FMR frequencies for $La_{0.7}Sr_{0.3}MnO_3$ film (A – 814 MHz, B – 1183 MHz, C – 1760 MHz) and for $TbCo_2$/FeCo nanostructure (D – 1172 MHz, E – 2174 MHz, F – 4918 MHz): solid line-experiment, dashed line-theory.*

*Fig. 10.* *Magnetic field dependence of the amplitude of sample vibrations at different FMR frequencies for $La_{0.7}Sr_{0.3}MnO_3$ film (A – 814 MHz, B – 1183 MHz, C – 1760 MHz) and for $TbCo_2$/FeCo nanostructure (D – 1172 MHz, E – 2174 MHz, F – 4918 MHz): solid line-experiment, dashed line-theory.*

*Fig. 11.* *Experimental setup. RF – radio frequency generator, C – circulator, ML – microstrip line, E. A. – easy axis, D – detector, A – amplifier, DAQ – data acquisition hardware, H – external magnetic field produced by electromagnet coils.*

*Fig. 12.* *Magnetic field dependence of the HF reflection coefficient R expressed in arbitrary units for TbCo/FeCo nanostructure at different FMR frequencies (A – 500 MHz, B – 660 MHz, C – 1100 MHz, D – 1800 MHz). The inset shows the FMR frequency vs magnetizing field. Solid lines –theory, dots – experiment.*

*Fig. 13.* *Magnetic field dependence of the magnetoelectric voltage for TbCo/FeCo nanostructure at different HF frequencies (A – 500 MHz, B – 660 MHz, C – 1100 MHz, D – 1800 MHz). Solid line –theory, dots – experiment.*

*Fig. 14.* *The structure (dm – the thickness of the magnetostrictive film; dPE – the thickness of the piezoelectric film; ds – the thickness of the substrate; Pt – platinum bottom electrode; d is the sample total thickness).*

*Fig. 15.* *Film with a linearly varying thickness.*

*Fig. 16.* *Cross sections of the dispersion surface (16) by planes perpendicular to the y axis.*

# List of tables

# Table of contents

# Introduction

High frequency (HF) and nonlinear phenomena in thin active ferromagnetic planar structures gained a lot of interest in the past 20 years mainly from their perspectives of practical applications in the microwave technology. These applications can serve as a component base of wave division multiplexing (WDM) filters, micro electro mechanical systems (MEMS), micro magneto mechanical systems (MMMS), actuators, etc. These phenomena are also relevant to the fundamental investigations of the interaction of the electromagnetic field with magneto-ordered materials [1]-[6].

One of the most promising objects for the nonlinear magnetic dynamics observation is thin planar structures that already became the basic element for integrated-circuit technologies [7]. In the recent years with the technological progress the new types of ferromagnetic planar structures become available for the experiment and production. These structures are regarded to be the main object of the present study.

The uniaxial magnetostrictive films with an artificial spin reorientation transition (SRT) induced by external magnetic field are of great practical interest for their applications to MEMS devices [19]-[22]. Rare earth intermetallic compositions like $TbCo_2$/FeCo, which are usually under consideration in this matter, provide giant magnetostriction and large values of the electromechanical coupling factor [23], [24]. The magnetoelastic sensitivity of MMMS can increase about two order of value near SRT in magnetostrictive multilayer nanostructures [19], [20], [25]. The area in the vicinity of SRT in magnets has a number of dynamic and nonlinear features [26]-[29]. In particular high efficiency of subharmonic excitation of elastic vibrations was observed in MMMS near SRT [30]. Magnetoelastic demodulation of electromagnetic waves can also become efficient in giant magnetostriction nanostructures near SRT. For microwave demodulation one can expect the most preferable conditions when SRT is combined with ferromagnetic resonance (FMR) in a magnetostrictive film.

Moreover, the magnetoelectric effect can also be considerably more efficient in a composite magnetostrictive-piezoelectric structure than in materials with intrinsic magnetoelectric properties [45], [46], [28]. The efficiency of magnetoelectrical energy conversion in stress-mediated structures is mostly defined by two factors: the value of electromechanical coupling factor in the piezoelectric component and magnetostriction value in the magnetic one. It was shown that magnetoelectric effect can be appreciably enhanced in a composite structure near SRT [29], [30]. Nevertheless, HF properties of these structures were not investigated. They can be of interest to the distance control of MEMS/MMMS and the practical applications on the base of them. Piezoelectric thin aluminium-nitride films, which were regarded here, gained a lot of interest in the applied physics because of available technology and significant value of electromechanical coupling factor due to comparatively small magnitude of dielectric constant [47], [48]. The resonant magneto-electric coefficient in thin film composite

multiferroic structures achieved more than 700 V/(cm*Oe). Various manifestations of magnetoelectric interaction in microwave frequency band were demonstrated in laminated or microparticle imbedded multiferroics [51]-[53]. The use of ferromagnetic resonance (FMR) in addition to acoustic resonance (AR) in composite structures appeared efficient to provide effective magnetoelectric energy conversion [54]. It was also clearly demonstrated the efficiency of reverse effect, when FMR is driven elastically [55]. HF electromagnetic excitation of low frequency (LF) alternating electrical polarization can be achieved using nonlinear magnetoelastic interaction in multiferroic structures. One can expect that the usage of FMR, SRT, AR, giant magnetostriction and a significant value of piezoelectric coefficient jointly enhance nonlinear magnetoelectric conversion in thin film structures.

In recent years, investigations of photonic crystals [62] have stimulated an interest in similar structures for other types of waves in solids. In particular, the investigations have been performed for acoustic structures similar to photonic crystals, in which the properties of acoustic microwaves are similar to those of electromagnetic waves in photonic crystals. Such media are called phonon crystals [**63**], [64]. In magnetic media (films and multilayer structures), the properties of spin (magnetostatic) waves have been investigated by analogy with photonic and phonon structures. These structures are called magnon crystals [65], [66]. Introduction of a periodic inhomogeneity brings about the occurrence of forbidden frequency bands, which is manifested in the existence of transmission and non-transmission bands for an optical signal in photonic crystals. A periodic variation of the properties of a magnetic medium leads to the same effects in the microwave range [68]-[70]. It should be noted that similar magnetic structures were considered earlier only in the case when the waveguiding carrier thickness was constant.

As the media for investigation of the properties of MSSWs propagating, ferromagnetic films and plates homogeneous in their parameters are used. However, as shown in [71]-[74], the introduction of a non-uniform magnetic bias field substantially changes the properties of surface magnetostatic waves, changing the wave number, the phase and group velocities, and also cardinally changes the trajectory configuration of surface magnetostatic wave beams. On the other hand, inhomogeneities in the geometric parameters of films, e.g., a change in the thickness, must cause similar effects as well. Ferromagnetic films with periodic structures are of specific interest owing to a possibility to control their dispersion characteristics by a magnetic field [75], [76].

It is believed that a combination of a periodic inhomogeneity and a variable thickness of the structure will lead to the manifestation of new properties of the waveguiding medium and will open new areas of magnon crystals application. The formulation of this problem [17] was caused by the intensive work in this domain that was provided in the last few years in the Kotel'nikov Institute of Radio-engineering and Electronics of RAS and by Pr. Sergey Nikitov particularly. In fact there were some important reasons to carry out the work in this direction as it has good perspectives in the HF

applications. The problem seemed to be the promising one from a perspective to provide us with the information on the new types of WDM filters. The methods that were used to estimate the influence of the varying thickness (WKB approximation) and the periodical structure (Kronig-Penny model) are quite simple and valid in the approximation of the small angles of a thickness variation. On the other hand, it gives us the basic advantages of these structures for practical applications.

Ferrite-dielectric-metal (FDM) planar structures also have some unique features to observe when magnetostatic surface waves (MSSWs) propagate in such media as the condition of a negative dynamic magnetic susceptibility can be complied. Typically, the media with negative values of magnetic susceptibility and permittivity exhibit a number of specific dynamic properties [12]. In particular, it is shown in [85] that an anomalous Doppler effect may be observed in these media. This effect shows itself as a decrease in the frequency of the received signal as the source moves toward the receiver and as an increase as the source moves away from the receiver.

A number of recent studies is devoted to the observation of the anomalous Doppler effect in transmission lines for backward electromagnetic waves [86]-[88]. Also studied is the anomalous Doppler effect observed in photonic and phononic crystals [89], [90], in which this effect is caused by the interaction of acoustic and electromagnetic wave with the crystal lattice characterized by a set of forbidden frequency bands.

Thin active ferromagnetic planar structures are also promising for observing the anomalous Doppler effect. In these materials, special oscillations - spin magnetostatic waves (MSWs) - can be excited. Depending on the mutual orientation of the radiating antenna and the external magnetic field, various types of MSWs can be observed: magnetostatic surface waves (MSSWs), magnetostatic backward volume waves (MSBVWs), and magnetostatic forward volume waves (MSFVWs). Propagation of MSSWs and MSBVWs in a free ferromagnetic film as well as the laws of reflection and refraction of MSSWs and MSBVWs at the interface between different media are studies in detail in [91], [92].

In study [93], an experimental observation of an anomalous Doppler effect during MSBVW propagation in a free ferromagnetic film is reported. In the experiment, the input MSW-exciting antenna was moved relative to the ferromagnetic film. The MSW-emitting source was moved toward the receiving antenna (wave receiver). Both types of MSWs were studied: forward MSSW and MSBVW. In this case, the Doppler effect was normal for the MSSW and anomalous for the MSBVW (for the MSBVW, the frequency of the received signal (MSW) decreased as the source was moved toward the receiver).

Generally **the main goal** of the work was the development of a theoretical description for the high frequency and non-linear waves propagation in thin planar ferromagnetic structures. Thus, for the achievement of the formulated goal following **research tasks** were assigned:

- Develop the theoretical description for second order non-linear and magnetostatic waves in thin ferromagnetic planar structures with different compositions such as multiferroics based on $TbCo_x$/FeCo intermetallic nanolayers, magnon crystals and ferrite-dielectric metal structures.
- Study the increase of magnetoelastic demodulation with LF vibrations of the cantilever when FMR is excited by HF electromagnetic field near SRT.
- Study the nonlinear magnetoelectric effect observation with the magnetoelastic demodulation and ferromagnetic resonance occurrence in thin planar magnetostrictive uniaxial nanostructures supplemented with a piezoelectric layer.
- Calculate the dispersion of a surface magnetostatic wave propagating in a film, whose thickness varies linearly, with a periodic structure in the form of parallel etched strips, and show the possible practical applications of these structures.
- Predict the occurrence of the anomalous Doppler effect during propagation of MSWs in a FDM structure in a certain range of system parameters.

General scientific content of the work consists of **five partitions**:

**Chapter 1** represents main theoretical models and calculations that were used in the further chapters. The Landau-Lifshitz-Gilbert model for ferromagnets underlies in the base of theoretical study of the phenomena. It was supplemented by magnetostatic approximation with corresponding computations for the study of MSWs propagating in the media. The second order approximation of the model was used to describe the nonlinear behavior of magnetization in cases of magnetoelastic demodulation and nonlinear magnetoelectric effect in multiferroic nanostructures.

**Chapter 2. Ferromagnetic resonance and magnetoelastic demodulation in thin active ferromagnetic films.** This work was a part of the research activity on micro electro mechanical systems (MEMS) that can be used in a hypothetical system "Smartdust". It was assumed to cover the question with the distance control of such systems and their efficiency. On the other hand, this work was also used in the further related studies, where the problems of inducing a SRT in giant magnetostrictive thin planar nanostructures for applications in MEMS and NEMS were regarded [11].

This chapter contains main experimental and theoretical results on the considered phenomenon. In particular, the magnetic field dependences of the HF reflection coefficient and the amplitude of sample vibrations at different FMR frequencies for $La_{0.7}Sr_{0.3}MnO_3$ film and for $TbCo_2$/FeCo nanostructure are presented here. The experiments and theoretical calculations have been provided at high frequencies from below 1 to above 4 GHz. The ancillary measurements of easy axis direction were

carried out as well. The results were discussed in details with respect to all previous works provided in this direction.

The experimental and theoretical data on FMR and magnetoelastic demodulation in the $TbCo_2$/FeCo nanostructure and $La_{0.7}Sr_{0.3}MnO_3$ thin film, deposited on Si and $NdGaO_3$ cantilevers, respectively, show that LF vibrations of the cantilever can be amplified when FMR is excited by HF electromagnetic field near SRT. Rare earth manganitestrontium perovskites demonstrated clear resonance properties in the majority of the high frequency range. The results of the calculations are in good agreement with the experimental data of measurements of the FMR line and with the data of the optical detection of elastic vibrations of the magnetostrictive cantilever under HF electromagnetic field. The phenomenon under consideration can find various applications in the field of MMMS controlled by a HF electromagnetic field.

**Chapter 3. Nonlinear magnetoelectric effect in multiferroic nanostructure TbCo/FeCo-AlN in high frequency electromagnetic field.** In this chapter the same magnetoelastic system TbCo/FeCo on Si substrate was supplemented with the piezoelectric aluminium-nitride layer to demonstrate the demodulation effect in the voltage oscillations. It contains experimental and theoretical data on the magnetic field dependence of the HF reflection coefficient and the magnetoelectric voltage at different FMR frequencies in 500MHz – 2GHz spectral range. The results were discussed in details with respect to all previous works provided in this direction.

The effect is studied in conditions of spin reorientation transition in magnetostrictive nanostructure. The results of calculations are in good agreement with the experimental data on magnetic field dependence of LF magnetoelectric voltage and on HF power absorption. It is shown that conductivity contribution to FMR line width is relatively weak in magnetostrictive nanostructure.

**Chapter 4. Propagation of the surface magnetostatic waves in an one dimensional magnon crystal with variable thickness.**

This chapter mainly contains basic results on the dispersion numerical calculation of a MSSW propagating in the structures represented by the ferromagnetic film and the one-dimensional magnon crystal made of a periodic structure in the form of parallel etched strips with variable thicknesses. In general, the linear dependence of the structure thickness variation was basically regarded. The questions of the calculations error was also under consideration.

Possible applications of the effects investigated for designing narrowband and comb microwave filters were considered. Varying the geometric parameters of the film, the period and the width of etched strips, a required transmission characteristic of a ferromagnetic film with such structures can be obtained.

For a more precise physical model one can see the further study that improved this work and was provided by Prof. Sergey Nikitov and Sergey Platonov [16].

**Chapter 5. Anomalous Doppler effect observed during propagation of magnetostatic waves in ferromagnetic films and ferrite–dielectric–metal (FDM) structures.** This chapter contains the theoretical study on the anomalous Doppler effect occurrence for the MSSWs in FDM structures and MSBVWs in a free ferromagnetic plate. It was considered a thin ferromagnetic film placed in a constant magnetic field and magnetized to saturation.

In this chapter the phenomenon of the anomalous Doppler effect observed during the MSBVW propagation in a free ferromagnetic film is theoretically substantiated. Plots of the Doppler shift are constructed for specified parameters. In addition, the possibility of the occurrence of the anomalous Doppler effect during propagation of MSSWs in a FDM structure in a certain range of system parameters is substantiated. It is found that the anomalous Doppler effect may be observed in these structures in a certain range of frequencies and dielectric interlayer thicknesses. A demonstration model that illustrates this effect with the use of equifrequency curves is constructed.

**Thesis conclusion** presented at the end of the manuscript summarizes the results obtained in the conducted studies of high frequency and nonlinear phenomena in thin active ferromagnetic planar structures and compares them with initially set goals and tasks of the work.

Thus, **the main results** of the thesis are:

- Theoretical description for high frequency and nonlinear phenomena in thin active ferromagnetic planar structures (multiferroics based on $TbCo_x$/FeCo intermetallic nanolayers, magnon crystals and ferrite-dielectric metal structures) is developed.
- The increase of efficiency of the magnetoelastic demodulation induced by HF electromagnetic field in the vicinity of SRT and combined with ferromagnetic resonance is theoretically and experimentally clearly demonstrated.
- Nonlinear resonance magnetoelectric effect induced by HF electromagnetic field in thin film composite multiferroic structure is observed experimentally and explained theoretically.
- The dispersion of a surface magnetostatic wave propagating in a film, whose thickness varies linearly, with a periodic structure in the form of parallel etched strips was calculated. Varying the geometric parameters of the film, the period and the width of etched strips, as well as the magnetic field strength a required transmission characteristic of a ferromagnetic film with such structures can be obtained.

- The prediction of the anomalous Doppler effect during propagation of MSSWs in a FDM structure in a certain range of system parameters is substantiated.

In total this work was conducted with the help of the numerical simulations methods, HF spectroscopy methods, analytical calculations, theoretical models, signal differential amplifying, longitudinal magneto-optical Kerr effect (MOKE), Landau-Lifshitz equation, magnetostatic approximation, WKB approximation, Kronig-Penny model.

# 1. High-Frequency and nonlinear dynamics of magnetic moment

In the first chapter we present general theoretical model and calculations on the second-order nonlinear dynamics and magnetostatic waves in thin ferromagnetic films that was used in the further research presented in the following chapters and could be also used as the base platform for other works in the area. The main results of the chapter are: the basic equations for HF and LF dynamics of magnetic system with a strong collinear magnetic order with an uniaxial anisotropy and magnetic relaxation in the substance in the approximation of a thin planar structure; the dispersion and main parameters of a magnetostatic wave propagating in a thin ferromagnetic plate.

## 1.1. General approach

General approach is useful as it introduces main concepts, system geometry and provides with several crucial theoretical results.

### 1.1.1. System geometry

The theory on low frequency (LF) elastic vibrations of the structure excited by LF electromagnetic field near SRT was already developed in ref. [28], [29]. Here this approach is extended for LF elastic vibrations excited by modulated HF electromagnetic field. The mechanism of such a process is explained by the combined contributions of two nonlinearities: the nonlinearity of magnetostriction and the nonlinearity of magnetic subsystem susceptibility.

The system geometry is presented in Fig. 1. We suppose that the thin film with magnetization $\vec{M}$ and thickness $d_m$ is placed on a thick nonmagnetic substrate with thickness d. The easy axis of the film is along the length of the sample corresponding to the x-axis and perpendicular to the external magnetic field H applied along the y-axis. The magnetization $\vec{M}$ has the direction defined by the competition between the external magnetic field and the anisotropy.

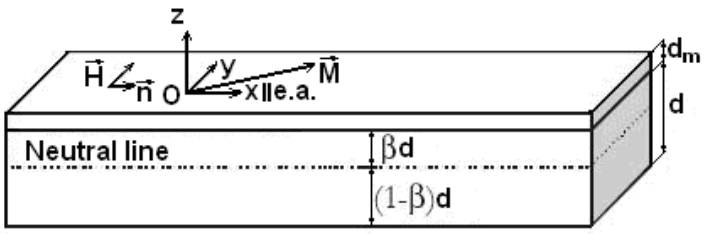


**Fig. 1. Geometry of the system: e.a. – Easy axis, M – magnetization of the magnetic film, dm and d – thicknesses of the magnetic film and substrate respectively, β - parameter defining the position of the neutral line, H – external magnetic field.**

Positions of the neutral lines defined by $\beta$ are different for the static and dynamic resonance cases [40]. In the static case, the neutral line defined by the parameter β has the position minimizing the sum of elastic and magnetoelastic energies: $\beta = 2/3$. For the dynamic case, the vibration modes have an antisymmetrical distribution of deformations relatively to the mean section of the cantilever and therefore: $\beta = 1/2$.

## 1.1.2.Free energy of the system

Following the classical approach [41], [42] one can derive the nonlinear equations of motion for magnetization and elastic strains by retaining high-order terms in the free energy. Overall energy of the sample consists of three parts: elastic $F_e$, magnetoelastic $F_{me}$ and magnetic $F_m$ ones.

$$F = F_e + F_{me} + F_m. \quad \textbf{(1)}$$

We assume that the structure is elastically isotropic. Thus the elastic part of energy volume density can be written in the following form [40]:

$$F_e^V = \frac{1}{2}C_{11}(u_{xx}^2 + u_{yy}^2 + u_{zz}^2) + C_{12}(u_{xx}u_{yy} + u_{xx}u_{zz} + u_{yy}u_{zz}) + (C_{11} - C_{12})(u_{xy}^2 + u_{xz}^2 + u_{yz}^2) \quad (2)$$

where $u_{ij}$ are components of the strain tensor; $C_{11}$ and $C_{12}$ - the two elastic stiffness constants. In this expression, the difference between elastic modules of the substrate and the film was neglected.

$$\begin{cases} C_{11} = \dfrac{E\,(1-\nu)}{(1+\nu)\,(1-2\,\nu)}, \\ C_{12} = \dfrac{E\,\nu}{(1+\nu)\,(1-2\,\nu)}. \end{cases}$$

Here E and $\nu$ are the integrated Young's modulus and Poisson's ratio of the material correspondingly. The magnetic part of energy volume density consists of the Zeeman energy, the anisotropy energy and the energy of demagnetization field.

$$F_m = -\left(\vec{M}\vec{H}\right) + \frac{H_{A0}}{2M_0}\left|\left[\vec{M}\times\vec{n}\right]\right|^2 + \frac{1}{2}\vec{M}\hat{N}\vec{M}. \tag{3}$$

with: $\vec{n}$ - the unit vector that is collinear to the easy axis of the sample (Fig. 1); $H_{A0}$ – the effective value of anisotropy field; $\vec{M}$ - the magnetic moment. $\hat{N}$ is the demagnetizating tensor which is assumed to be the same as for an infinite plate. Thus it has just only one non-zero element $N_{zz}=4\pi$.

The magnetoelastic energy volume density is defined by the magnetostrictive term in isotropic model:

$$F_{me} = \frac{1}{3}b^{\alpha,0}(u_{xx}+u_{yy}+u_{zz}) + b^{\gamma,2}[u_{xx}(\alpha_1^2-\tfrac{1}{3}) + u_{yy}(\alpha_2^2-\tfrac{1}{3}) + u_{zz}(\alpha_3^2-\tfrac{1}{3}) + \\ +2(\alpha_1\alpha_2u_{xy}+\alpha_1\alpha_3u_{xz}+\alpha_2\alpha_3u_{yz})] \tag{4}$$

.

Here following designations have been introduced: $\alpha_1 = \frac{M_x}{M_0}$, $\alpha_2 = \frac{M_y}{M_0}$, $\alpha_3 = \frac{M_z}{M_0}$, $b^{\gamma,2} = b$ is the magnetoelastic constant.

Finally we can write:

$$F = -(\vec{M}\vec{H}) + \frac{H_A}{2M_0}(M_z^2+M_y^2) + b\,[((M_x/M_0)^2-1/3)u_{xx} + ((M_y/M_0)^2-1/3)u_{yy} + \\ ((M_z/M_0)^2-1/3)u_{zz} + 2/M_0^2[M_xM_yu_{xy}+M_yM_zu_{yz}+M_xM_zu_{xz}]] + F_e + \frac{1}{2}\vec{M}\hat{N}\vec{M}. \tag{5}$$

The free energy of the system contains the magnetoelastic term that provides with the second order non-linearity of mechanical vibrations amplitude dependence on the magnetization. This causes the part of magnetoelastic demodulation phenomenon depending on high frequency magnetization precession amplitude.

## 1.1.3.HF-dynamics of magnetic moment

High-frequency magnetization precession of the ferromagnetic film is the system reaction to the influence of an external high-frequency electromagnetic field.

Calculations of the components of magnetization are carried out using the Landau-Lifshits equation [81]:

$$\frac{\partial \vec{m}}{\partial t} = -\gamma\,[\vec{m} \times \overrightarrow{H_{eff}}], \qquad \textbf{(6)}$$

Where $\overrightarrow{H_{eff}} = -\frac{\partial F}{\partial \vec{M}}$ is the effective value of an internal magnetic field in the substance and $F = F\,(\vec{M},\vec{H},\hat{u})$ is generally non-linear on $\vec{M}$.

In our problem we deal with sums of static and small alternating parameters:

$\vec{M} = \vec{m}\,(t) + \vec{M}_0, \vec{H} = \overrightarrow{h\,(t)} + \vec{H}_0, \hat{u} = \hat{\epsilon}(t) + \hat{u}_0.$

One can represent the energy of magnetic system in Taylor series for the first order of magnetization:

$$F_1(\vec{M}_0 + \overrightarrow{m\,(t)}, \overrightarrow{H_0} + \overrightarrow{h\,(t)}, \hat{u}_0 + \hat{\epsilon}(t)) = F\,(\vec{M}_0, \overrightarrow{H_0}, \hat{u}_0) + \frac{\partial F}{\partial M_i}(M_i - M_{i0}) + \frac{\partial F}{\partial H_i}(H_i - H_{i0}) + \frac{\partial F}{\partial u_{ij}}(\epsilon_{ij} - \epsilon_{ij}^0).$$

Thus the expression for the intensity of an effective magnetic field:

$$H_{effi} = -\frac{\partial F}{\partial M_i} = H_{effi}^0 + \frac{\partial H_{eff}^0}{\partial M_i} m_i(t) + \frac{\partial H_{eff}^0}{\partial H_i} h_i(t) + \frac{\partial H_{eff}^0}{\partial u_{ij}} \epsilon_{ij}(t).$$

Linearization of the Landau-Lifshits equation gives us:

$$\frac{\partial \vec{m}}{\partial t} = -\gamma\,[\vec{m} \times \overrightarrow{H_{eff}^0}] - \gamma\,[\vec{M} \times \frac{\partial H_{eff}^0}{\partial \vec{M}} \vec{m}(t) + \frac{\partial H_{eff}^0}{\partial \vec{u}} \vec{\epsilon}(t) + \frac{\partial H_{eff}^0}{\partial \vec{H}} \vec{h}(t)] \qquad \textbf{(7)}$$

High-frequency magnetization precession is caused by the linear part of Landau-Lifshitz equation and can be theoretically represented by the susceptibility tensor $\chi$ connecting the amplitudes of alternating HF magnetization and HF external magnetic field components.

## 1.1.4.LF-dynamics of magnetic moment

Let us represent the system energy in the second-order dependency on the magnetization in the Taylor series:

$$F_2\left(\vec{M}+\overrightarrow{m\,(t)},\overrightarrow{H_0}+\overrightarrow{h\,(t)},\hat{u}_0+\hat{\epsilon}(t)\right)=F_1\left(\vec{M}+\overrightarrow{m\,(t)},\overrightarrow{H_0}+\overrightarrow{h\,(t)},\hat{u}_0+\hat{\epsilon}(t)\right)$$

$$+\frac{\partial^2 F}{\partial M_i l M_j}m_i(t)m_j(t)\ +\frac{\partial^2 F}{\partial H_i \partial H_j}h_i(t)h_j(t)\ +\frac{\partial^2 F}{\partial u_{ij}\partial u_{nk}}\epsilon_{ij}(t)\epsilon_{nk}(t)\ +2\frac{\partial^2 F}{\partial M_i \partial H_j}m_i(t)h_j(t)$$

$$+2\frac{\partial^2 F}{\partial \mathrm{M}_i \partial u_{ij}}m_i(t)\epsilon_{ij}(t)+2\frac{\partial^2 F}{\partial u_{ij}\partial H_k}\epsilon_{ij}(t)h_k(t)$$

Averaging the final second-order non-linear Landau-Lifshits equation by time-parameter, we obtain the equation of LF magnetization precession:

$$\frac{\partial\vec{\mu}}{\partial t}=-\gamma\,[\vec{\mu}\times\overrightarrow{H^0_{eff}}]\ -\ \gamma\,[\vec{M}\times\frac{\partial H^0_{eff}}{\partial\vec{M}}\vec{\mu}(t)\ +\frac{\partial H^0_{eff}}{\partial\vec{u}}\vec{\epsilon}(t)\ +\frac{\partial H^0_{eff}}{\partial\vec{H}}\vec{h}(t)]-\overline{\gamma[\overrightarrow{m\,(t)}\times\overrightarrow{h\,(t)}]}^{\tau}$$

$$-\overline{\gamma[\overrightarrow{m\,(t)}\times\frac{\partial H^0_{eff}}{\partial\vec{M}}\vec{m}(t)\ +\frac{\partial^2 H^0_{eff}}{\partial M_i\partial M_j}m_i(t)m_j(t)]}^{\tau} \qquad (8)$$

Where: $1/\Omega \gg \tau \gg\ 1\ /\ \omega$.

Low-frequency magnetization precession is caused by the non-linearity of Landau-Lifshitz equation and can be theoretically presented by the susceptibility tensor $\kappa$ connecting the amplitudes of alternating LF magnetization and HF external magnetic field components.

## 1.2. Magnetostatic approximation

This part of work is mostly based on the fundamental article of Damon and Eshbach **[77]**. It was carried out with the same geometry and assumptions. On the other hand, it provides with theoretical results derived in a quite different manner. It can be useful as an introduction to the calculations provided in the Chapter 4 and the Chapter 5. Moreover, here one can find the simplified expression for the MSSW dispersion equation that were not presented in the mentioned article.

### 1.2.1.Basics.

The general magnetostatics equations obtained from the corresponding Maxwell equations in the approximation of a quasi-static mode **[81]**:

$$rot\vec{H}=0; \qquad (9)$$

$$div\vec{B}=0 \qquad (10)$$

Here: $\vec{B}=\vec{H}+4\pi\vec{M}$ .

Let us suppose that the field and magnetization can be presented in the following form:

$$\vec{H}=H_i\cdot\vec{n}_z+\vec{h}\cdot e^{i\omega t}; \quad (11)$$

$$\vec{M}=M_0\cdot\vec{n}_z+\vec{m}\cdot e^{i\omega t}. \quad (12)$$

Here: $H_i$ - an interior constant field; $h\sim m<<H_i\sim M_0$.

Substituting **(**11), **(**12) in **(**9), **(**10), and considering that

$$rot\left(H_i\cdot\vec{n}_z\right)=0,$$

$$div\left(M_0\cdot\vec{n}_z\right)=0$$

(As $H_i=const$, $M_0=const$),

we have:

$$rot\vec{h}=0; \quad (13)$$

$$div\left(\vec{h}+4\pi\vec{m}\right)=0. \quad (14)$$

From the equation (13) one can assume the introduction of potential $\psi$ of an alternating magnetic field such that:

$$\vec{h}=grad\psi=\left\{\frac{\partial\psi}{\partial x};\frac{\partial\psi}{\partial y};\frac{\partial\psi}{\partial z}\right\}. \quad (15)$$

Thus the equation (14) becomes:

$$div\left(grad\psi+4\pi\vec{m}\right)=0, \quad (16)$$

Thus one can obtain the basic equation for a potential in the medium with the magnetization:

$$\Delta\psi+4\pi div\vec{m}=0. \quad (17)$$

It includes an alternating magnetization $\vec{m}$ that could be expressed from the Landau-Lifshits equation of magnetization vector motion through an alternating magnetic field $\vec{h}$ and a susceptibility tensor $\vec{\vec{\chi}}$. The alternating field components can be expressed through potential $\psi$ according to **(15)**. In this way the components of $\vec{m}$ could be derived by the potential $\psi$ and then substituted directly to the obtained expressions (16). Thus we have the equation only for the potential $\psi$. It is the Walker's equation, which is defined by the susceptibility tensor $\vec{\vec{\chi}}$.

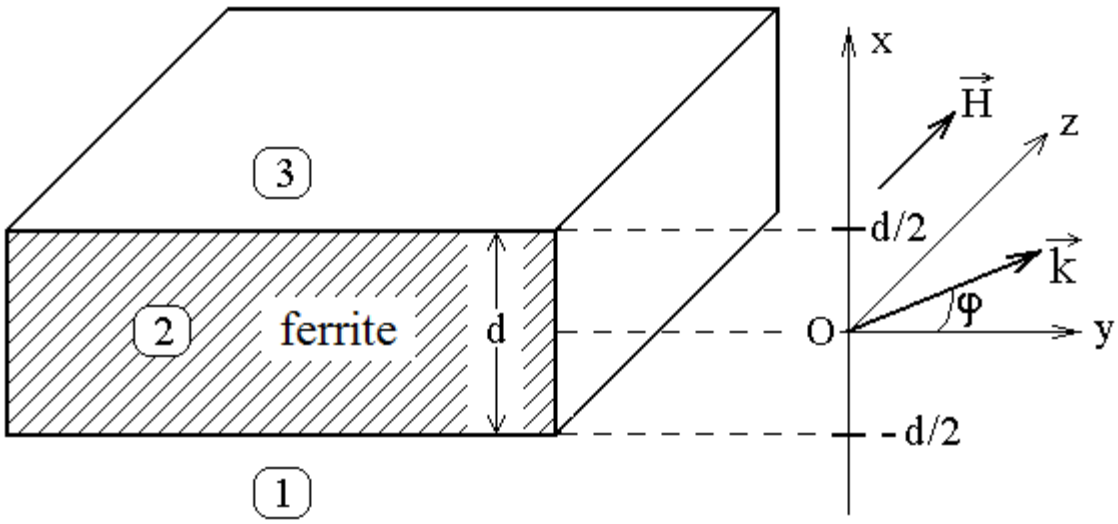


**Fig. 2. Problem geometry.**

One can consider the problem geometry. The structure represents an unfinit ferrite plate 2 with the thickness $d$ and limited by semispaces 1 and 3. The coordinate system $Oxyz$ is chosen as its plane $Oyz$ is parallel to the planes of ferrite plate, and the axis $Ox$ is perpendicular to them. Thus the axis $Oz$ is oriented along an external field direction. The center of coordinate system O is in the middle between the surface planes of ferrite plate, which coordinates are equal to $\pm d/2$.

The boundary conditions on plate surfaces is the continuity of normal components of the magnetic displacement $\vec{B}$ and tangential components of the magnetic strength $\vec{H}$:

$$B_x^i\Big|_{x=\pm\frac{d}{2}} = B_x^e\Big|_{x=\pm\frac{d}{2}},$$

$$H_{y,z}^i\Big|_{x=\pm\frac{d}{2}} = H_{y,z}^e\Big|_{x=\pm\frac{d}{2}}.$$

Calculating components of $\vec{B}$ and $\vec{H}$, boundary conditions become (there are only 4 boundary conditions):

$$\mu\frac{\partial\psi^i}{\partial x} + i\nu\frac{\partial\psi^i}{\partial y}\Big|_{x=\pm\frac{d}{2}} = \frac{\partial\psi^e}{\partial x}\Big|_{x=\pm\frac{d}{2}}; \qquad (18)$$

$$\psi^i\Big|_{x=\pm\frac{d}{2}} = \psi^e\Big|_{x=\pm\frac{d}{2}}. \qquad (19)$$

The second pair of boundary conditions are obtained from the equality of derivatives that is carried out with the assumption of an arbitrary constant, which is added to the potential (as a result of integration). In the Damon-Eshbah work **[77]** this constant is supposed to be equal to zero as all fields are calculated through the derivatives of potential, and the derivative of a constant equals to zero.

Thus, the full problem formulation is:

Space 1 (out of ferrite):

$$\frac{\partial^2\psi_1}{\partial x^2}+\frac{\partial^2\psi_1}{\partial y^2}+\frac{\partial^2\psi_1}{\partial z^2}=0. \tag{20}$$

Space 2 (in ferrite):

$$\mu\cdot\left(\frac{\partial^2\psi_2}{\partial x^2}+\frac{\partial^2\psi_2}{\partial y^2}\right)+\frac{\partial^2\psi_2}{\partial z^2}=0. \tag{21}$$

Space 3 (out of ferrite):

$$\frac{\partial^2\psi_3}{\partial x^2}+\frac{\partial^2\psi_3}{\partial y^2}+\frac{\partial^2\psi_3}{\partial z^2}=0.$$

Boundary conditions for the low $\left(x=-\frac{d}{2}\right)$ and top $\left(x=\frac{d}{2}\right)$ surfaces:

$$\mu\frac{\partial\psi_2}{\partial x}+i\nu\frac{\partial\psi_2}{\partial y}\bigg|_{x=-\frac{d}{2}}=\frac{\partial\psi_1}{\partial x}\bigg|_{x=-\frac{d}{2}}; \tag{22}$$

$$\mu\frac{\partial\psi_2}{\partial x}+i\nu\frac{\partial\psi_2}{\partial y}\bigg|_{x=\frac{d}{2}}=\frac{\partial\psi_3}{\partial x}\bigg|_{x=\frac{d}{2}}; \tag{23}$$

$$\psi_2\big|_{x=-\frac{d}{2}}=\psi_1\big|_{x=-\frac{d}{2}}; \tag{24}$$

$$\psi_2\big|_{x=\frac{d}{2}}=\psi_3\big|_{x=\frac{d}{2}}. \tag{25}$$

Here:

$$\mu = 1 + \frac{\Omega_H}{\Omega_H^2 - \Omega^2};$$

$$\nu = \frac{\Omega}{\Omega_H^2 - \Omega^2};$$

$$\Omega = \frac{\omega}{\omega_M} = \frac{\omega}{4\pi\gamma M_0};$$

$$\Omega_H = \frac{\omega_H}{\omega_M} = \frac{H_i}{4\pi M_0}.$$

### 1.2.2. Frequency ranges for backward volume and surface magnetostatic waves

Let us find frequency ranges for backward volume and surface magnetostatic waves. For this purpose we will regard the dependency $\mu(\Omega)$, which is:

$$\mu = 1 + \frac{\Omega_H}{\Omega_H^2 - \Omega^2},$$

Following cases are possible:

1) $\Omega = 0$, then: $\mu = 1 + \Omega_H^{-1}$;

2) $0 < \Omega < \Omega_H$, then: $1 + \Omega_H^{-1} < \mu < +\infty$;

3) $\Omega_H < \Omega < \sqrt{\Omega_H(\Omega_H + 1)}$, then: $-\infty < \mu < 0$;

4) $\Omega = \sqrt{\Omega_H(\Omega_H + 1)}$, then: $\mu = 0$;

5) $\sqrt{\Omega_H(\Omega_H + 1)} < \Omega < +\infty$, then: $0 < \mu < 1$.

The dependency $\mu(\Omega)$ is presented on Fig. 3.

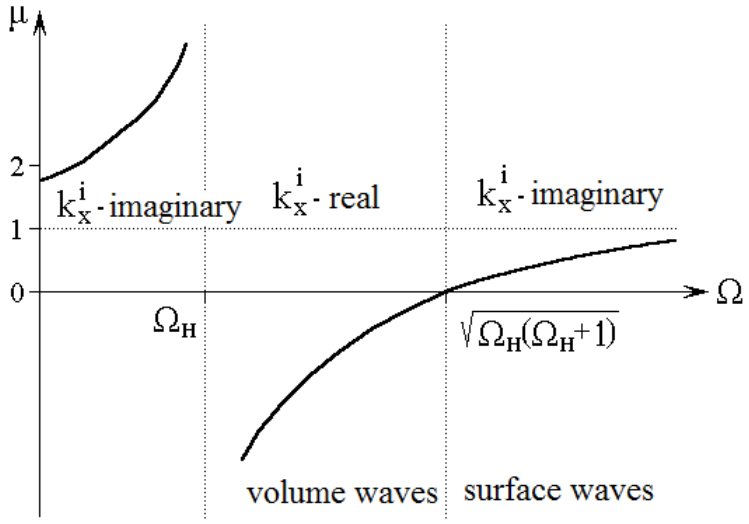


**Fig. 3. The dependency $\mu(\Omega)$.**

There is a range: $\Omega_H<\Omega<\sqrt{\Omega_H(\Omega_H+1)}$, where $\mu<0$ and the wave number inside the film $k_x^i$ can be the real. It is the range of volume waves, for which the dependence of potential $\psi_2$ on the coordinate x oscillates periodically.

In the 2nd space: $0<\Omega<\Omega_H$ where $\mu>0$, waves do not propagate, as in this case their frequency would be below the frequency of homogeneous ferromagnetic resonance.

In the 5th space: $\sqrt{\Omega_H(\Omega_H+1)}<\Omega<+\infty$, where $\mu>0$, the quantity of $k_x^i$ is always imaginary. It is the range of surface waves, for which the dependence of potential $\psi_2$ on the coordinate x decreases expnonentially from a plate surface.

The final dispersion equation follows from the determinant of the system (22)-(25). In general it includes four wave numbers: $k_x^e$, $k_x^i$, $k_y$, $k_z$. Two of them, $k_x^e$ and $k_x^i$, can be excluded by the Walker's equation. Thus the dispersion relation can contain only $k_y$ and $k_z$. It means that if $k_y$ is defined then the dispersion relation allows to derive $k_z$ through $k_y$. As the problem has a cylindrical symmetry one can introduce the polar coordinate system:

$$k_y = k \cdot \cos\varphi; \qquad (26)$$

$$k_z = k \cdot \sin\varphi. \qquad (27)$$

In this coordinate system the wave numbers become:

$$k_x^e = \sqrt{k_y^2 + k_z^2} = k;$$

$$k_x^i = i \cdot \sqrt{k_y^2 + \frac{k_z^2}{\mu}} = i \cdot k \cdot \sqrt{\cos^2\varphi + \frac{\sin^2\varphi}{\mu}} = ik\alpha,$$

Where the following designation is made:

$$\alpha = \sqrt{\cos^2\varphi + \frac{\sin^2\varphi}{\mu}}.$$

$$\beta = \left(\nu^2 - \mu^2 + \mu\right)\cos^2\varphi - \mu. \qquad (28)$$

Finally the basic dispersion relation for the isotropic ferrite plate magnetised in the plane with free surfaces is:

$$k = \frac{1}{2d\alpha} \cdot \ln\frac{\beta - 1 + 2\mu\alpha}{\beta - 1 - 2\mu\alpha}. \qquad (29)$$

This equation is mainly used in the Chapter 4 and the Chapter 5.

## 1.3. Conclusion

The magnetic susceptibility tensors for high frequency and low frequency magnetization dynamics cases were obtained for the specificity of the system geometry. It is of interest for the further theoretical research on the magnetoelastic energy conversion. Low frequency magnetization dynamics was considered as a consequence of the second-order non-linearity of the Landau-Lifshitz equation. The HF magnetic damping influence was proposed to be considered in the form offered by Gilbert. The magnetoelastic coupling was taken under consideration in the internal magnetic field strength calculation. It was found to have a neglectibly small contribution to the final result and was taken out of the further calculations. In fact its contribution can be significant in the vicinity of the spin reorientation transition as it forms the gap for the resonant frequency. In the present work this gap was near 23 MHz and was much lower than the lowest frequency limit of FMR observation (500 MHz).

Magnetostatic approximation regarded here is mostly based on the work of Damon and Eshbach **[77**]. The dispersion equation and the other results obtained here are mainly used in the chapters 4 and 5, where the related problems of magnetostatic surface wave propagation in a magnon crystal with a variable thickness and the anomalous Doppler effect occurrence during the magnetostatic surface waves propagation in the ferrite-dielectric-metal structures are under consideration.

## 2. Ferromagnetic resonance and magnetoelastic demodulation in thin active films with an uniaxial anisotropy

Here we study FMR and magnetoelastic demodulation in the uniaxial $TbCo_2$/FeCo nanostructure deposited on Si cantilever. The results are compared with the ones obtained on $La_{0.7}Sr_{0.3}MnO_3$ thin film grown on $NdGaO_3$ substrate. The latter rare earth manganitestrontium perovskite thin film was chosen for its low high frequency (HF) absorption and its significant magnetostriction coefficient at room temperature [34], [37]. In both cases the technology provides uniaxial in plane magnetic anisotropy and clearly expressed SRT [38], [39]. Creation of SRT in giant magnetostriction $TbCo_2$/FeCo exchange coupled nanostructures was achieved technologically by means of RF deposition under a steady state external magnetic field, while creation of SRT in the $La_{0.7}Sr_{0.3}MnO_3$ perovskite films was achieved technologically by means of lattice mismatch of the film and the substrate.

The results of measurements of FMR lines and magnetic field dependencies of amplitudes of low frequency (LF) magnetoelastic vibrations in the samples are compared with calculations.

### 2.1. Looking to the theory of phase transitions

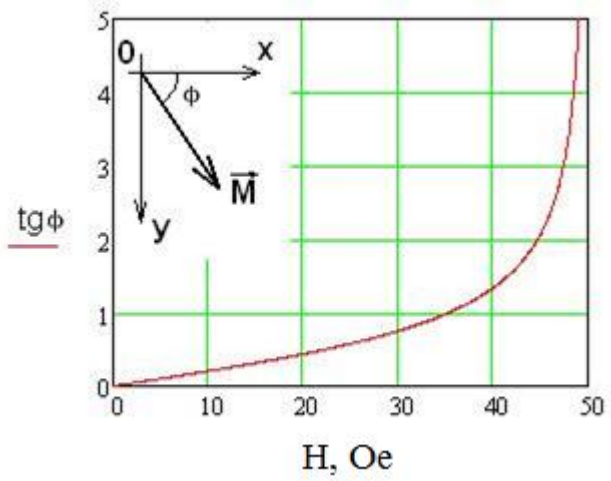


**Fig. 4. Change of equilibrium orientation of static magnetization of the sample $tg\ \phi = \frac{M_y}{M_x}$ under the influence of an external magnetic field.**

Let us consider behavior of the system directly in the vicinity of the spin reorientation transition.

External magnetic field can be introduced to change an equilibrium phase of the system, and the direction of magnetization (Fig. 4). As the order parameter (here, the magnetization) changes continuously according to the external influence from one equilibrium state to another, it is obvious that we have a phase transition of the second order.

For the convenience we will introduce a small parameter $\eta = M_0 - M_y$. Then $M_x \approx M_z \approx 0$. Thus the energy of the system can be written as:

$$F = -(H - H_A + 2b\frac{1}{M_0}u_{yy}^0)\,\eta + (b(\frac{1}{M_0})^2 u_{yy}^0 + \frac{H_A}{2M_0})\eta^2 + const. \qquad (30)$$

One can see that factor $\eta$ critically depends on the external field and especially in the vicinity of the spin reorientation transition $H = H_A$, where it is equal to zero.

We introduce a small external magnetic field changing in time much more slowly than the characteristic time of spin precession. Thus the change of system energy can be written as $\delta F = -\delta h M_0$. Then the change of order parameter caused by this influence is:

$$\delta\eta = \frac{1}{\frac{\partial F}{\partial \eta}} h = \frac{1}{\left(H - H_A + 2b\frac{1}{M_0}u_{yy}^0\right) - (2b(\frac{1}{M_0})^2 u_{yy}^0 + \frac{H_A}{M_0})\,\eta}\,\delta h = \chi(H)\,\delta h.$$

Thus, the susceptibility of the sample for quasistatic influence by a small external magnetic field has been calculated. One can see that in the vicinity of SRT it has a singularity, which disappears with taking into account of the magnetoelastic coupling factor: $H \to H_A \sim \eta \to 0 \sim \chi \to \frac{1}{2b(\frac{1}{M_0})^2 u_{yy}^0}$.

One can calculate the resonant frequency $\omega_0$ corresponding to the maximum of mechanical response of the system. Neglecting the magnetoelastic coupling contribution, one can obtain:

$$(\frac{\omega_0}{\gamma})^2 = (H + 4\pi(M_0 - \eta))(-H + H_A + \frac{H_A}{M_0}\eta) \qquad (31)$$

In the vicinity of spin reorientation transition in this assumption the resonant frequency decreases to zero. This phenomenon is a so-called "soft mode" **[44]**: $H \to H_A \sim \eta \to 0 \sim \omega_0 \to 0$. One can be easily shown that the high-frequency susceptibility diverges in this case.

## 2.2. Flexural bulk vibrations

The magnetization can be subdivided into three parts: static, HF and LF:

$$M_i(t) = M_i^0 + m_i(t) + \mu_i(t). \qquad (32)$$

Elastic deformations contain static and LF dynamic parts.

$$\hat{u}(t) = \hat{u}_0 + \hat{\varepsilon}(t) \qquad (33)$$

HF part of elastic strains is assumed to be negligibly small because of relatively thick substrate and the high value of HF mechanical absorption in the sample.

To obtain the energetic form of the flexural vibrations we can introduce the vertical displacement $U = u_z$. In this case the dynamic part of the deformations is defined by the second

derivatives of the displacement: $\varepsilon_{ij} = -(z - z_0)\dfrac{\partial^2 U}{\partial x_i \partial x_j}$, where *i,j* are equal to 1 or 2, and $\varepsilon_{zz} = -\dfrac{C_{12}}{C_{11}}\left(\varepsilon_{xx} + \varepsilon_{yy}\right)$. Here $z_0$ is the position of the neutral section.

It can be shown [40] that Lagrangian of the system after integration by *z* may be expressed via kinetic and potential components of the surface energy density:

$$L = \int_S dS[1/2\rho_S \dot{U}^2(x,y,t) - F_e^S(\hat{U}(x,y,t)) - F_{me}^S(\vec{M},\hat{U}(x,y,t))] \tag{34}$$

Taking into account presentation (32) one can obtain the following expressions for elastic and magnetoelastic potential energy parts related to the LF excitations:

$$F_e^S = 1/2\hat{e}\hat{U}^2(x,y,t) = \frac{d^3}{3}(3\beta^2 - 3\beta + 1)(C_{11} - C_{12})[\frac{1}{2}(1 + \frac{C_{12}}{C_{11}})(\Delta U)^2 + (\frac{\partial^2 U}{\partial x \partial y})^2 - \frac{\partial^2 U}{\partial x^2}\frac{\partial^2 U}{\partial y^2}] \tag{35}$$

$$\begin{aligned} F_{me}^S(t) = {} & \frac{\beta d d_m b^{\gamma,2}}{M_0^2}[\frac{\partial^2 U}{\partial x^2}(-2M_x^0\mu_x(t) - \overline{((m_x(t))^2 - (m_z^2(t))\frac{C_{12}}{C_{11}})}^{\tau}) - \\ & - \frac{\partial^2 U}{\partial y^2}(-2M_y^0\mu_y(t) - \overline{((m_y(t))^2 - (m_z^2(t))\frac{C_{12}}{C_{11}})}^{\tau}) - \\ & - \frac{\partial^2 U}{\partial x \partial y}(M_x^0\mu_y(t) + M_y^0\mu_x(t) + \overline{m_x(t)m_y(t)}^{\tau})] \end{aligned} \tag{36}$$

The averaging in (36) is made over the time period τ which is much higher than the period of HF oscillations of magnetization but much smaller than the period of LF vibrations.

One can expand overall elastic deformation into normal vibration modes:

$$U(x,y,t) = \sum_n U_n(x,y)A_n(t) \tag{37}$$

Substituting these expansion in (34), (35), (36) one can write Lagrangian of mode n:

$$L_n = 1/2M_n\dot{A}_n^2 - 1/2k_nA_n^2 + F_n(t)A_n \tag{38}$$

where the following notations are used:

$$\begin{cases} M_n = \int_S dS\, \rho_S U_n^2, \\ k_n = \int_S dS\, \hat{e} \hat{U}_n^2, \\ F_n(t) = \int_S dS\, F_{me}^S(\vec{M}, \hat{U}). \end{cases} \tag{39}$$

Equation of motion for $A_n(t)$ can be derived from Lagrange's differential equation:

$$\frac{\partial}{\partial t}\frac{\partial L_n}{\partial \dot{A}_n} - \frac{\partial L_n}{\partial A_n} + \frac{\partial D}{\partial \dot{A}_n} = 0 \tag{40}$$

Here we used Rayleigh dissipation function in the form [43]: $D = \delta_n \dot{A}_n^2$.

Hence we can obtain the equation of motion for amplitude $A_n(t)$ of a mode "n" in the form of an oscillator equation:

$$M_n\left(\ddot{A}_n + 2\delta_n \dot{A}_n + \Omega_n^2 A_n\right) = F_n(t) \tag{41}$$

Here $\Omega_n$ is the resonance frequency of the mode $\Omega_n = (\kappa_n / M_n)^{1/2}$.

Following (39) and (41) one can obtain the Fourier amplitude of elastic vibrations that is proportional to the LF and to the averaged value of the square of the HF magnetization components.

$$A_n(\Omega) = \frac{\eta_n \beta d_m d b^{\gamma,2}}{M_n \sqrt{(\Omega^2 - \Omega_n^2)^2 + (2\delta_n \Omega)^2}} \frac{1}{T} \int_{-T/2}^{T/2} dt \cdot e^{-i\Omega t} \cdot \left[ \overline{m_x^2(t) - m_z^2(t)\frac{C_{12}}{C_{11}}}^{\tau} + 2M_{0x} \cdot \mu_x(t) \right] / M_0^2 \tag{42}$$

Here $\eta_n = \int \frac{\partial^2 U_n}{\partial x^2} dS$, $T = 2\pi / \Omega_n$, and $\Omega$ is a frequency divisible by $\Omega_n$. The explicit form of the function $U_n(x)$ is presented in Appendix C.

It could be derived from (42) that the amplitude of elastic vibrations of the fundamental flexural mode at resonance frequency is equal to:

$$A_n(\Omega_n) = 0.231 \cdot b^{\gamma,2} \Gamma \frac{1}{T} \int_{-T/2}^{T/2} dt \cdot e^{-i\Omega t} \cdot \left[ \overline{m_x^2(t) - m_z^2(t)\frac{C_{12}}{C_{11}}}^{\tau} + 2M_{0x} \cdot \mu_x(t) \right] / M_0^2 \tag{43}$$

Here $\Gamma$ is a parameter which is composed of the geometric and acoustic properties of the sample: $\Gamma = d_m / \rho_S c_s \delta_n$, where $c_S$ is the longitudinal sound velocity in the sample and $\rho_S$ is the surface density of the structure. The equation (43) together with the results of calculations of $m_x(t)$ and $\mu_x(t)$ are used to obtain the magnetic field dependence of the vibration amplitudes presented in Fig. 10.

Calculations of the components of magnetization are carried out using the Landau-Lifshitz-Gilbert equation:

$$\frac{\partial \vec{M}}{\partial t} = -\gamma[\vec{M} \times \vec{H}_{eff}] + \frac{\alpha}{M_0}[\vec{M} \times \frac{\partial \vec{M}}{\partial t}] \tag{44}$$

Where α is the coefficient of magnetic relaxation and $\vec{H}_{eff}$ is the effective magnetic field.

$$\vec{H}_{eff} = -\frac{\partial F}{\partial \vec{M}} \tag{45}$$

The effective magnetic field is divided in static, LF and HF components:

$$\vec{H}_{eff} = \vec{H}^0_{eff} + \vec{h}^{\Omega}_{eff}(t) + \vec{h}^{\omega}_{eff}(t), \tag{46}$$

where superscripts Ω and ω correspond to LF and HF parts respectively. The equilibrium ground state of the magnetic system is given by the static equation:

$$[\vec{M}_0 \times \vec{H}^{eff}_0] = 0 \tag{47}$$

According to the system energy one can obtain the components of the static effective field:

$$\vec{H}^0_{eff} = \begin{pmatrix} 0 \\ -H + \frac{H_A}{M_0} M^0_y \\ \frac{H_A}{M_0} M^0_z + 4\pi M^0_z \end{pmatrix} \tag{48}$$

In the definition of $H_A$ we took into account the contribution of the static magnetostrictive strains. Generally the static strain contains two parts. One of them is created during the preparation of the films and corresponds to the direction of magnetization parallel to the easy axis in the non-stressed structure. This part contributes to the anisotropy field with value $H_{me} = 2(b^{\gamma,2})^2 / M_0(C_{11} - C_{12})$. It is included in definition of $H_A$ in equation (48): $H_A = H_{A0} + H_{me}$.. The second component of the static strain follows variations of the equilibrium direction of $\vec{M}_0$. These deformations are proportional to the ratio of the film and the substrate thicknesses $\frac{d_m}{d} \sim 10^{(-3)\div(-4)}$ and introduce a negligibly small contribution in $H^0_{eff}$.

The HF component of the effective magnetic field can be presented as:

$$h^{\omega}_{eff}(t) = h_i(t) + S^{ij} m_j(t) \tag{49}$$

where: $S^{ij} = \partial(H^0_{eff})_j \big/ M_i$ .

One can describe HF magnetization dynamics in a linear approximation of the Landau-Lifshitz equation:

$$\frac{\partial \vec{m}}{\partial t} = -\gamma[\vec{M}_0 \times (\frac{H^0_{eff}}{M_0}\vec{m}(t) - \vec{h}^{\omega}_{eff}(t) - \frac{\alpha}{\gamma M_0}\frac{\partial \vec{m}}{\partial t})] \tag{50}$$

The solution of equation (50) is expressed via the magnetic susceptibility tensor: $\vec{m}(t) = \hat{\chi}(\omega)\vec{h}(t)$. The explicit form of $\hat{\chi}(\omega)$ is presented in the Appendix E.

Low-frequency dynamics of magnetization is described by the second-order nonlinear part of the Landau-Lifshitz equation:

$$\frac{\partial \vec{\mu}}{\partial t} = -\gamma[\vec{M}_0 \times (\frac{H^0_{eff}}{M_0}\vec{\mu}(t) - \vec{h}^{\Omega}_{eff}(t) - \frac{\alpha_{\Omega}}{\gamma M_0}\frac{\partial \vec{\mu}}{\partial t})] - \gamma\overline{[\vec{m} \times \vec{h}^{\omega}_{eff}]}^{\tau} \tag{51}$$

where $\alpha_\Omega$ is LF magnetic relaxation coefficient. The low frequency part of the effective field is equal to:

$$h_{eff}^{\Omega}(t) = S^{ij}\mu_j + S^{ilj}\overline{m_l m_j}^{\tau} \tag{52}$$

where $S^{ilj} = \partial^2 (H_{eff}^0)_j \Big/ \partial M_i \partial M_l$

As it was mentioned above the nonlinear alternative terms are averaged for the time period τ: $1/\Omega \ll \tau \ll 1/\omega$. In the expression (52) we neglected by elasto-magnetic feedback effect caused by the LF deformations and proportional to the ratio $d_m/d$.

Following (51) and (52) one can obtain the LF part of the magnetization:

$$\mu_i(t) = \kappa_{ikl}\overline{h_k(t)h_l(t)}^{\tau} \tag{53}$$

where:

$$\kappa_{ikl} = -4\Theta_{ij}(\varepsilon_{jmk}\chi'_{ml} + \varepsilon_{juv}S^{vv}(\chi'_{uk}\chi'_{vl} + \chi''_{uk}\chi''_{vl}))/(\pi \det\hat{\Theta}) \tag{54}$$

Here: $\varepsilon_{ijk}$ is the Levi-Civita symbol; $\chi'_{vl}$ and $\chi''_{vl}$ are real and imaginary components of the HF magnetic susceptibility, respectively; $\hat{\Theta} = \hat{A}(\Omega)$ is the operator of the linear Landau-Lifshitz equation for low-frequency vibrations which differs from the high-frequency operator by the low frequency Ω instead of HF ω (see Appendices B and D).

## 2.3. Experimental setup.

Experimentally observed excitation of low frequency elastic vibrations of the cantilevers due to magnetoelastic demodulation of microwave electromagnetic field at FMR frequency is presented in this part. The scheme of the experimental setup is shown in Fig. 5. A high-frequency sinusoidal signal modulated by low-frequency square signal was used to feed the sample by means of the microstrip line ML. The first sample was made of 25 bilayers of ($TbCo_2$/FeCo) composition, and thickness 10 nm, deposited by RF sputtering on Si substrate of 20mm×4mm×60 μm dimensions. The second $La_{0.7}Sr_{0.3}MnO_3$ film, of thickness 200 nm, was deposited by laser ablation on a (110) $NdGaO_3$ substrate of 5mm×5mm×500 μm size. The samples parameters are presented in Table 1.

| Film material | Substrate material | $H_A$, Oe | $M_0$, G | $\delta$, $s^{-1}$ | Length, cm | Width, cm | $\beta^{\gamma,2}$, MPa |
|---|---|---|---|---|---|---|---|
| $TbCo_2/FeCo$ | $SiO_2$ | ~25-50 | 1400 | 0.1 | 2 | 0.5 | ~6 |
| $La_{0.7}Sr_{0.3}MnO_4$ | $NdGaO_3$ | 110 | 350 | 0.25 | 0.5 | 0.5 | ~0.1 |

**Table 1. Parameters of samples.**

According to **[39]** at this crystal orientation of substrate the perovskite film has an uni-axial anisotropy with [001] hard axis. The hard axis was perpendicular to the long side of the samples. Both samples were successively installed in the static bias field **H** of an electromagnet. Mechanical vibrations of the samples were observed optically by measurement of the deflection of a laser beam (λ = 650 nm) using a position sensitive photo detector PSD. Simultaneously, a part of the HF signal was split via the circulator C to the detector D, amplified by the lock-in amplifier and registered by the DAQ block.

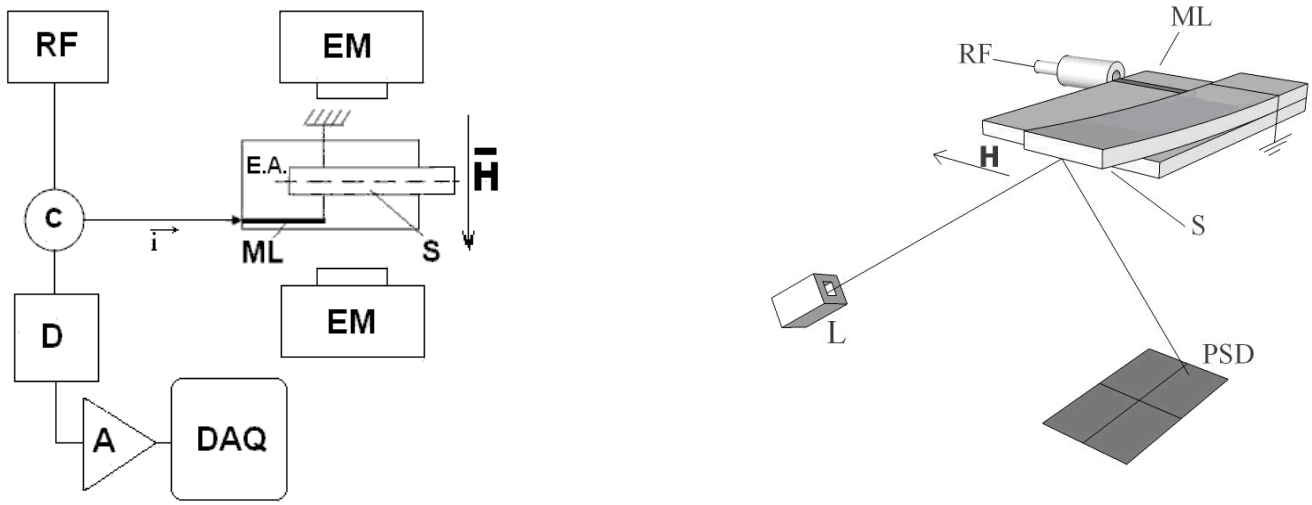


A. B.

**Fig. 5. Description of the experimental setup: A) HF excitation and measurement system : RF – radio frequency generator, C – circulator, EM – electromagnet, ML – microstrip line, E. A. – easy axis, S – sample, D – detector, A – amplifier, DAQ – data acquisition hardware ; B) Optical system for the measurement of mechanical deflections: L – laser λ = 650 nm, PSD – position sensitive detector).**

## 2.3.1.Methods for hard axis setting

We used the longitudinal magneto-optical Kerr effect (MOKE) to define the hard axis direction. The experimental setup is presented in Fig. 6. The change of polarization of the light beam from the semi-conductor laser L ($\lambda = 630\ nm$, $P = 5\ mW$) passing through the polarizer P and beam splitter and then reflected from a film was measured by the system of analyzers A1 and A2 and semi-conductor photodetectors D1 and D2. The signal from both channels was fed to the differential amplifier and then to the DAQ block. Such scheme of optical measurements allowed to reduce the influence of laser noises and to increase the amplitude of resulting signal.

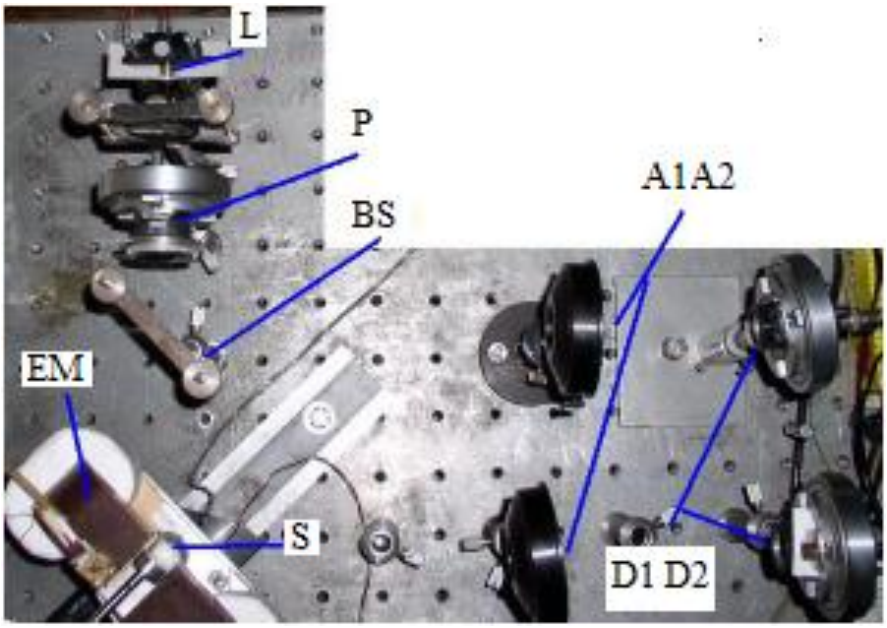


**Fig. 6. Experimental setup for longitudinal the MOKE measurements: L - the semi-conductor laser, P - a polarizer, BS – beam splitter, A1 and A2 - analyzers of reference and main channels, S - the sample, EM - electromagnet, D1 and D2 - photodetectors.**

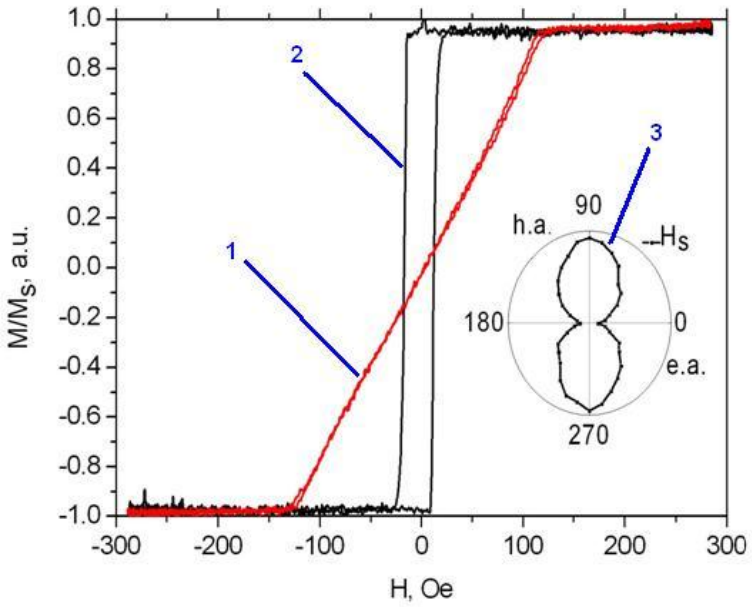


**Fig. 7. Results of measurements of the hysteresis loop for manganite lanthanum:**

**1 - exact adjustment for hard axis; 2 - rectangular loop of a hysteresis, exact adjustment for easy axis;**

**3 - polar dependence of the saturation field on the rotation angle of the sample in an external magnetic field.**

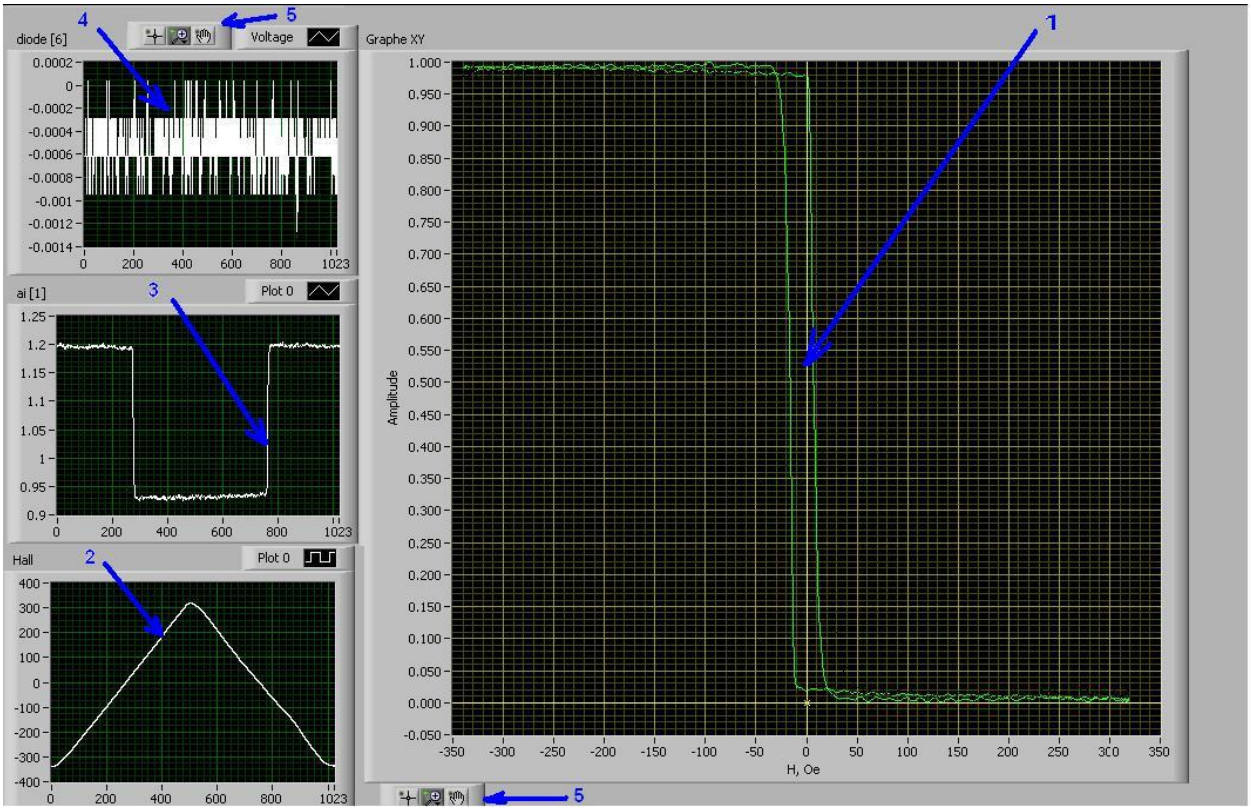


**Fig. 8. The screen of the working virtual device.**

**1 - the image of a rectangular loop of a hysteresis of thin film $TbCo_2$/FeCo, it is received by averaging of the saved up signal;**

**2 - time sweep of a signal from the Hall cell;**

**3 - time sweep of the signal supplied to the DAQ block;**

**4 - noise signal from the microwave detector that is not involved in the experiment;**

**5 - tools for the formatting of graphic representation.**

According to longitudinal MOKE theory **[99]**, the Kerr angle rotation for s-polarized incident light is defined by first order of the film surface magnetization:

$$\theta_{xy}(h) = \frac{\cos\varphi \tan\psi}{\cos(\varphi+\psi)} \frac{inQ}{n^2-1} M(h)$$

Here n is the relative refractive index of the air and the film material, *M(h)* – the film magnetization in the longitudinal direction, $\varphi$ and $\psi$ – the angles of reflection and refraction, *Q* is the magnetooptical imaginary constant. This equation shows that polarization of the reflected wave is linearly dependent on the film magnetization.

The results of optical measurements for the film of manganite lanthanum are presented in Fig. 7. Fig. 8 represents the virtual device graphic interface.

The description of the method can also be found in the Ref. **[39]**.

## 2.4. Microwave measurements

The value of the bias field which induced SRT was equal to the value of the effective anisotropy field $H_A$ = 25 Oe for the $TbCo_2$/FeCo nanostructure and $H_A$ = 105 Oe for the $La_{0.7}Sr_{0.3}MnO_3$ perovskite film. Measured FMR curves are presented in Fig. 9 (solid lines). One can see that FMR amplitude is twice higher, when FMR conditions verge towards SRT (compare Fig. 9(a) and Fig. 9(b); Fig. 9(d) and Fig. 9(e)) and decreases sharply when FMR is far from SRT (Fig. 9(c) and Fig. 9(f)). This phenomenon is caused by the increase of the magnetic susceptibility imaginary part.

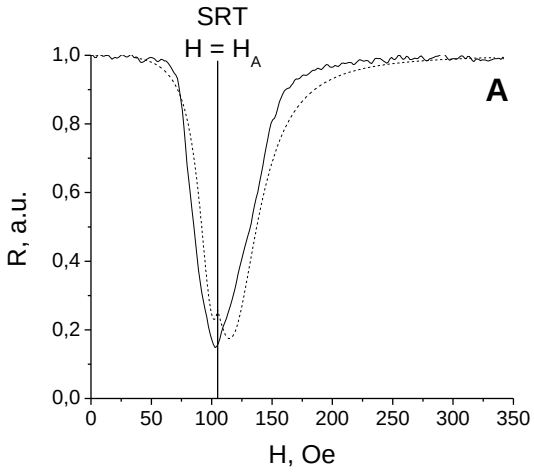
SRT
H = H_A
A
R, a.u.
H, Oe

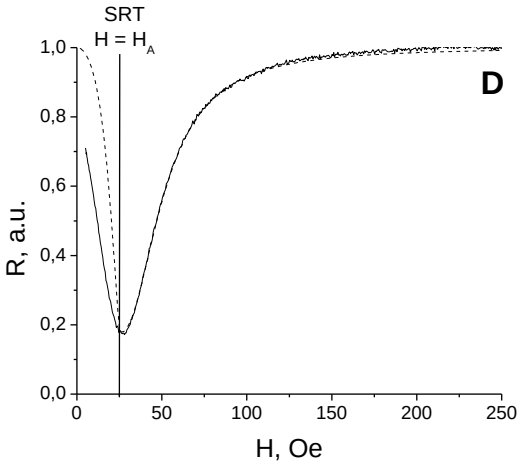
SRT
H = H_A
D
R, a.u.
H, Oe

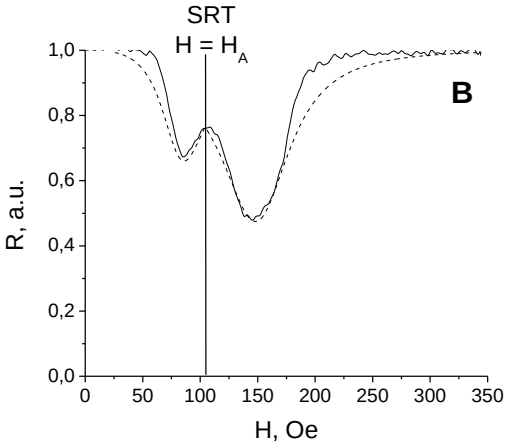
SRT
H = H_A
B
R, a.u.
H, Oe

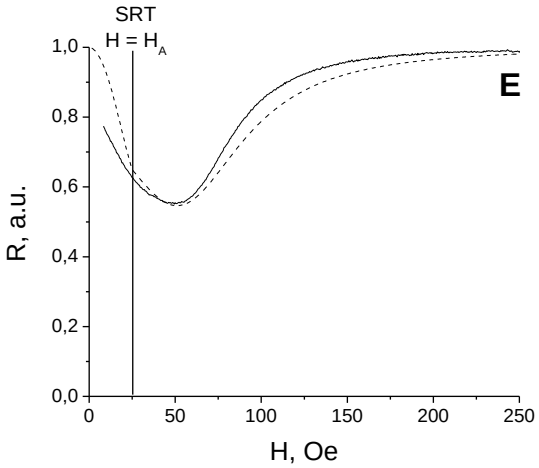
SRT
H = H_A
E
R, a.u.
H, Oe

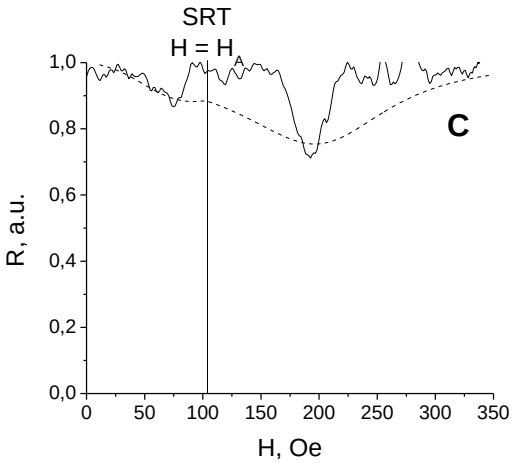
SRT
H = H_A
C
R, a.u.
H, Oe

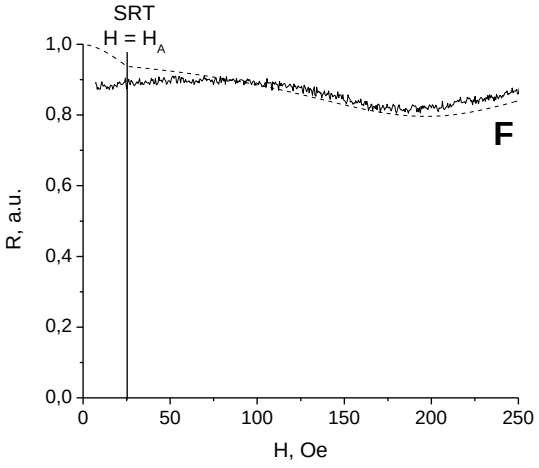
SRT
H = H_A
F
R, a.u.
H, Oe

**Fig. 9. Magnetic field dependence of the HF reflection coefficient R expressed in arbitrary units at different FMR frequencies for $La_{0.7}Sr_{0.3}MnO_3$ film (A – 814 MHz, B – 1183 MHz, C – 1760 MHz) and for $TbCo_2$/FeCo nanostructure (D – 1172 MHz, E – 2174 MHz, F – 4918 MHz): solid line-experiment, dashed line-theory.**

## 2.5. Optical measurements

The results of the optical detection of the flexural vibrations of the cantilever are presented in Fig. 10. One can see that the amplitude of the vibrations increases when FMR is excited near SRT. All results were observed at room temperature when $La_{0.7}Sr_{0.3}MnO_3$ still has ferromagnetic order and a significant magnetoelastic coupling factor **[34]**, **[37]**.

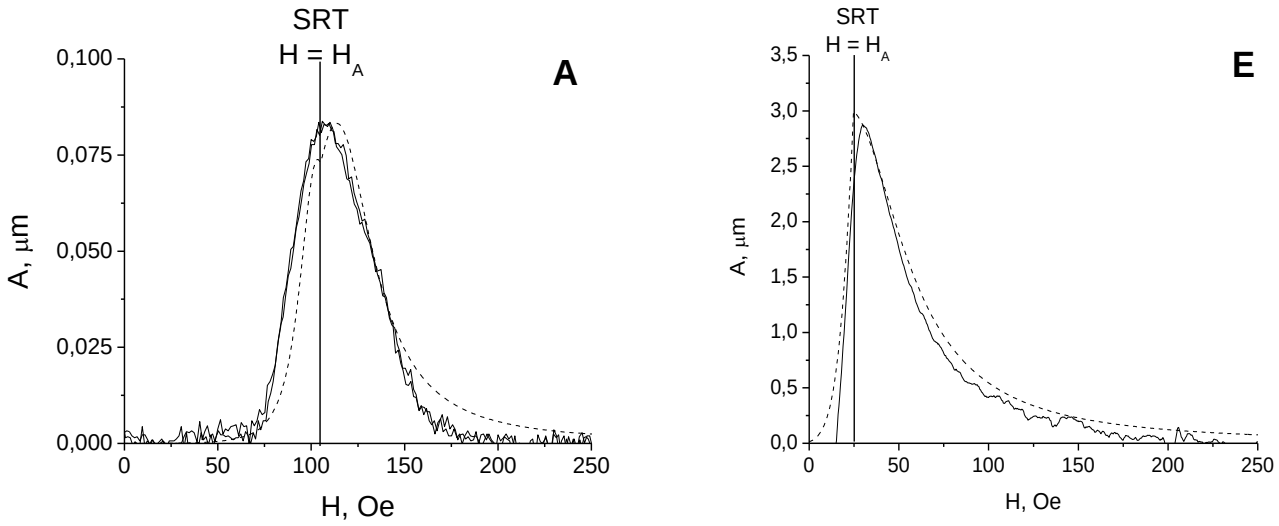

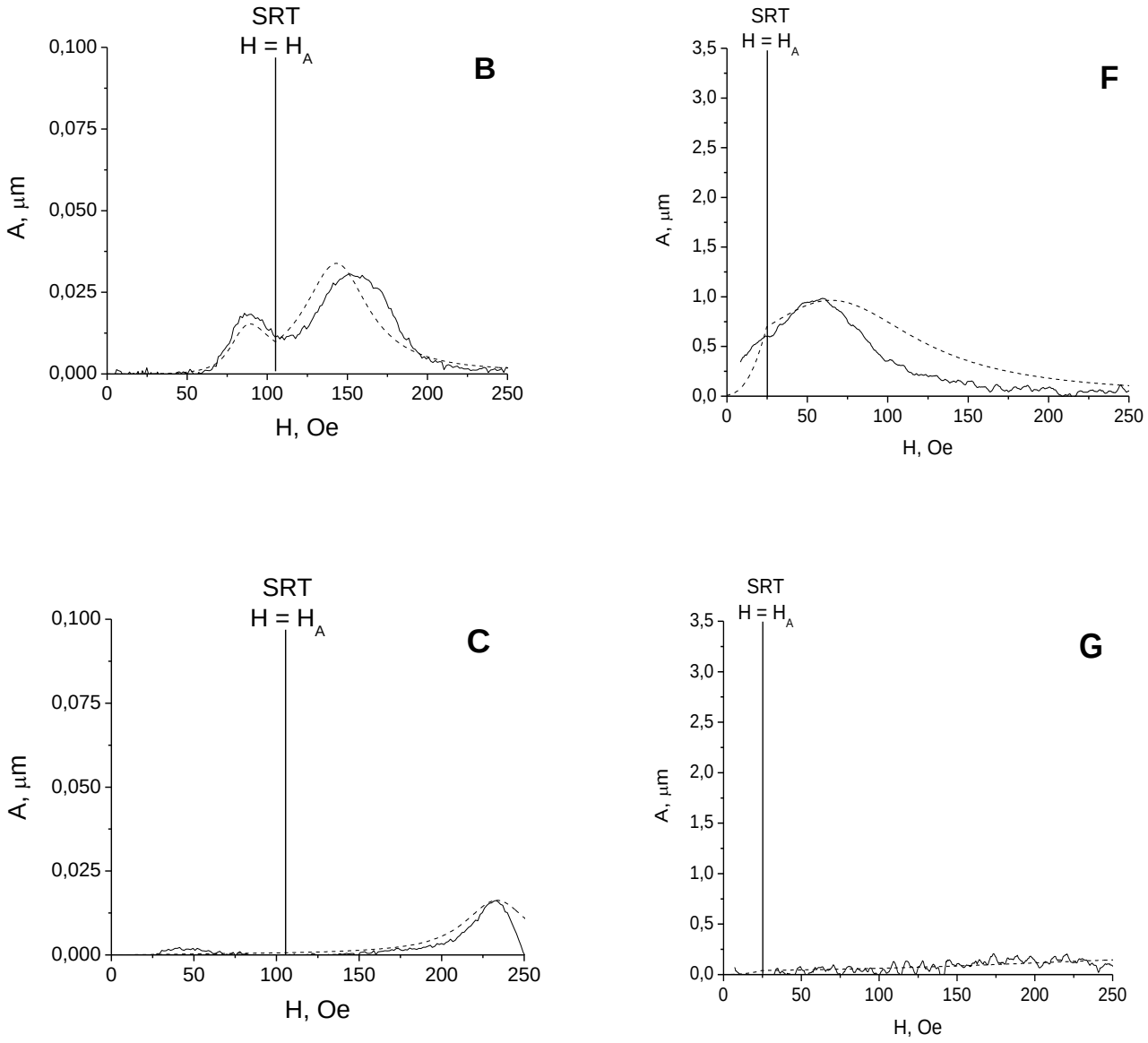


**Fig. 10. Magnetic field dependence of the amplitude of sample vibrations at different FMR frequencies for $La_{0.7}Sr_{0.3}MnO_3$ film (A – 814 MHz, B – 1183 MHz, C – 1760 MHz) and for $TbCo_2$/FeCo nanostructure (E – 1172 MHz, F – 2174 MHz, G – 4918 MHz): solid line-experiment, dashed line-theory.**

The attenuation coefficients of the mechanical vibrations of both samples were also measured. They were defined by the measurements of relaxation time for the fundamental flexural mode assuming that the vibration amplitude was decaying exponentially. The obtained attenuation coefficients were $\delta = 0.1\ s^{-1}$ for the $TbCo_2$/FeCo nanostructure, and $\delta = 0.25\ s^{-1}$ for the perovskite film.

## 2.6. Theory and experiment comparison

Analysis of the matrix $\chi(\omega)$ shows that the FMR line for uni-axial magnetic film has two maxima near SRT: one for saturation ($H>H_A$) and another for angular phases ($H<H_A$) which are caused by $\chi''$ and $\kappa_{ikl}$ maximas. In the case of the $TbCo_2$/FeCo nanostructure only one resonance peak was observed in all the involved frequency range. That is explained by the strong attenuation of HF spin excitations in rare earth compounds. On contrary, the curves for the perovskite film have two resonant peaks in most part of frequency range except the area near SRT where the HF relaxation increases. The best fitting of calculations with the experimental data in the case of the perovskite film was obtained for relative HF magnetic attenuation factors equal to $\alpha_A = 0.605$ for 1172 MHz, $\alpha_{B,C} = 0.355$ for 1172 MHz and for 2174 MHz, which are almost twice lower than for the $TbCo_2$/FeCo nanostructure: $\alpha_A = 0.925$ for 1172 MHz, $\alpha_B = 0.575$ for 2174 MHz and $\alpha_C = 0.275$ for 4918 MHz. In the area which is sufficiently far from SRT the relative HF magnetic attenuation factors decrease slowly. This fact is probably caused by the domain structure that appears in the vicinity of SRT.

According to the calculations using (43), the increase of amplitude of the LF vibrations excited by the HF electromagnetic field in FMR conditions near SRT is clearly seen. The behaviour of the curves for the vibration amplitude presented in Fig. 10 is similar to the behaviour of FMR curves presented in Fig. 9. One can see that the mechanical response for the $TbCo_2$/FeCo nanostructure is by order of magnitude greater than for the perovskite film. The comparison of the multipliers $\Gamma$ gives the ratio: $\Gamma_{LSMO} \Big/ \Gamma_{TbCo_2/FeCo} \approx 1.126$. This data, together with the magnetostriction coefficient ratio $b^{\gamma,2}_{LSMO} \Big/ b^{\gamma,2}_{TbCo_2/FeCo} \approx 0.1$, explain the favourable mechanical response of the $TbCo_2$/FeCo structure in spite of the higher HF attenuation relatively to the one in the $La_{0.7}Sr_{0.3}MnO_4$ sample.

## 2.7. Conclusion

The experimental and theoretical data on FMR and magnetoelastic demodulation in the $TbCo_2$/FeCo nanostructure and $La_{0.7}Sr_{0.3}MnO_3$ thin film deposited on Si and $NdGaO_3$ cantilevers respectively, show that low-frequency vibrations of the cantilever can be amplified when FMR is excited by HF electromagnetic field near SRT. The experiments have been carried out at high frequencies from below 1 GHz to above 4 GHz. Rare-earth manganitestrontium perovskites demonstrated clear resonance properties in the majority of the high-frequency range. At the same time it is shown that the $TbCo_2$/FeCo nanostructure has one order higher mechanical response in spite of the higher HF attenuation. This is caused by the fact that the $TbCo_2$/FeCo nanostructure has a high value of

magnetoelastic coupling factor (approximately one order higher than for the $La_{0.7}Sr_{0.3}MnO_3$ thin film). The results of calculations are in good agreement with the experimental data of measurements of FMR line and with the data of the optical detection of elastic vibrations of the magnetostrictive cantilever under HF electromagnetic field. The phenomenon under consideration can find applications in the area of MMMSs distantly controlled by a HF external electromagnetic field.

# 3. Nonlinear magnetoelectric effect in multiferroic nanostructure TbCo/FeCo-AlN in high frequency electromagnetic field

In the present chapter we report the results of observation of the low frequency electric voltage induced by a HF electromagnetic field in the nanostructured thin film multiferroic TbCo/FeCo-AlN in the vicinity of SRT. Observed magnetoelectric effect is described in the framework of nonlinear model of spin dynamics and magnetoelastic interaction taking into account intrinsic absorption in magnetic subsystem and electric conductivity of magnetic component of the structure.

## 3.1. Experimental technique and results

In this part experimentally observed excitation of LF electric voltage generated by magnetoelectric demodulation of microwave electromagnetic field in nanostructured thin film multiferroic is presented. The experimental setup is shown in Fig. 11. A high frequency sinusoidal signal modulated by low frequency harmonic excitation was used to feed the sample via the microstrip line ML. The sample represented the multiferroic structure deposited on $<100>$ silicon substrate of $50\ \mu m$ thick and $18 \times 3\ mm^2$ surface. The platinum electrode coated the surface of the substrate. The aluminum nitride (AlN) thin film layer of $5.5\ \mu m$ thick was deposited above the electrode. Magnetostrictive nanostructure of 25 TbCo/FeCo bilayers was deposited on AlN surface by rf sputtering in a static magnetic field. The thickness of each bilayer was equal to 10 nm. The methodology of sample production is presented in detail in **[29]**. The magnetoelastic coupling constant, measured via the bending cantilever method **[56]** on a test sample, was found to be $b^{y,2} \sim -7\ MPa$. The magnetostricive layer possessed a significant conductivity and served as the top electrode. The easy axis induced during deposition process was directed at an angle of $\varphi_0 = 70°$ to the long side of the sample. The sample was installed in the static bias field **H** that was perpendicular to the easy axis direction and the microstrip line was parallel to the short side of the sample. Simultaneously, a part of the HF signal was split via the circulator C to the detector D, amplified by the lock-in amplifier and registered by the DAQ block. The modulation frequency of HF signal was chosen equal to the resonance frequency $\Omega/2\pi = 843\ Hz$ of the fundamental flexural mode of the sample vibrations. The vibrations occurred for the flexural mode with vertical displacement $U(\xi)$ were $\xi$ direction is parallel to the long side of the sample. The voltage oscillations caused by elastic strains were observed by the oscilloscope with pre-amplifying system.

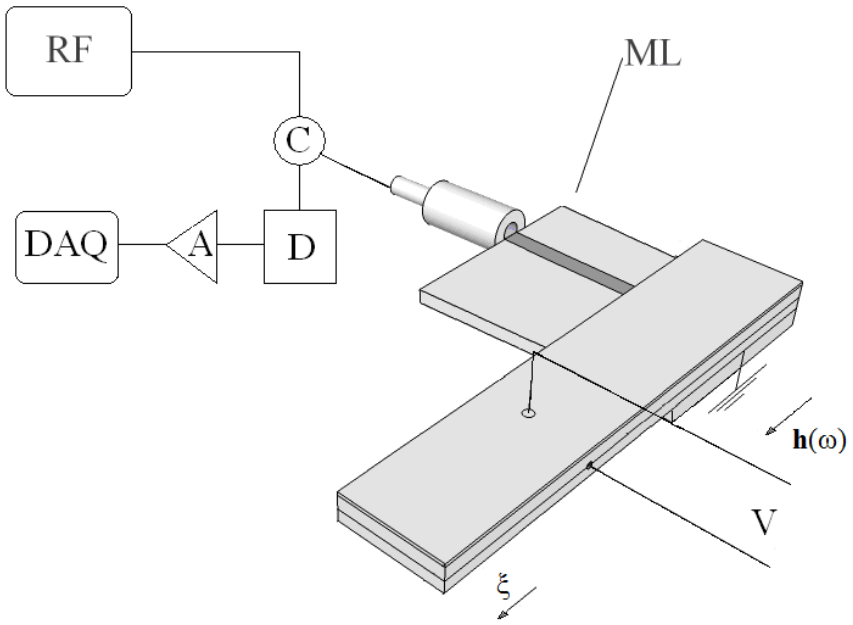


**Fig. 11. Experimental setup. RF – radio frequency generator, C – circulator, ML – microstrip line, E. A. – easy axis, D – detector, A – amplifier, DAQ – data acquisition hardware, H – external magnetic field produced by electromagnet coils.**

The value of the bias field, which induced SRT, was equal to the value of the effective anisotropy field $H_A = 95\ Oe$, which was defined by vibrating sample magnetometer (VSM) measurements.

The attenuation coefficients of the mechanical vibrations of the sample were also measured. They were obtained by measurement of the relaxation time for the fundamental flexural mode assuming that the vibration amplitude was decaying exponentially. The attenuation coefficient was found equal to $\delta = 0.1\ s^{-1}$ for the resonant mode ($\Omega/2\pi = 843\ Hz$).

The Fig. 12 represents the results of measurements of HF reflection coefficient versus magnetizing field strength H in the frequency range *500- 2000 MHz*. In the inset of Fig. 12A the measured FMR frequencies versus magnetic field are presented by dots. The minima of reflection coefficient correspond to ferromagnetic resonance (FMR) in magnetostrictive nanostructure. The resonant value of the magnetizing field strength is always smaller than anisotropy field of the sample. It means that FMR is observed in angular phase of magnetic system corresponding to spin reorientation from magnetizing field direction. This feature of spin system excitation by HF electromagnetic field is explained below by specificity of relative orientation of micro-stripe line and easy axis of anisotropy in our experimental setup.

The Fig. 13 shows the results of measurement of magnetic field dependence of electric voltage induced in the structure at modulation frequency by HF electromagnetic field. Contribution of FMR to

the nonlinear magnetoelectric conversion (NMEC) is more clearly expressed on Fig. 13B. The peak value of conversion coefficient defined as voltage- to- absorbed energy ratio is found as $K_{NMEC}$= *100 μV/mW*.

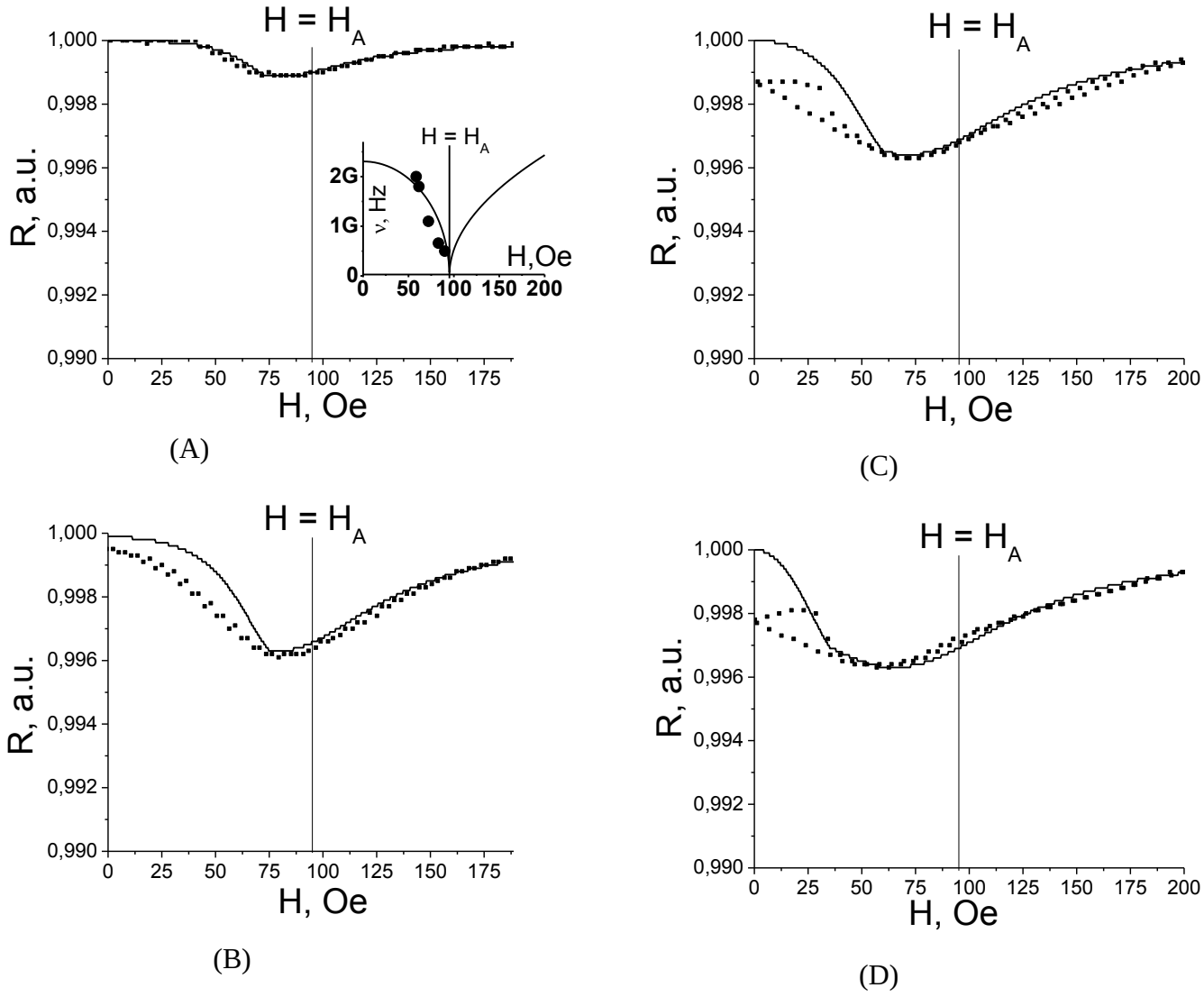


**Fig. 12. Magnetic field dependence of the HF reflection coefficient R expressed in arbitrary units for TbCo/FeCo nanostructure at different FMR frequencies (A – 500 MHz, B – 660 MHz, C – 1100 MHz, D – 1800 MHz). The inset shows the FMR frequency vs magnetizing field. Solid lines –theory, dots – experiment.**

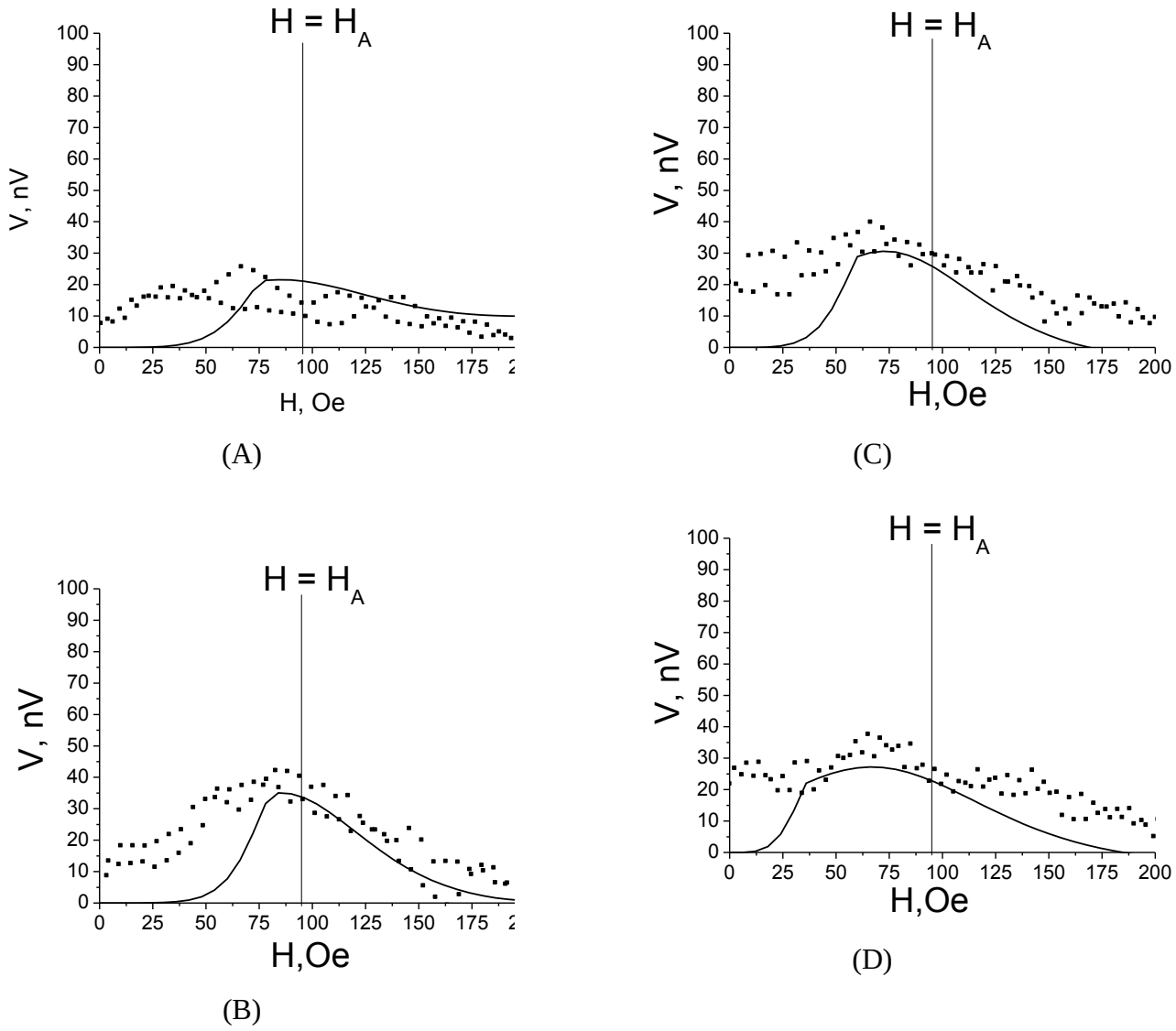


**Fig. 13. Magnetic field dependence of the magnetoelectric voltage for TbCo/FeCo nanostructure at different HF frequencies (A – 500 MHz, B – 660 MHz, C – 1100 MHz, D – 1800 MHz). Solid line –theory, dots – experiment.**

## 3.2. Theory of nonlinear magnetoelectric conversion

The theoretical description of LF elastic vibrations of such structure excited by modulated HF electromagnetic field near SRT was already developed in **[13]**. In the present paper, this approach is extended for piezoelectric layer introduction. As it can be shown the mechanism of the process is described by the joint contributions of two nonlinearities: the nonlinearity of magnetostriction and the nonlinearity of magnetization dependence on the alternating external magnetic field value.

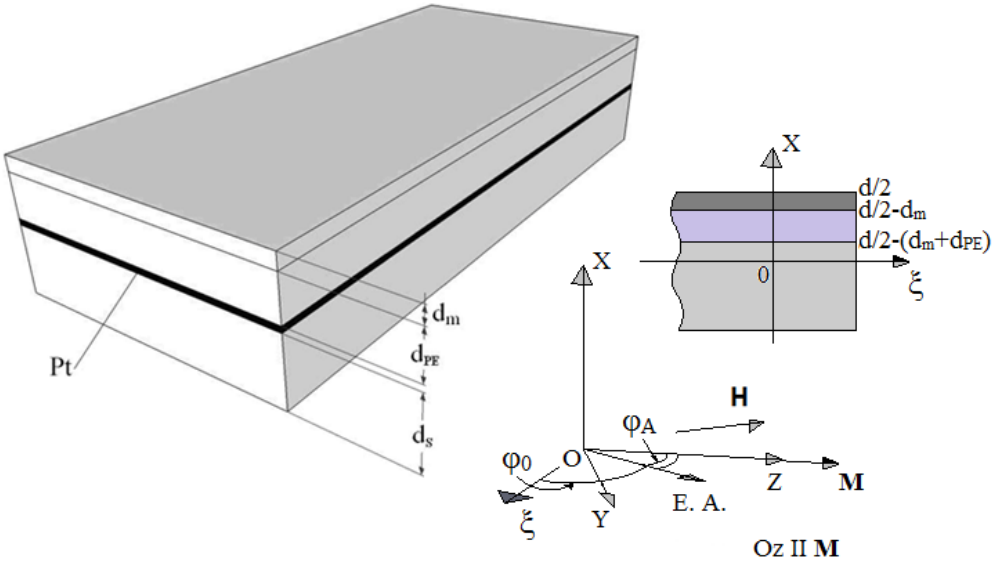


**Fig. 14. The structure ($d_m$ – the thickness of the magnetostrictive film; $d_{PE}$ – the thickness of the piezoelectric film; $d_s$ – the thickness of the substrate; Pt – platinum bottom electrode; d is the sample total thickness).**

According to the experimental conditions we suppose that the thin film with magnetization $M$ and thickness $d_m$ is placed on a thick piezoelectric layer with thickness $d_{PE}$. The Oz axis on Fig. 14 corresponds to the equilibrium magnetization direction and $Ox$ axis labels direction perpendicular to the sample surface. The magnetic film is assumed to be conductive and serves as a top electrode. The piezoelectric layer is deposited on the ultrathin conductive layer that is followed by nonmagnetic substrate with thickness $d_S$ and serves as a low electrode for the piezoelectric system. The magnetization $\boldsymbol{M}$ has the direction defined by the competition between the external magnetic field and the anisotropy. The initial direction of magnetization is along the easy axis. With the biasing field **H** value increase it simultaneously changes the direction clockwise with the angle $\sin\varphi_A = \dfrac{H}{H_A}$ to the $Oz$ up to the moment, when $H \geq H_A$ and it fixes along $Oy$ while the magnetization is directed along the bias field direction **[81]**. Following the classical approach **[41]**, **[42]** one can derive the nonlinear equations of motion for magnetization, voltage and elastic strains by retaining high-order terms in the free energy. Overall free energy of the sample consists of four parts: elastic $F_e$, magnetoelastic $F_{me}$, magnetic $F_m$, and piezoelectric $F_{PE}$ ones:

$$F = F_e + F_m + F_{me} + F_{PE} \tag{55}$$

We assume isotropic model for elastic and magnetoelastic properties of magnetic film thus:

$$F_e^V = \tfrac{1}{2} C_{11}(u_{xx}^2 + u_{yy}^2 + u_{zz}^2) + C_{12}(u_{xx}u_{yy} + u_{xx}u_{zz} + u_{yy}u_{zz}) + (C_{11} - C_{12})(u_{xy}^2 + u_{xz}^2 + u_{yz}^2) \tag{56}$$

$$F_{me}^V = b^{\gamma,2}[((M_x / M_0)^2 - 1/3)u_{xx} + ((M_y / M_0)^2 - 1/3)u_{yy} + ((M_z / M_0)^2 - 1/3)u_{zz} + 2/M_0^2[M_x M_y u_{xy} + M_y M_z u_{yz} + M_x M_z u_{xz}]] \tag{57}$$

Here, $\boldsymbol{M}$ is magnetization of the film, $u_{ij}$ are components of the strain tensor; $C_{11}$ and $C_{12}$ are the elastic stiffness constants, $b^{\gamma,2}$ is the magnetoelastic constant. We neglect by the difference between elastic moduli of the substrate and the films.

The magnetic part of energy volume density consists of the Zeeman energy, the anisotropy energy and the energy of demagnetization field.

$$F_m^V = -(\vec{M}\vec{H}) + \frac{H_{A0}}{2M_0}\left\|\left[\vec{M} \times \vec{n}\right]\right\|^2 + \frac{1}{2}\vec{M}\hat{N}\vec{M} \tag{58}$$

where $\boldsymbol{n}$ is the unit vector collinear to the easy axis of the film; $H_{A0}$ is the value of anisotropy field, $\hat{N}$ is the demagnetizing tensor, which is assumed to be the same as for an infinite plate: $N_{ij}=0$ excepting $N_{zz}=4\pi$.

In piezoelectric energy density we will take into account only one component of deformation $u_{\xi\xi}$ along $\xi$ direction related to the flexural deformation of the structure:

$$F_{PE}^V = \lambda E_x u_{\xi\xi}(t) \tag{59}$$

where: $\lambda = -(e_{31} - \frac{C_{12}}{C_{11}} e_{33})$ and $e_{ij}$ are piezoelectric constants.

The LF piezoelectric polarization is defined by deformation:

$$P_x = -\frac{\partial F_{PE}^V}{\partial E_x} = -\lambda \cdot u_{\xi\xi}(t) \tag{60}$$

The deformation $u_{\xi\xi}$ is expressed via flexural displacement $U(\xi)$ by the equation:

$$u_{\xi\xi} = -(x - x_0)\frac{\partial^2 U}{\partial \xi^2} \tag{61}$$

where $x_0$ is the position of the neutral section of the structure. For dynamic resonant deformations the neutral section is defined in the middle of the sample section $x_0=0$.

The equations (60) and (61) reduce the problem of magnetoelectric polarization to the problem of electromagnetic excitation of LF flexural elastic vibrations.

Taking into account the relationship (60) one can derive the Lagrangian functional of the system related to the elastic displacement *U(ξ,t)* **[40]**:

$$L = \iiint_V \{1/2\rho(x,\dot{U}(\xi,t))^2 - F_e^V(x,U(\xi,t)) - F_{me}^V(\vec{M},x,U(\xi,t)) - F_{PE}^V(\vec{E},x,U(\xi,t))\}dV \quad (62)$$

Where $\rho$ is the mass density assumed equal for substrate and piezo- and magnetic components, $V$ is the total volume of the structure.

The elastic displacement can be represented as a superposition of the normal vibration modes:

$$U(\xi,t) = \sum_n U_n(\xi)\cdot A_n(t) \quad (63)$$

Expansion (63) allows presentation of the equation (62) in the form of Lagrangian of the assembly of oscillators driven by effective magnetostrictive $f_{me}$ and piezoelectric $f_{PE}$ forces:

$$L = \sum_n L_n = \sum_n \left[\frac{1}{2}M_n(\dot{A}_n^2 - \Omega_n^2\cdot A_n^2) - (f_{me}^{(n)} + f_{PE}^{(n)})\cdot A_n\right] \quad (64)$$

where $M_n = \iiint_V \rho(U_n)^2 dV$ and $\Omega_n$ are the effective mass and the eigen frequency of the mode,

$$f_{me}^{(n)} = -b^{\gamma,2}\iiint_{V_m}\frac{1}{M_0^2}\left[x\cdot(M_\xi^2 - \frac{C_{12}}{C_{11}}M_x^2)\cdot\frac{\partial^2 U_n}{\partial\xi^2}\right]dV \quad (65)$$

$$f_{PE}^{(n)} = -\lambda\iiint_{V_p}\left[x\cdot E_x\cdot\frac{\partial^2 U_n}{\partial\xi^2}\right]dV \quad (66)$$

here $V_m$ and $V_p$ are the volumes of magnetic and piezoelectric films respectively.

The vibration amplitude for given resonant mode one can calculate using the Lagrangian equation of motion:

$$\frac{\partial}{\partial t}\frac{\partial L_n}{\partial\dot{A}_n} - \frac{\partial L_n}{\partial A_n} + \frac{\partial D}{\partial\dot{A}_n} = 0 \quad (67)$$

Here we introduced Rayleigh dissipation function in the form **[43]**: $D = \delta_n M_n \dot{A}_n^2$, where $\delta_n$ is the attenuation coefficient of the mode. Piezoelectric force linearly dependent on electric field strength

does not contribute to the demodulation effect. Thus the problem of vibrations generated by magnetostrictive force is reduced to the simple oscillator problem:

$$\ddot{A}_n + 2\delta_n \dot{A}_n + \Omega_n^2 A_n = \frac{1}{M_n} \overline{f_{me}^{(n)}}$$

(68)

where line means averaging by the period of HF oscillations.

In order to describe demodulation effect the magnetisation in equation (65) has to be defined up to the second order approximation relatively to HF magnetic field:

$$\vec{M}(t) = \vec{M}_0 + \vec{m}(t) + \vec{\mu}(t).$$

(69)

where the first, second and third components are static, HF and LF components respectively. The last one appears under HF electromagnetic excitation due to proper nonlinearity of magnetic subsystem. We assume internal HF magnetic field modulated harmonically with modulation frequency Ω and modulation depth η: $h_i(t) = h_i \cos(\omega t) \cdot \left[1 + \eta \cdot \cos(\Omega t)\right]$. Correspondingly the dynamic components of magnetisation can be expressed via linear $\chi_{ij}$ and nonlinear $\chi_{ijk}$ magnetic susceptibilities calculated using equation (4) in the Appendix A and the Appendix D:

$$m_i = \frac{1}{2}\chi_{ij}(\omega) h_j e^{i\omega t} + \frac{\eta}{4}\chi_{ij}(\omega+\Omega) \cdot h_j e^{i(\omega+\Omega)t} + \frac{\eta}{4}\chi_{ij}(\omega-\Omega) h_j e^{i(\omega-\Omega)t} + c.c.$$

(70)

$$\mu_i = \frac{\eta}{2}\chi_{ijk}(\Omega) \cdot h_j h_k e^{i\Omega t} + c.c.$$

(71)

Taking into account conductivity of the magnetic film the internal HF magnetic field is proportional to the external field $\boldsymbol{h_0}$ with an inhomogeneous factor $\beta_{ij}(x)$ calculated in the Appendix B: $h_i = \beta_{ij}(x) h_{0j}$.

Using equations (65), (70), (71) one can find the magnetostrictive force:

$$\overline{f_{me}^{(n)}} = \frac{-b^{\gamma,2}\eta}{8M_0^2}\left[\nu_{\xi,jk}(\omega,\Omega) - \frac{C_{12}}{C_{11}}\nu_{x,jk}(\omega,\Omega)\right] \iiint_V x \frac{\partial^2 U_n}{\partial \xi^2} \beta_{jl}(x)\beta_{kq}^*(x) dV \cdot h_{0l} h_{0q} e^{i\Omega t} + c.c.$$

(72)

where

$$\nu_{i,jk}(\omega,\Omega) = \chi_{ij}(\omega)\chi_{ik}^*(\omega-\Omega) + \chi_{ij}(\omega+\Omega)\chi_{ik}^*(\omega) + 8 \cdot M_{0i}\chi_{ijk}(\Omega)$$

(73)

Using the equations (68) and (72) one can find the amplitude of elastic vibrations:

$$A_n = \frac{-b^{\gamma,2}\eta \cdot h_{0l} h_{0q}}{8M_0^2 M_n(\Omega^2 - \Omega_n^2 + i\delta_n\Omega)} \cdot \left[ \nu_{\xi,jk}(\omega,\Omega) - \frac{C_{12}}{C_{11}} \nu_{x,jk}(\omega,\Omega) \right] \iiint_V x \frac{\partial^2 U_n}{\partial \xi^2} \beta_{jl}(x) \beta_{kq}^*(x) dV \tag{74}$$

According to the equations (60) and (61), contribution of LF piezoelectric polarization to the normal component of electrical displacement is equal to:

$$D_x = \varepsilon E_x + 4\pi \cdot \lambda \cdot x \frac{\partial^2 U_n}{\partial \xi^2} A_n \tag{75}$$

The open electrical circuit condition requires the LF alternating charge $q = \int_S D_x dS$ equal to zero, it means:

$$\int_{S_x} E_x dS = -\frac{4\pi\lambda}{\varepsilon} A_n \int_{S_x} x \cdot \frac{\partial^2 U_n}{\partial \xi^2} dS \tag{76}$$

where $S_x$ is the inside piezoelectric surface parallel to the electrodes. The amplitude of magnetoelectric voltage induced by HF electromagnetic field at resonance frequency $\Omega=\Omega_n$ is equal to:

$$\begin{aligned} V_{me} &= \frac{1}{S} \int_S dS \int_{d/2-d_m-d_p}^{d/2-d_m} E_x dx = \\ &= \frac{-i \cdot \pi\lambda \cdot b^{\gamma,2}\eta \cdot h_{0l} h_{0q}}{\varepsilon \cdot S \cdot M_0^2 M_n \Omega_n^2} Q_n \cdot \left[ \nu_{\xi,jk}(\omega,\Omega) - \frac{C_{12}}{C_{11}} \nu_{x,jk}(\omega,\Omega) \right] \cdot \\ &\iiint_{V_M} x \frac{\partial^2 U_n}{\partial \xi^2} \beta_{jl}(x) \beta_{kq}^*(x) dV \iiint_{V_P} x \cdot \frac{\partial^2 U_n}{\partial \xi^2} dV \end{aligned} \tag{77}$$

where $Q_n=\Omega_n/2\delta_n$ is the quality factor of the elastic mode, $S$ is the surface of electrodes. Calculation of integrals in equation (77) is given in the Appendix C.

## 3.3. Discussion

The results of calculation of magnetoelectric voltage as function of magnetizing field using equation (77) are presented in Fig. 13 in comparison with the experimental data. The HF parameters of magnetic film involved in susceptibility matrixes (73) were determined by fitting the theoretical field

dependence of HF absorption with the results of measurements presented in Fig. 12. Calculations of HF absorption taking into account conductivity of the film and intrinsic attenuation in magnetic subsystem are given in Apendix C. Gilbert attenuation coefficient and saturation magnetisation were found as $\alpha = 0.2$, $4\pi M_0 = 14.5$ *kGs*. The conductivity value was assumed to be close to the one for Fe films $\sigma = 2*10^7$ *Mho* **[57**]. Calculations show that conductivity contribution to the HF absorption does not exceed *10%* of the total loss.

We considered AlN as a piezoelectric material. One can show that with the symmetry of this material piezoelectric coefficient λ may be derived through the piezoelectric modulus $d_{33}$ as $\lambda = 3C_{12}d_{33}$ **[40**], **[58**]. According to the common data **[59**], we used the following piezoelectric coefficient and dielectric permeability for AlN: $d_{33} = 5*10^{-12}$ *C/N*, $\varepsilon = 8.42$.

The data presented in Fig. 12 and Fig. 13 demonstrates good agreement between theoretical and experimental results. The relative orientation of HF magnetic field and anisotropy axis defined by the angle $\varphi_0 = 70°$ allows observation of only one brunch of FMR (see inset of Fig. 12A) corresponding to declination of magnetic moment from magnetizing field in the SRT process. The nonlinear magnetoelectric convertion coefficient $K_{NMEC}$ increases in FMR conditions (see Fig. 13B). Decrease of FMR frequency corresponding to approach the SRT point leads to increase of $K_{NMEC}$ (compare Fig. 13B and Fig. 13D). However in the close vicinity of the SRT point the conversion efficiency decreases because of widening of FMR line width twice.

## 3.4. Conclusion

Nonlinear resonance magnetoelectric effect induced by HF electromagnetic field in thin film composite multiferroic structure TbCo/FeCo-AlN is observed experimentally and described theoretically. The effect is studied in conditions of spin reorientation transition in magnetostrictive nanostructure. The results of calculations are in good agreement with the experimental data on magnetic field dependence of LF magnetoelectric voltage and on HF power absorption. It is shown that conductivity contribution to FMR line width is relatively weak in magnetostrictive nanostructure. The unusual disappearing of the FMR line in the saturation phase, where magnetisation is collinear to magnetizing field, is explained by specific geometry of the experiment and strong HF absorption. Obtained value of nonlinear magnetoelectric conversion coefficient amounts to $100\ \mu V/mW$. Calculations show for optimal orientation of anisotropy axis $\varphi_0 = 0$ increase the conversion coefficient one order of value.

# 4. Propagation of surface magnetostatic waves in an one dimensional magnon crystal of variable thickness

Here a theoretical model of propagating surface magnetostatic wave in a ferromagnetic film with a variable thickness and a planar periodic structure in the form of etched parallel strips (one-dimensional magnon crystal) is developed. The results are analyzed for their possible practical applications.

The work consists of three parts. In the first part, the features of propagating surface magnetostatic waves in a variable-thickness film are considered in a dipole—dipole approximation. Based on the solution of the equation of propagating surface magnetostatic waves in a medium with geometric inhomogeneity in the Wentzel—Kramers—Brillouin approximation, we derived a dispersion relationship. In the second part, the effect of the coordinate dependence of the film thickness on the dispersion of surface magnetostatic waves propagating in a planar periodic structure in the form of etched parallel strips is considered. In the third part, we discuss possible applications of investigated phenomena in the designing of microwave devices.

## 4.1. Propagation of surface magnetostatic waves in a ferromagnetic film with variable thickness

Consider the propagation of surface magnetostatic waves in a film the thickness of which is linearly dependent on the coordinate.

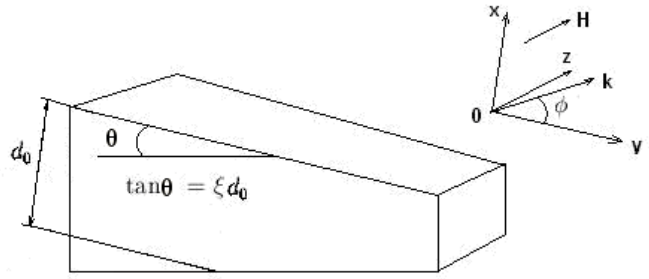


**Fig. 15. Film with a linearly varying thickness.**

Fig. 15 depicts a ferromagnetic film with a variable thickness, which is linearly dependent on the coordinate x and the related rectangular coordinate system. The coordinate plane *yz* is parallel to the upper surface of the film, and axis *x* is perpendicular to it. The origin of coordinates is in the point where the segment connecting the upper surface of the film with the bottom surface at a right angle is $d_0$. In what follows, such a segment length is called the film thickness. The magnetic field is directed

along the tangent to the film along the *z* axis. A wave propagates along the upper film surface at an angle φ to axis y. The film is not limited in the *yz* plane and is magnetized to saturation.

In the geometry of the problem set, the film thickness is varied by the law

$$d(y) = d_0(1 - \xi y). \tag{78}$$

where $d_0$ is the film thickness at the origin of coordinates and ξ is an angular coefficient characterizing the value of varying the film thickness.

The dispersion relationship was derived for the propagation of surface magnetostatic waves in a plane-parallel film with allowance for the dipole- dipole interaction (29):

$$k_0 = \frac{1}{2d_0\alpha}\ln\frac{\beta - 1 + 2\mu\alpha}{\beta - 1 - 2\mu\alpha}.$$

Where:

$$\begin{gathered}\beta = (\nu^2 - \mu^2 + \mu)\cos^2\phi - \mu, \\ \alpha = \sqrt{\cos^2\phi + \frac{\sin^2\phi}{\mu}}, \\ \mu = 1 + \frac{\omega_H\omega_M}{\omega_H^2 - \omega^2}, \\ \nu = \frac{\omega\omega_M}{\omega_H^2 - \omega^2}, \\ \omega_H = \gamma H, \omega_M = 4\pi\gamma M.\end{gathered} \tag{79}$$

Here, *H* is the external magnetic field strength, *M* is the static magnetization of the film, γ is the magneto- mechanical ratio, and ω is the frequency of the surface magnetostatic wave.

In a zero approximation, the dispersion relation of surface magnetostatic waves in a film whose thickness varies linearly (78) can be written in the form similar to relationship (29)

$$k(y) = \frac{1}{2d(y)\alpha}\ln\frac{\beta - 1 + 2\mu\alpha}{\beta - 1 - 2\mu\alpha}. \tag{80}$$

With allowance for the coordinate dependence of the wave number, the equation for the *y* component of the vector-potential of surface magnetostatic waves [77] is transformed to the differential equation with a variable coefficient

$$Y'' + k^2(y)\sin^2\varphi Y = 0.$$

(81)

The Wentzel—Kramers—Brillouin method [79], [80] allows, to some accuracy (the limiting condition is $||k'(y)\sin\varphi| << k^2(y)\sin^2\varphi$), the solution of the equation. In this case, an approximate solution of the Eq. (81) is

$$Y(y) = \exp(iu(y)).$$

(82)

After substituting Eq. (82) into Eq. (81) and rearranging, Eq. (81) takes the form

$$-(u'(y))^2 + iu''(y) + k^2(y)\sin^2\varphi = 0.$$

(83)

Putting |u"(y)| small, we obtain

$$u'(y) = \pm k(y)\sin\varphi.$$

(84)

Hence,

$$u(y) = \pm\int k(y)\sin\varphi dy.$$

(85)

The condition of validity (smallness of |u"(y)| in relationship (83)) takes the form

$$|u''(y)| \approx |k'(y)\sin\varphi| << k^2(y)\sin^2\varphi.$$

(86)

Substituting relationship (85) into relationship (82) gives

$$Y(y) = Y_1\exp(i\int k(y)\sin\varphi dy) + Y_2\exp(-i\int k(y)\sin\varphi dy).$$

(87)

where *k(y)* is determined using relationship (80).

In the case of the linear coordinate dependence (78), the solution of Eq. (81) is

$$Y(y) = Y_1(1-\xi y)^{\frac{1}{2\alpha d_0\xi}\sin\phi\ln\frac{\beta-1+2\mu\alpha}{\beta-1-2\mu\alpha}} + Y_2(1-\xi y)^{-\frac{1}{2\alpha d_0\xi}\sin\phi\ln\frac{\beta-1+2\mu\alpha}{\beta-1-2\mu\alpha}} =$$
$$= Y_1(1-\xi y)^{\frac{1}{\xi}k_0\sin\phi} + Y_2(1-\xi y)^{-\frac{1}{\xi}k_0\sin\phi}$$

(88)

Repeating the line of arguments proposed in [77], we write the general solution of the problem of propagation of surface magnetostatic waves in a ferromagnetic film for the ψ potential

$$\Psi(x,y,z) = X(x)Y(y)Z(z).$$

(89)

The functions $X(x)$ and $Z(z)$ are the solutions of the wave equation with the parameters that are constant in x and $z$ and are determined by the medium parameters, the wave frequency, and the coordinate $y$,

$$\begin{cases} X(x) = X_1 \exp(i\alpha k(y)\, x) + X_2 \exp(-i\alpha k(y)\, x); \\ Z(z) = Z_1 \exp(ik(y)\cos\varphi\, z) + Z_2 \exp(-ik(y)\cos\varphi\, z). \end{cases}$$

(90)

Beyond the ferromagnetic film, $\alpha = 1$.

Substituting the obtained values of the $\psi$ potential into the boundary continuity conditions of the normal induction component and the tangent components of the magnetic field strength gives

$$\begin{cases} \mu \dfrac{\partial \psi_2}{\partial x} + i\nu \dfrac{\partial \psi_2}{\partial y}\Big|_{x=-d(y)} = \dfrac{\partial \psi_1}{\partial x}\Big|_{x=-d(y)}; \\ \mu \dfrac{\partial \psi_2}{\partial x} + i\nu \dfrac{\partial \psi_2}{\partial y}\Big|_{x=0} = \dfrac{\partial \psi_3}{\partial x}\Big|_{x=0}; \\ \psi_2\big|_{x=-d(y)} = \psi_1\big|_{x=-d(y)}; \\ \psi_2\big|_{x=0} = \psi_3\big|_{x=0}. \end{cases}$$

(91)

In relationships (91) the notations are introduced as follows: $\psi_2$ is the value of the magnetostatic potential inside the ferromagnetic film; $\psi_\chi$ and $\psi_3$ are the magnetostatic potentials in the space above and under the film, respectively.

From the compatibility condition of relationships (91) with allowance for relationships (80) and (88)— (90), we obtain the dispersion relationship for the first Wentzel—Kramers—Brillouin approximation

$$k(\xi, y, z) = \frac{1}{2d(y)\alpha} \ln \frac{\beta - 1 + 2\mu\alpha + (\phi(\xi, y) - \psi(\xi, y, z))}{\beta - 1 - 2\mu\alpha - (\phi(\xi, y) + \psi(\xi, y, z))}.$$

(92)

The distinction of relationship (92) from the initial form of the dispersion relation for surface magneto - static waves in a film with a constant thickness is determined by the correction functions under logarithm

$$\psi(\xi, y, z) = \left(U^2(\xi, y, z) - k_0^2 - V_1^2 - V_2^2(\xi, y) + 2V_2(\xi, y)k_0\right) \cdot k_0^{-2} - \beta + 1,$$

$$\phi(\xi, y) = (2V_1 k_0 - 2V_1 V_2(\xi, y)) \cdot k_0^{-2} - 2\mu\alpha \,, \tag{93}$$

where

$$k_0 = \frac{1}{2d_0\alpha} \ln \frac{\beta - 1 + 2\mu\alpha}{\beta - 1 - 2\mu\alpha} \,,$$

$$V_1 = \mu\alpha k_0 \,,$$

$$V_2(\xi, y) = i\nu\alpha k_0 \left[ \frac{\xi}{1 - \xi y} \right] \cdot \frac{d(y)}{2} \,, \tag{94}$$

$$U(\xi, y, z) = \nu \left[ k_0 \cos\varphi + z \sin\varphi \frac{\xi}{1 - \xi y} k_0 - i \frac{\xi}{1 - \xi y} \frac{1}{2} \frac{\xi}{1 - \xi y} \right].$$

Other notations are given in relationship (79). It is easily seen that, at $\xi = 0$, $\varphi(\xi, y) = 0$, $\psi(\xi, y) = 0$, $k(y) = k_0$.

Estimate the correction of the first Wentzel— Kramers—Brillouin approximation for the parameters characteristic of ferrite-garnets [81]. Assume that $\xi = 0.1$, $H = 550$ Oe, $M = 139$ G, and $d_0 = 10$ μm. At these conditions, the first approximation correction gives very small relative contribution to the real value of the wave number $\sim 10^{-11}$. Additional calculation shows that the corrections of successive approximations are negligible as compared to the first correction. In this case, the wave number becomes complex. The imaginary part magnitude is $\sim 10^{-4}$—$10^{-3}$ of the real part value.

The solution taking into account the first approximation corrections contains the dependence on *z* (relationship (92)). Thus, the dispersion relation obtained is an equation of the four-dimensional surface in the (ω, k, *y, z)* space. In the case when a wave propagates perpendicularly to the direction of an external magnetic field ($\sin\varphi = 0$), the four-dimensional surface degenerates into a three-dimensional surface that can be constructed using only three coordinates (ω, k, *y).* The cross sections of this surface by planes $y = 0$, 3, 6, and 9 for the system parameters $\xi = 0.1$, $H = 550$Oe, $M = 139$G, and $d_0 = 10$μm are shown in Fig. 16.

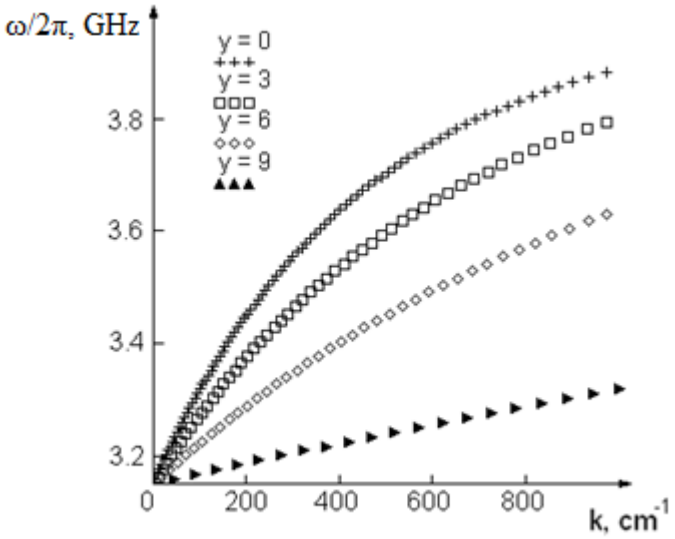


**Fig. 16. Cross sections of the dispersion surface (16) by planes perpendicular to the y axis.**

As the wave propagates along the positive direction of axis y, the ω(k) curve becomes smoother as the coordinate increases, and *k* increases.

In the region where the film thickness approaches zero, the solutions of the zero and first approximations tend to infinity. Following **[79]**, let us estimate the method error which determines how much the system parameters satisfy the condition (86). The error magnitude is

$$\varepsilon(y) = \exp(i\delta)(-\xi)\ln(1-\xi y)\frac{1}{2k_0}\left(\frac{1}{\cos^2\phi} - \frac{5}{8\cos\phi}\right) + \exp(-i\delta)\frac{1}{2}\frac{\xi^2\left(\frac{1}{\cos\phi} - \frac{5}{8}\right)}{k_0\cos\phi}\left(2i\frac{k_0\cos\phi}{\xi}\right)\times$$

$$\times\left[(1-\xi y)^{2i\frac{k_0\cos\phi}{\xi}-1}\frac{-\xi}{1-\xi y} + 1^{2i\frac{k_0\cos\phi}{\xi}}\xi\right]. \qquad (95)$$

where δ is the component of the phase factor that does not influence the absolute error value.

It is seen from relationship (95) that, as ξ = 0 (plane-parallel film), the error becomes zero. As $y \to \frac{1}{\xi}$ the error tends to infinity. The error diverges as the film thickness decreases ($y \to 10$ relative units of length). The value $y \sim 7$—8 corresponds to the error of 10%.

Note that the solution of Eq. (81) by the Wentzel— Kramers—Brillouin method leads to the appearance of the imaginary component of the wave number

$$k = k' + ik''.$$

(96)

Upon propagation of the surface magnetostatic wave along axis *y (φ = 0)*, as the angular parameter ξ is changed, only the imaginary part of the wave number is changed. The real part changes as well at an arbitrary angle φ.

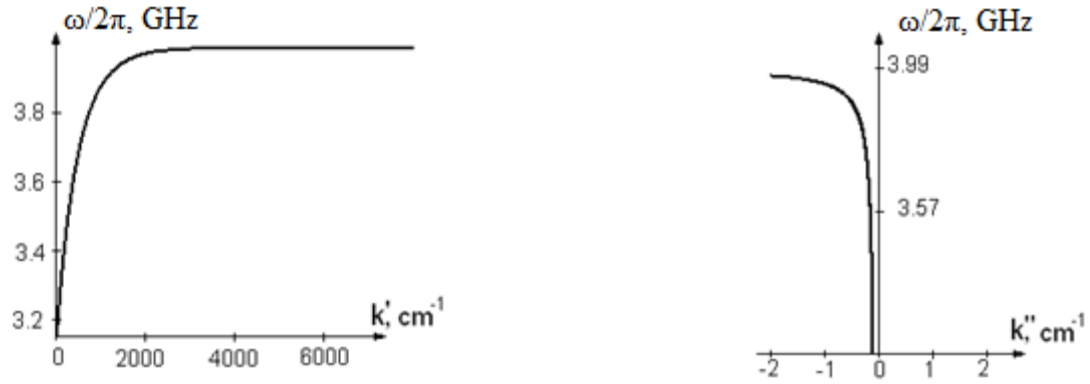


A. B.

**Fig. 17. Dispersion curves for the (A) real and (B) imaginary components of the wave number k || *y*.**

Fig. 17 depicts the plots of the dispersion curves of the real and imaginary components of the wave number for the film thickness $d_0 = 10\ \mu m$ and the angular coefficient $\xi = 0.1$. The curve of the imaginary component of the wave number on the angular coefficient is symmetric with respect to the origin of the coordinates.

According to **[77]**, the solution for the wave propagating along the film surface along axis *y* is

$$\psi = \left(A_1 \exp(kx) + B_1 \exp(kx)\right)\left(A_2 \exp(iky) + B_2 \exp(-iky)\right) \tag{97}$$

In this case, $A_1 << B_1$ for the wave propagating along the upper film boundary and - $A_1 >> B_1$ for the wave propagating along the lower boundary. This fact brings about a number of results.

Because of asymmetry of the geometric parameters of the film, the wave amplitude propagating in the negative direction along axis *y* decreases, and the wave amplitude propagating in the positive direction increases.

As a complex component of the wave number appears, the wave ceases to be surface wave, it takes a volume component, i.e., the traveling wave along axis x.

The nonreciprocity of the Damon—Eshbach solution **[77]** leads to the fact that the wave volume component is mainly radiated deep to a ferromagnet. The wave propagating in positive direction (clockwise when looking in the direction of the external magnetic field) has significantly larger

amplitude than the wave propagating in the negative direction, and the wave traveling along axis x radiated deep to the ferromagnetic film corresponds to the latter wave.

Now, we consider the case of an arbitrary coordinate dependence of the film thickness. The solution of the problem when *d(y)* is given by an arbitrary functional dependence has the form identical to relationship (92); however, the correction functions appear differently.

We introduce the denotation

$$d(y) = d_0 \xi(y) \,. \tag{98}$$

Then,

$$\psi(\xi, y) = \left(U^2(\xi, y) - k_0^2 - V_1^2 - V_2^2(\xi, y) + 2V_2(\xi, y)k_0\right) \cdot k_0^{-2} - \beta + 1,$$
$$\phi(\xi, y) = (2V_1 k_0 - 2V_1 V_2(\xi, y)) \cdot k_0^{-2} - 2\mu\alpha \,, \tag{99}$$

where

$$k_0 = \frac{1}{2d_0\alpha} \ln \frac{\beta - 1 + 2\mu\alpha}{\beta - 1 - 2\mu\alpha},$$
$$V_1 = \mu\alpha k_0,$$
$$V_2(\xi, y) = -i\nu\alpha k_0 \left[ \frac{d\xi / dy}{\xi(y)} \right] \cdot \frac{d(y)}{2}, \tag{100}$$
$$U(\xi, y) = \nu \left[ k_0 \cos\varphi - z \sin\varphi \frac{d\xi / dy}{\xi(y)} k_0 + i \frac{1}{2} \frac{d\xi / dy}{\xi(y)} \right].$$

With $\xi(y) = 1 - \xi y$, the solution (99) is changed to relationship (92).

Fig. 18 shows the dispersion surface for the film thickness that varies by the law $d(y) = d_0(1 - y^2 + y^4)$. The dispersion surface for such a functional dependence is strongly different from the linear case.

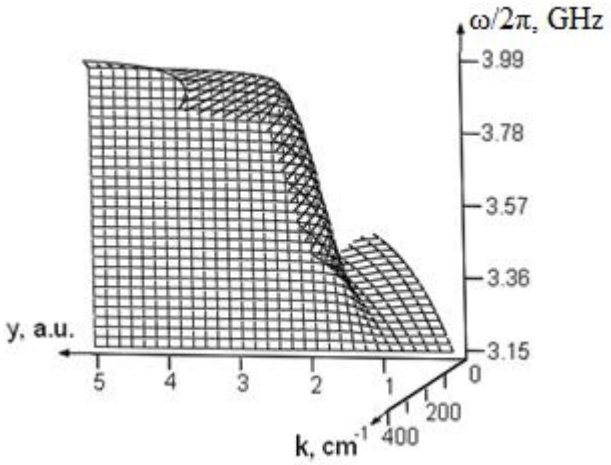


**Fig. 18. Dispersion surface. The first Wentzel–Kramers–Brillouin approximation.**

$$d(y) = d_0(1 - y^2 + y^4).$$

As noted in **[70]**, the dipole—dipole approximation using here agrees well with the experiment at large wavelengths (small values of k). In the case when *k* exceeds a threshold value, it is necessary to take into account the exchange interaction.

## 4.2. Propagation of the surface magnetostatic wave in a ferromagnetic film with variable thickness and periodic magnetic inhomogeneity

In **[65]**, **[68]**, the method of calculating the characteristics of propagation of a surface magnetostatic wave in a magnetically ordered periodic structure based on the Kronig—Penney model **[82]** was described.

We calculate the manner in which a surface magnetostatic wave propagates along the surface of a film whose thickness varies linearly and in which a periodic plane-parallel strip structure is etched.

We use the model of scanted film and the denotation taken in the preceding Section. We introduce a periodic structure of a magnetic inhomogeneity consisting of ferromagnetic material strips alternating with unfilled strips: *a* is the structure period; *b* is the unfilled area width (Fig. 19).

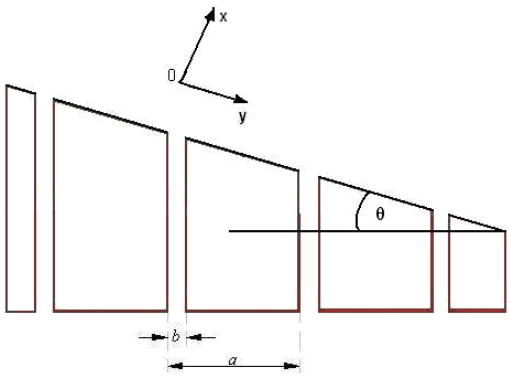


**Fig. 19. Film with a linearly varying thickness and an etched periodic structure.**

Consider a wave propagating along axis *y* perpendicularly to the external magnetic field. The origin of coordinates is at the boundary of an etched cavity where the film thickness is equal to $d_0$.

For the sake of convenience of further consideration, we denote the wave number of the surface magnetostatic wave in the ferroelectric film by $\alpha_1$. According to relationship (92),

$$\alpha_1 = \frac{1}{2d(y)\alpha} \ln \frac{\beta - 1 + 2\mu\alpha + (\phi(\xi, y) - \psi(\xi, y))}{\beta - 1 - 2\mu\alpha - (\phi(\xi, y) + \psi(\xi, y))}$$

(101)

The potential of the surface magnetostatic wave takes the form

$$\psi = A\exp(i\alpha_1 y) + A'\exp(-i\alpha_1 y)$$

(102)

In the free space of the etched cavities, the dispersion relation has the form

$$\alpha_2 = \frac{\omega}{c},$$

(103)

where *c* is the velocity of light in free space.

The potential is

$$\psi = B\exp(i\alpha_2 y) + B'\exp(-i\alpha_2 y)$$

(104)

The Kronig—Penney method gives the general solution as a function which is continuous and differentiable in given range of values of y. In this case, the conditions of continuity and differentiability of the potential are fulfilled at the ferromagnet—air boundary near the etched cell edge

$$\begin{cases} \psi(0^-) = \psi(0^+), \\ \psi'(0^-) = \psi'(0^+). \end{cases}$$

(105)

From the solvability condition of this system and also using the Bloch condition of the potential periodicity, we can obtain the dispersion relation

$$\cos ka = \cos[\frac{\alpha_2 b}{\cos\theta}]\cos[\frac{\alpha_1(a-b)}{\cos\theta}] + [\frac{\alpha_1}{2\alpha_2} + \frac{\alpha_2}{2\alpha_1}]\sin[\frac{\alpha_2 b}{\cos\theta}]\sin[\frac{\alpha_1(a-b)}{\cos\theta}]$$

(106)

The appearance of the periodic structure brings about the formation of band gaps in the surface magnetostatic wave spectrum. The appearance of writing of expression (106) is similar to the dispersion relation of electromagnetic waves in layer optical structures **[67]**. However, the initial surface magnetostatic wave spectrum (101) is more complex. Fig. 20 shows, in particular, the surface magnetostatic wave spectra in the structure with the parameters as follows: $H$ = 550 Oe, $M$ = 139 G (it corresponds to iron-yttrium garnet at room temperature), $a$ = 1 mm, $b$ = 10 μm, the film thickness $d$ = 6 μm.

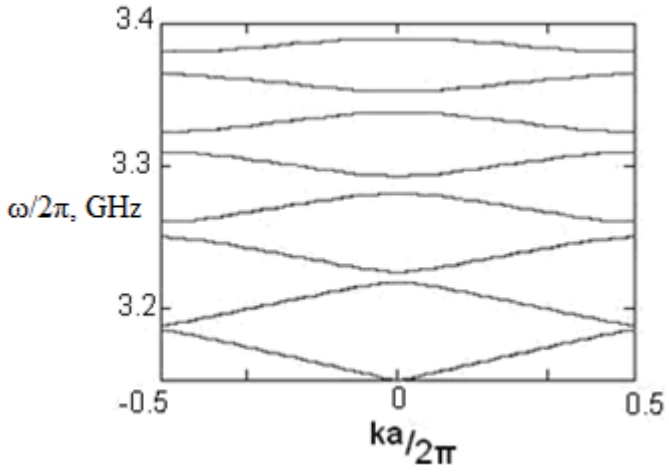


**Fig. 20. Surface magnetostatic wave spectra at the film thickness $d$ = 6 μm.**

The dependence of the dispersion characteristics of the film with a periodic magnetic inhomogeneity on the parameters of the periodic structure was discussed earlier in **[70]**. Of our interest is the effect of a variable thickness on the structure spectrum. It turns out that, as the film thickness increases, the energy gap width increases and the density of energy levels decreases.

Thus, it is believed that, for a variable-thickness film, the three-dimensional plot of the (ω, k, y) dispersion surface of a surface magnetostatic wave is a periodic sequence of surfaces which converges as the film thickness decreases.

Because of variation of the thickness, the energy band pattern is different in different portions of the film, which lead to their partial mutual overlapping; i.e., the summary pattern of the energy bands is very complex. Some features of this phenomenon are demonstrated in Fig. 21.

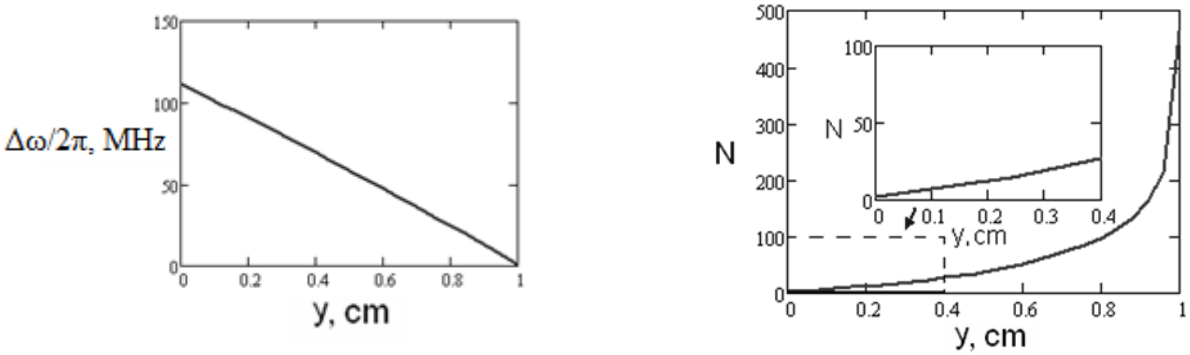


A. B.

**Fig. 21. Dependences of the changes in (a) the first band gap and (b) the density of energy states on the coordinate. ξ = 0.99 cm$^{-1}$.**

Fig. 21a depicts the dependence of the first energy gap width on the coordinate along the surface of a film whose thickness varies linearly. It is seen that the dependence is easily approximated by a linear dependence with a negative angular coefficient.

Fig. 21b shows similar dependence for the number of the energy levels lying in the frequency range under consideration. At the initial segment, the dependence is practically linear; its slope increases sharply at small film thicknesses.

Falling into the frequency range of the energy gap, the wave is weakened. The dispersion relation (106) is solved in complex numbers. Thus, in this case, the wave vector is the sum $k = k + ik''$, where the k" component determines the amplitude of the surface magnetostatic wave. The value of the imaginary component of the wave number can be obtained from the dispersion relation

$$k'' = \frac{1}{a}\mathrm{Im}[\arccos(\cos[\frac{\alpha_2 b}{\cos\theta}]\cos[\frac{\alpha_1(a-b)}{\cos\theta}]+[\frac{\alpha_1}{2\alpha_2}+\frac{\alpha_2}{2\alpha_1}]\times\sin[\frac{\alpha_2 b}{\cos\theta}]\sin[\frac{\alpha_1(a-b)}{\cos\theta}])] \quad (107)$$

Mathematically, the case when the right part of relationship (106) exceeds unity corresponds to the condition of appearance of the imaginary component of the wave number and damping of the Bloch wave.

Our theoretical conclusions on the existence of a new type of dispersion of a surface magnetostatic wave in a medium with a periodic magnetic inhomogeneity are valid at the condition that the mean free path of magnon excitations significantly exceeds the structure period.

## 4.3. Coarse WDM filters based on the phenomenon of MSW propagation in an one dimensional magnon crystal of variable thickness

Consider possible practical applications of the obtained results of investigation of the properties of surface magnetostatic waves in ferromagnetic variable-thickness films with periodic structures for processing of microwave signals. The idea of applying photonic crystals as filters of electromagnetic signals has just been considered in a number of reports **[62**], **[83**]. A variable-thickness film with periodic magnetic inhomogeneity manifests a number of peculiarities.

As indicated above, as the film thickness decreases, the energy gaps in the surface magnetostatic wave spectrum can overlap allowed bands, thus decreasing the frequency range of the waves which can propagate in the film without losses. Thus, choosing a corresponding thickness and the angular coefficient of a film, we can select a narrow band of allowed frequencies, which is of interest for the frequency filtration of the signals. Estimate the spectral characteristic of similar filter.

Assume that a wave number has an imaginary component $k''(\omega, y)$. We follow the reasonings identical to those used upon the deduction of the Bouguer-Lambert-Beer law in the optics **[84**]. In a small interval $dy$ where the imaginary component of the wave number can be taken constant, the relative change in the wave amplitude is

$$\frac{d\psi}{\psi} = -k'' dy \quad . \tag{108}$$

Integrating relationship (32), we obtain

$$\psi(\omega, y2) = C \exp(-\int_{y_1}^{y_2} k''(\varpi, y) dy) \tag{109}$$

where $y_1$ and $y_2$ are the coordinates of the radiator and the detector, respectively.

The relative change in the traveling wave amplitude at a certain detector coordinate is

$$r(\omega) = \frac{\psi(\omega, y2)}{\psi(\omega, y1)} = \exp(-\int_{y_1}^{y_2} k''(\varpi, y)dy).$$

(110)

The energy transmission coefficient (ratio of the energy fluxes of the transmitted and incident waves) is equal to the squared amplitude ratio

$$T(\omega) = r^2(\omega) = \exp(-2\int_{y_1}^{y_2} k''(\varpi, y)dy)$$

(111)

Fig. 22 depicts the spectral characteristic of the $10\mu$-thick ferromagnetic film as the distance from the exciting antenna to the receiving antenna is 1 cm with the magnetic system parameters taken in this work. In this case, transmission spectrum is completely determined by the imaginary component of the wave number.

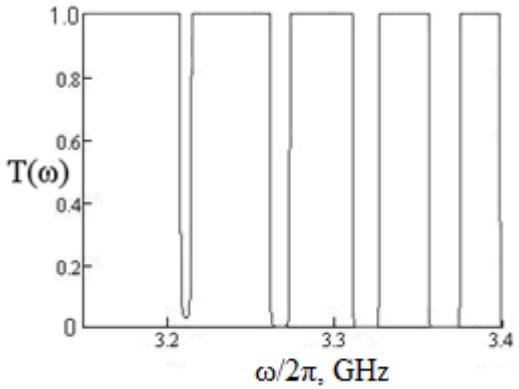


**Fig. 22. Transmission spectrum of the ferromagnetic film with the periodic structure from parallel strips.**

Varying the angular coefficient of the film, we can obtain different spectral characteristics, the examples of which are shown in Fig. 23. Depending on the angular coefficient, the spectrum at the filter output can be comb (Fig. 22, Fig. 23a, and Fig. 23c) or narrow-band (Fig. 23b and the inset to Fig. 23c) spectra.

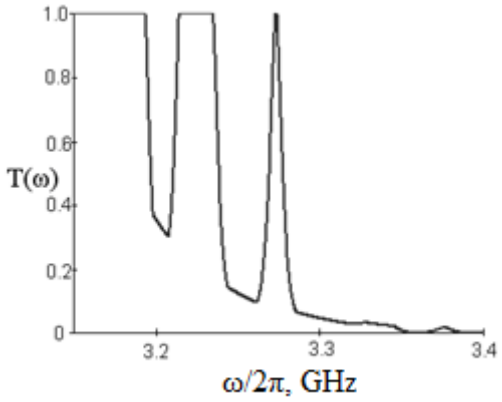


A.

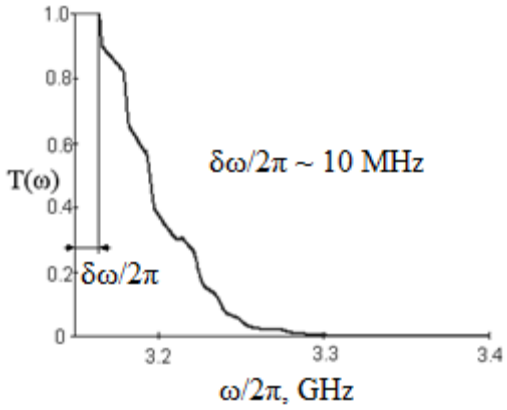


B.

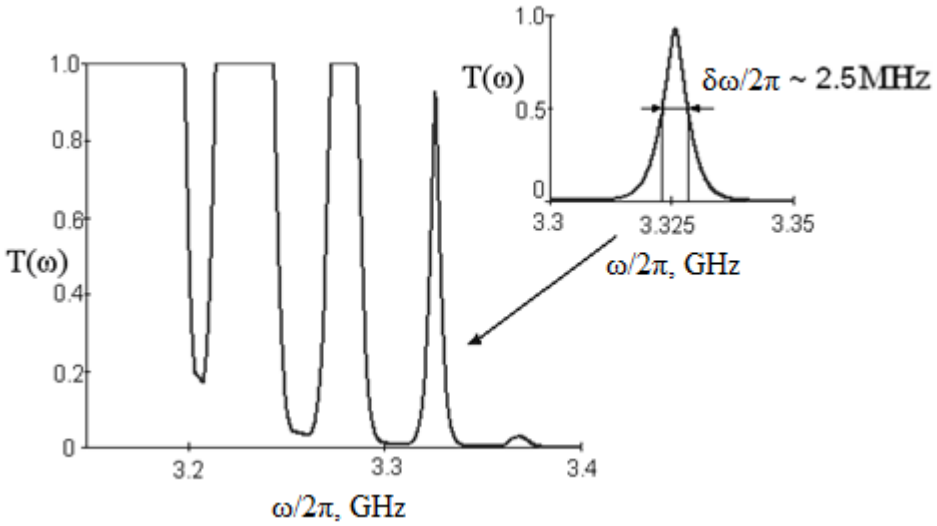


C.

**Fig. 23. Spectral characteristics of the filter of surface magnetostatic waves on the basis of the ferromagnetic variable thickness film with the periodic structure of parallel strips. ξ = (a) 0.25, (b) 0.75, and (c) 0.17 cm$^{-1}$.**

It is seen that the transmission spectra of microwave filters based on a variable-thickness ferromagnetic film with a periodic magnetic inhomogeneity shown in Fig. 22 have the transmission bands *2—10 MHz*. Filters with such bands can be applied, e.g., in devices intended for detection and transmission of TV signals and also in other areas of engineering where the communication channel width is assumed to be fairly large.

## 4.4. Conclusion

Thus, in this work, the Wentzel—Kramers—Brillouin method was used to calculate the properties of a surface magnetostatic wave propagating in a ferromagnetic variable-thickness film magnetized along the tangent (one-dimensional magnon crystal). We derived the dispersion relation for the wave propagating perpendicularly to the field and estimated the intrinsic error of the method. Calculations were provided for the system with the following parameters: $H$ = 550 Oe, $M$ = 139 G, the film thickness, which was mainly supposed to decrease from $d_0 = 10\ \mu m$ with the factor $\xi = 0.1$.

On the assumption that the wave propagates at a constant frequency, the wave number must increase with decreasing the film thickness. The allowance for the correction calculated using the Wentzel—Kramers—Brillouin method shows that, as a surface magnetostatic wave propagates in a film whose thickness varies linearly, the wave ceases to be surface wave; it takes a volume component radiated deep to the ferromagnetic film. The surface magnetostatic wave amplitude increases as the film thickness decreases and decreases as its thickness increases. This term is in agreement with the law of energy conservation.

Using the Kronig—Penney method, we calculated the dispersion of a surface magnetostatic wave propagating in a film, whose thickness varies linearly, with a periodic structure in the form of parallel strips of width $b = 10\ \mu m$ etched with the space period $a = 1\ mm$. It is shown that, as a surface magnetostatic wave propagates in such a medium, the spectrum of its energy states becomes more saturated as the film thickness decreases.

Possible applications of the effects investigated for designing narrow-band and comb microwave filters were considered. Varying the geometric parameters of the film, the period and the width of etched cavities, a required transmission characteristic of a ferromagnetic film with such structures can be obtained. In particular, it was shown that varying the parameters of system one can obtain the transmission bands of order of one MHz at the carrier frequency of 3-4 GHz.

# 5. Anomalous Doppler effect observed during propagation of magnetostatic waves in ferromagnetic films and ferrite–dielectric–metal (FDM) structures

In the fourth chapter the Doppler shift is calculated for both MSW types: the MSBVW and the MSSW propagating in a free ferromagnetic film in the case of the exciting antenna moving toward the receiving antenna. In addition, the assumption of the existence of the anomalous Doppler effect for MSSWs propagating in ferrite—dielectric-metal (FDM) structures is theoretically substantiated. Despite the fact that, in this case, the dynamic magnetic susceptibility and permittivity can simultaneously be greater than zero, it is assumed that, under certain conditions, the anomalous Doppler effect can also be observed.

## 5.1. Doppler effect observed during propagation of MSBVWs and MSSWs in a free ferromagnetic film

Let us consider a thin ferromagnetic film placed in a constant magnetic field and magnetized to saturation. Magnetostatic waves are excited in the film. Depending on the orientation of the radiating antenna with respect to the direction of the magnetic field and on the frequency of the exciting signal, either MSBVWs or MSSWs are observed (Fig. 24). It is assumed that the radiating antenna is moved toward the receiving antenna.

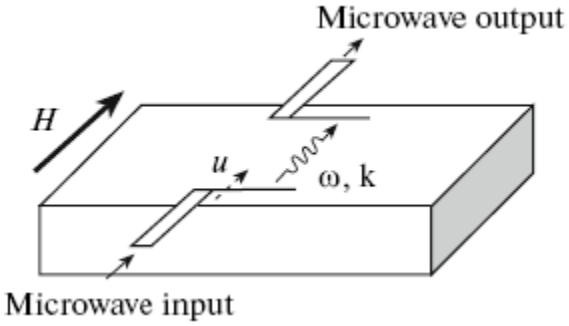


A.

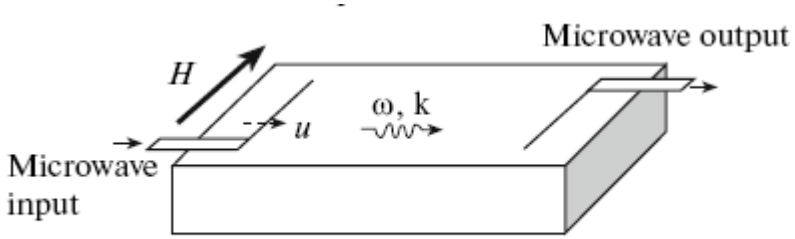


B.

**Fig. 24. Conditions for observing (a) MSBVW and (b) MSSW.**

As is known **[95]**, in a nonrelativistic case, the value of the Doppler frequency shift is determined as

$$\Delta\omega = \omega_0 \frac{u}{c}\cos\alpha = ku\cos\alpha. \tag{112}$$

where $k$ is the wave number, $u$ is the velocity of the source with respect to the receiver, α is the angle between the vectors of the source velocity and the phase velocity of the radiated wave, $\omega_0$ is the frequency of the radiated wave, and $c$ is the speed of light.

Let the direction at which the group velocity of the wave emitted by the source moving toward the receiver be positive. At $u > 0$ and at angles α such that $\cos\alpha < 0$, $\Delta\omega < 0$.

In this case the received frequency is smaller than the radiated frequency, a circumstance that may cause an anomalous Doppler effect. At $u > 0$ and such angles α that $\cos\alpha > 0$, $\Delta\omega > 0$, and the Doppler effect is a normal one.

Both cases can be implemented in a magnetically ordered structure in the form of a free ferromagnetic film. As noted above, in such a structure, spin wave modes can be excited, the MSSW and MSBVW being special cases of these modes. In the case of the MSSW, the wave is a forward one, its phase and group velocities have the same directions (when the wave propagates completely perpendicular to the magnetic field). In the case of the MSBVW, the wave is a backward one and its phase and group velocities are oppositely directed (the direction of the wave propagation being strictly parallel to the direction of the magnetic field).

For the MSBVW propagating along the direction of the magnetic field in a free ferromagnetic film of thickness $d$ (Fig. 24a), the dispersion law has the form:

$$tg\frac{kd}{2\sqrt{-\mu}}=\sqrt{-\mu} \tag{113}$$

where

$$\mu=1+\frac{\omega_H\omega_M}{\omega_H^2-\omega^2}, \qquad \omega_H=\gamma H, \omega_M=4\pi\gamma M. \tag{114}$$

$H$ is the external magnetic field, $M$ is the static magnetization of the film, γ is the magnetomechanical ratio, and ω is the MSW frequency.

The dispersion curves for the first four MSBVW modes are shown in Fig. 25. Here and below, in the calculating and graphical plotting, the parameters that are typical of the magnetic films are used. For example, for the yttrium iron garnet, $H$ = 367 Oe, $4\pi M$ = 1870 Gs, and $d$ = 82 μm. In addition to the fact that the MSBVW dispersion has a multimode composition, it also has a number of other specific features. It can be seen that all dots marked on the plot correspond to negative values of the projection of wave vector k, but the projection of the group velocity $U_{gr} = \delta\omega/dk$ on the *0y* axis corresponding to these dots is everywhere positive. Thus, the phase and group velocities of the wave are collinear and are oppositely directed, i.e., the direction of propagation of the electromagnetic energy is opposite to that of the phase. Therefore, the received signal, coming from the approaching source, will have a phase velocity whose direction is opposite to the direction of the source velocity, i.e., α = π and cosα = -1 in expression (112). Therefore, we can assume that, in this case, an anomalous Doppler effect is observed.

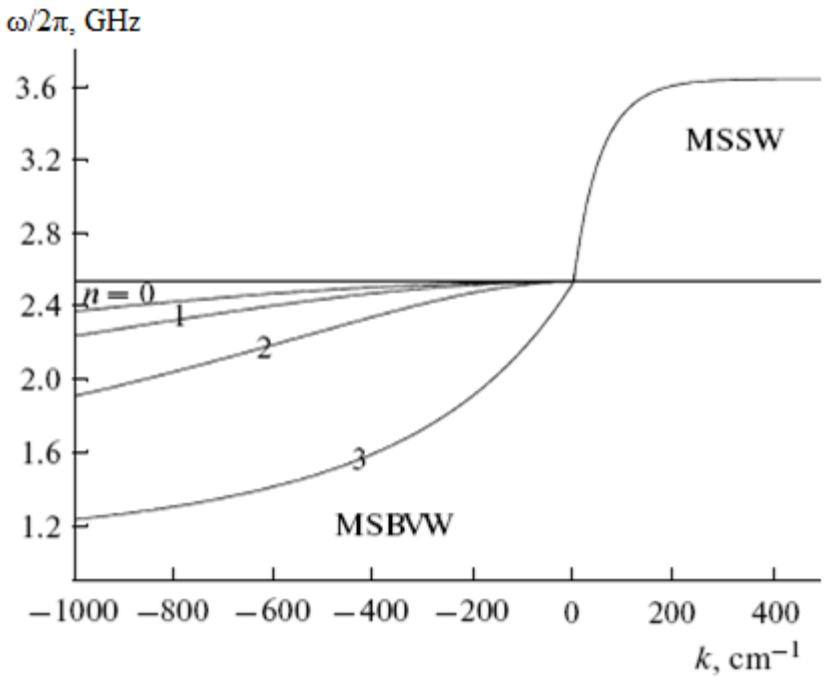


**Fig. 25. Dispersion curves for the first four MSBVW modes (n = 0−3) and for an MSSW in a free ferromagnetic plate.**

In a free ferromagnetic film, the MSSWs obeys a dispersion law of the form (29) or also it can be written as:

$$k = \frac{1}{d\alpha} arcth(\frac{2\mu\alpha}{\beta - 1}).$$

where

$$\beta = \left(\nu^2 - \mu^2 + \mu\right)\cos^2\varphi - \mu$$

$$\alpha = \sqrt{\cos^2\varphi + \frac{\sin^2\varphi}{\mu}}$$

$$\nu = \frac{\omega\omega_M}{\omega_H^2 - \omega^2},$$

φ is the angle between the direction of the MSSW phase velocity and the perpendicular to the direction of the external magnetic field. The dispersion curve for an MSSW propagating in the direction perpendicular to the direction of the external magnetic field (see Fig. 24b) is also shown in Fig. 25. It can be seen that here the vectors of the phase and group velocities are collinear and directed in the same direction. Therefore, a normal Doppler effect occurs.

The curves of the Doppler shift constructed as a function of frequency for the first four MSBVW modes and for an MSSW propagating in a free ferromagnetic film in accordance with expression

(112) are shown in Fig. 26. Here and below, the velocity of the source with respect to the receiver is assumed to be the same: $u$ = 8 mm/s.

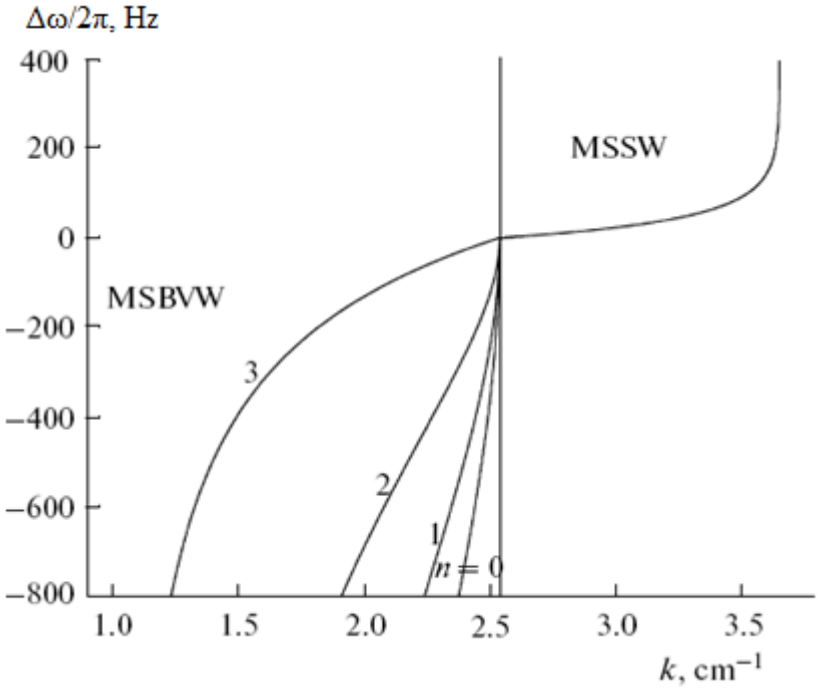


**Fig. 26. Doppler frequency shift for an MSSW and the first four MSBVW modes (n = 0−3) at the source speed u = 8 mm/s.**

## 5.2. Doppler effect observed during propagation of MSSWs in a FDM structure

Of greater interest for studying the MSSW propagation in a ferromagnetic film proved to be an FDM structure. The dispersion law for a MSSW propagating in this structure perpendicularly to the magnetic field has the form **[96]**

$$th(kt)+\mu(th(kt)+1)cth(kd)-\nu(th(kt)-1)+\mu^2-\nu^2=0. \quad (115)$$

where $t$ is the thickness of the dielectric interlayer in the FDM structure.

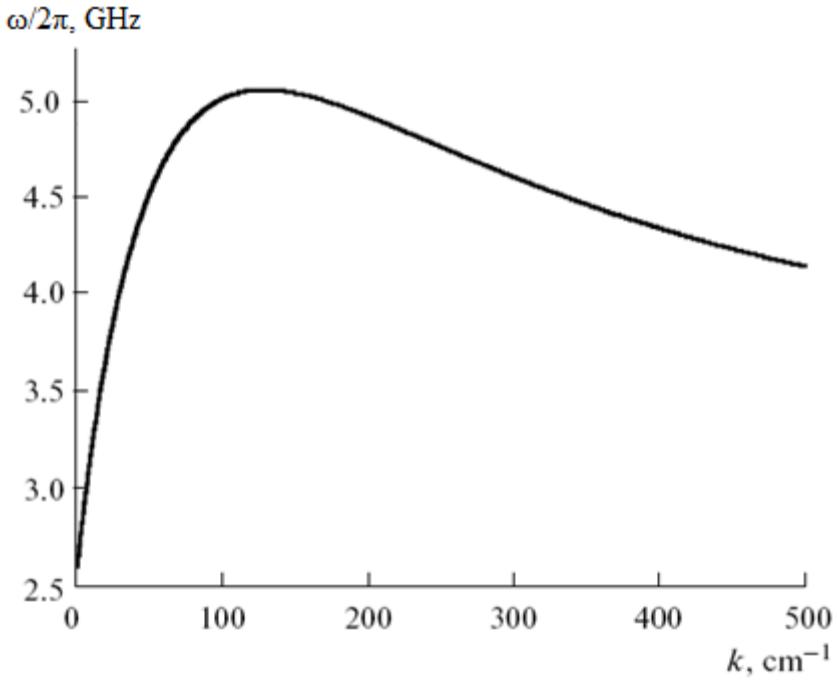


**Fig. 27. MSSW dispersion in an FDM structure with t = 0.5d.**

The curve of the MSSW dispersion in the FDM structure corresponding to the dielectric thickness t = 0.5d is shown in Fig. 27. It can be seen that the presence of a metal plate near the surface of the ferromagnetic film adds certain specific features to the MSSW dispersion. It is known that, beginning from a certain thickness of the dielectric interlayer, the dispersion curve ceases to be single-valued in *k* **[96]**, **[97]**. In addition, curve segments with both positive and negative slopes are formed. This fact indicates that, for these segments, the projections of the group velocity

$$\vec{u}_g = \frac{\partial \omega}{\partial \vec{k}}$$

on the *0y* axis differ in sign.

It can be shown that, at a certain wave-number value, the sign of the group-velocity projection changes to the opposite one. The directions of the phase and group velocities become opposite in direction. This circumstance suggests that, at the given parameters, the conditions for the anomalous Doppler effect are formed in the system.

By using expression (112), we can calculate the Doppler shift for each frequency in the MSSW-observation interval (Fig. 28).

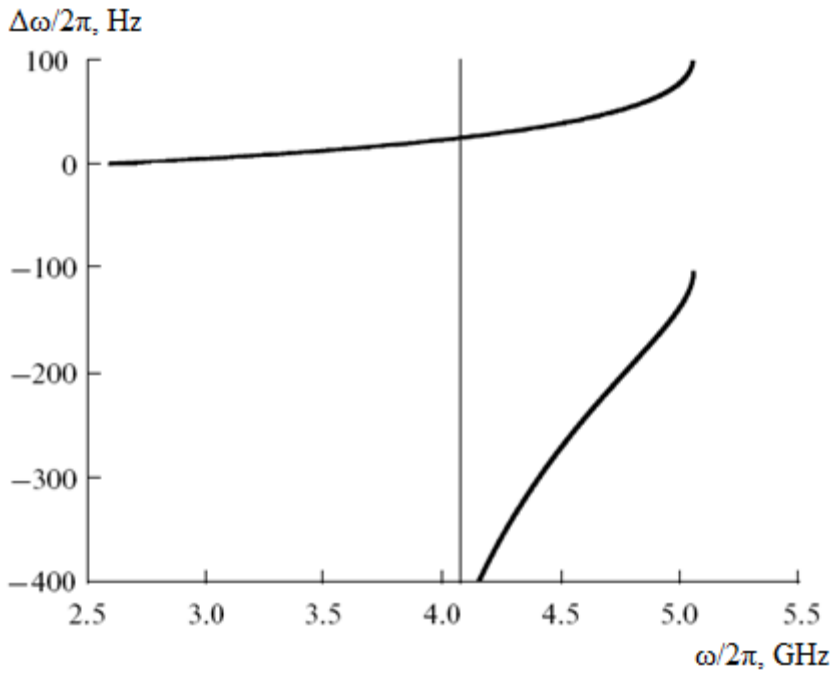


**Fig. 28. Doppler shift for an MSSW propagating in an FDM structure.**

Let us derive a dispersion relation for an arbitrary direction of the MSSW propagation in the FDM structure. We will use the line of reasoning similar to that of **[96]**, **[97]**.

The behavior of an MSW in a medium is described by Maxwell's equations:

$$rot\vec{h}=0;$$

(116)

$$div\vec{b}=0\ .$$

(117)

The form of the coupling equations is determined by the Landau—Lifshits equation:

$$\frac{d\vec{M}}{dt}=-\gamma\cdot\left[\vec{M}\times\vec{H}\right].$$

(118)

The simultaneous solution of equations (116)—(118) results in a system of equations for potential ψ:

$$\vec{h}=grad\Psi$$

$$\mu_{11}\left(\frac{\partial^2\psi_i}{\partial x^2}+\frac{\partial^2\psi_i}{\partial y^2}\right)+\frac{\partial^2\psi_i}{\partial t^2}=0$$

$$\frac{\partial^2 \psi_e}{\partial x^2} + \frac{\partial^2 \psi_e}{\partial y^2} + \frac{\partial^2 \psi_e}{\partial z^2} = 0$$

where ψ,· is the value of potential ψ inside the ferromagnetic film and $\psi_\beta$ is the value of potential ψ in the dielectric; potential ψ inside and on the surface of the metal film is zero (up to an arbitrary constant, which is assumed to be zero in the solutions of Damon and Eshbach **[77**]).

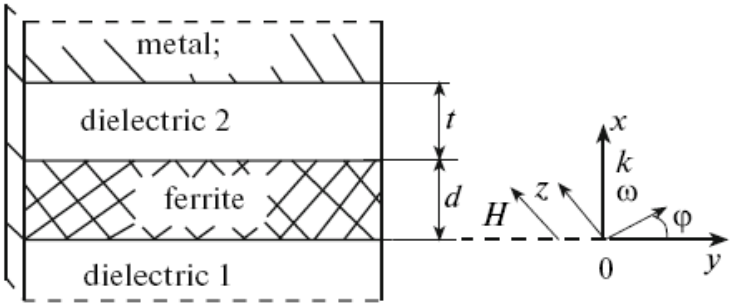


**Fig. 29. Geometry of the MSSW propagation in an FDM structure.**

This system should be supplemented with boundary conditions for continuity of the normal component of the induction and of the tangential components of the magnetic field for each interface in the FDM structure (Fig. 29):

$$\begin{cases} \mu \dfrac{\partial \psi_i}{\partial x} + i\nu \dfrac{\partial \psi_i}{\partial y}\Big|_{x=0} = \dfrac{\partial \psi_e^1}{\partial x}\Big|_{x=0}; \\ \psi_i\big|_{x=0} = \psi_e^1\big|_{x=0}; \\ \mu \dfrac{\partial \psi_i}{\partial x} + i\nu \dfrac{\partial \psi_i}{\partial y}\Big|_{x=d} = \dfrac{\partial \psi_e^2}{\partial x}\Big|_{x=d}; \\ \psi_i\big|_{x=d} = \psi_e^2\big|_{x=d}; \\ \psi_e^2\big|_{x=d+t} = 0. \end{cases}$$

(119)

From the necessary condition for consistency of the obtained system (equality of its determinant to zero), we obtain the desired dispersion relation

$$-\left(\mu\sqrt{-(\sin\varphi)^2-\frac{(\cos\varphi)^2}{\mu}}\right)^2-th(-t\cdot|k|)+\nu\cos(\varphi)(th(-t\cdot|k|)+1)-\nu^2(\cos\varphi)^2+$$

$$+(-th(-t\cdot|k|)+1)\mu\sqrt{-(\sin\varphi)^2-\frac{(\cos\varphi)^2}{\mu}}\cdot ctg\left(d\cdot|k|\cdot\sqrt{-(\sin\varphi)^2-\frac{(\cos\varphi)^2}{\mu}}\right)=0 \qquad (120)$$

At φ = 0, this expression can be reduced to form (115) or, on imposing the additional condition $t \to \infty$, to form (29).

Let us rewrite law of the MSSW dispersion in an FDM structure (120) in designations of the wave-vector projections:

$$-\left(\mu\sqrt{-k_y^2-\frac{k_z^2}{\mu}}\right)^2-\left(k_y^2+k_z^2\right)th(-t\cdot\sqrt{k_y^2+k_z^2})+\nu k_y\sqrt{k_y^2+k_z^2}\,(th(-t\cdot\sqrt{k_y^2+k_z^2})+$$

$$+1)-\nu^2k_y^2+(-th(-t\cdot\sqrt{k_y^2+k_z^2})+1)\mu\sqrt{k_y^2+k_z^2}\sqrt{-k_y^2-\frac{k_z^2}{\mu}}\times$$

$$\times ctg\left(d\cdot\sqrt{k_y^2+k_z^2}\cdot\sqrt{-k_y^2-\frac{k_z^2}{\mu}}\right)=0 \qquad (121)$$

Based on (121), we can introduce a function that allows the dispersion relation to be written in a more compact form:

$$F(k_y,k_z)=0. \qquad (122)$$

The expression for the dependence of the direction of the group velocity on the direction of the phase front has the form **[93]**

$$\psi=arctg\frac{\partial k_z}{\partial k_y}+n\pi, \qquad (123)$$

$$\frac{\partial k_z}{\partial k_y}=-\frac{\partial F/\partial k_y}{\partial F/\partial k_z}. \qquad (124)$$

It can be shown that, in accordance with (123) and (124), the direction of the group velocity is a function of angle $\varphi$: $\psi=\psi(\varphi)$.

The direction of the group velocity plotted as a function of the direction of the phase front of the MSSW with a frequency of *4.2 GHz* propagating in the FDM structure with $t = 0.5d$ at $n = 0$ is shown in Fig. 30. The angles are measured counterclockwise with respect to the 0y axis.

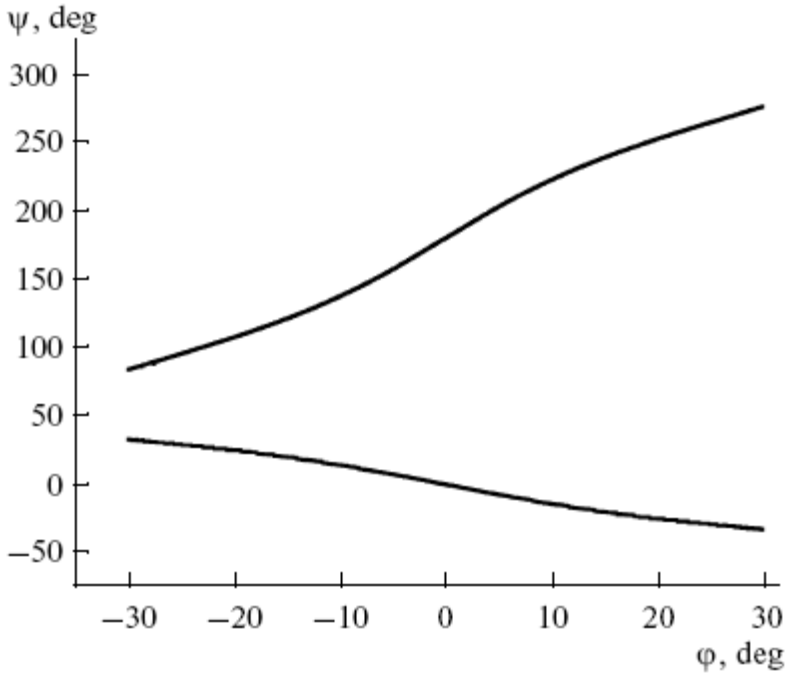


**Fig. 30. Direction of the group velocity against the direction of the phase velocity for an MSSW propagating in an FDM structure.**

In the frequency range in which the dispersion curve (see Fig. 27) intersects the straight line $\omega = \omega_0$ at only one point, one would expect to see a clear, one-to-one dependence in Fig. 30. This dependence is presented in studies **[92]**, **[93]**. In the frequency range in which ambiguity in $k$ occurs, which is the case under consideration, a second branch appears in Fig. 30, which corresponds to the points of intersection of the segment with a negative slope of the dispersion curve and of the straight line $\omega = \omega_0$. This branch is located higher and changes more rapidly than the first branch. The cosine of angle $\alpha$, which determines the behavior of the Doppler frequency shift in expression (112), is equal, according to the selected measurement procedure, to $\cos\alpha = \cos(\psi-\varphi)$. As one would expect, the cosine is everywhere negative for the upper branch in Fig. 30 and everywhere positive for the lower branch. The branches converge at the point where $\cos(\psi-\varphi)=0$, i.e., $\psi - \varphi = \pi/2$. This point corresponds to the case where the straight line $\omega = \omega_0$ intersects the dispersion curve (see Fig. 27) at the point of maximum. In this case, the vectors of the phase and group velocities are mutually orthogonal.

## 5.3. Anomalous Doppler effect on the equifrequency curves

Let us see how all these phenomena can be described with the use of equifrequency curves, which are constructed on the basis of expression (121) and correspond to MSSWs with various frequencies propagating in the FDM structure (Fig. 31). It is seen that, as the frequency increases, the curve takes a “roundish” shape. This phenomenon can be explained by the formation of a segment of the dispersion curve with a negative angular coefficient (see Fig. 27).

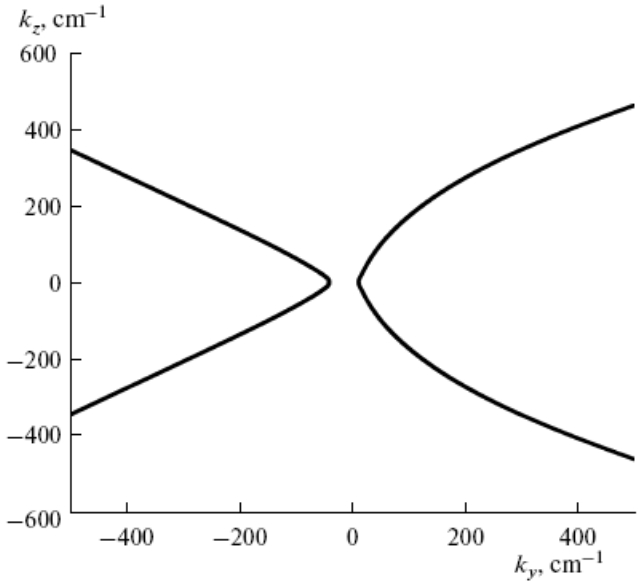


A.

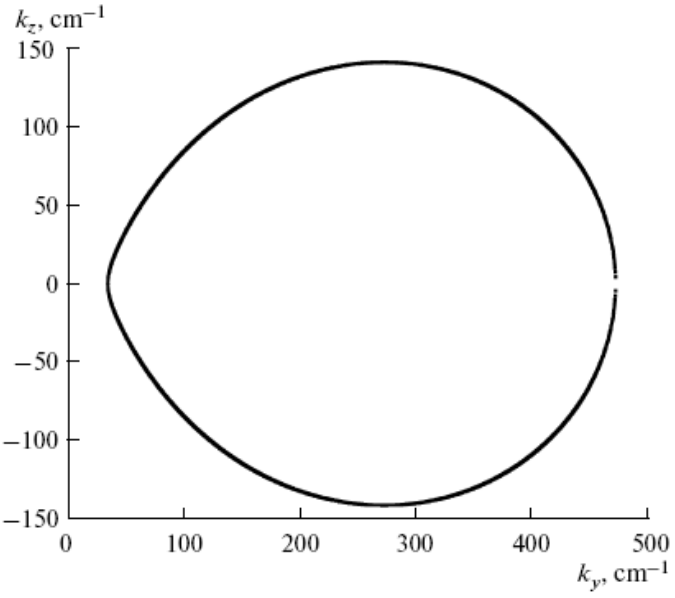


B.

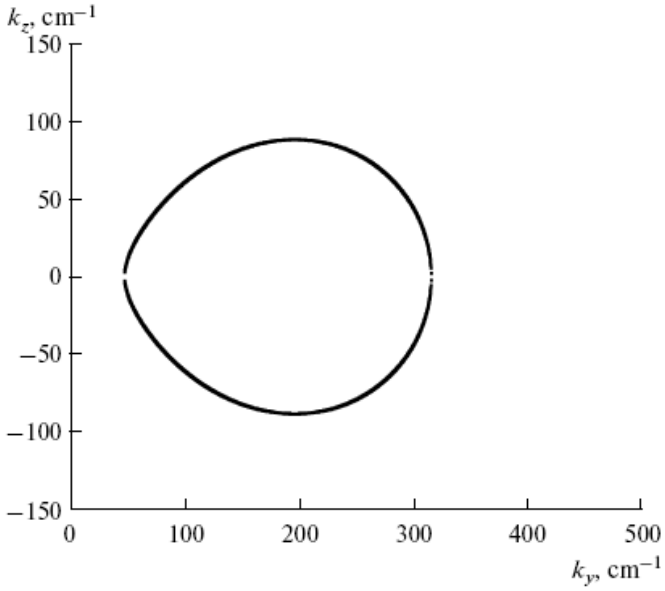


C.

**Fig. 31. Equifrequency curves for various MSSW frequencies: (a) 3.2 GHz, (b) 4.2 GHz, and (c) 4.55 GHz.**

Thus, in a certain angular range, there exist two points of intersection of the equifrequency curve with radius vector **k** drawn from the origin of coordinates at angle φ. It can be shown that the vector of the group velocity is perpendicular to the tangent to the equifrequency curve. Fig. 32 shows the equifrequency curve for the MSSW with a frequency of *4.55 GHz*. It is clearly seen that, in a certain angular range, a second point of intersection of the radius vector with the equifrequency curve appears. It can be seen that the group-velocity vector and the radius vector for this point form angle α such that $\cos\alpha<0$ and that there exists a boundary angle $\varphi_0$ at which the radius vector is a tangent to the isofrequency curve. At this point, the group-velocity vector is perpendicular to the wave vector, the circumstance that corresponds to the case when, at specified angle of the MSSW propagation $\varphi_0$, the dispersion curve is intersected with the straight line $\omega = \omega_0$ at the point of maximum. The value of angle $\varphi_0$ is determined by the MSSW frequency and by the parameters of the magnetic system.

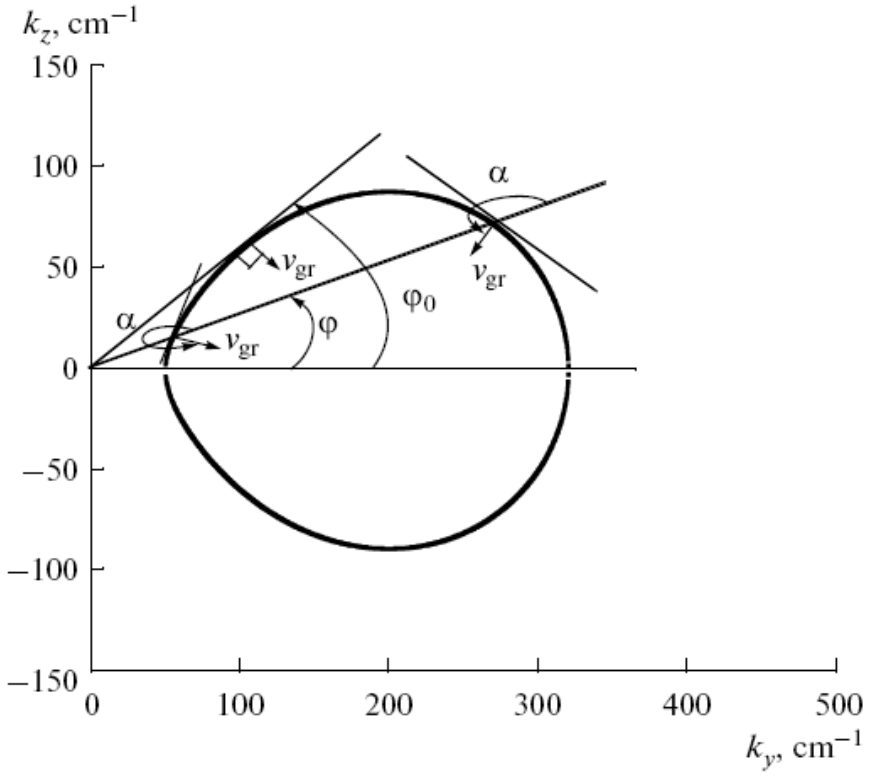


**Fig. 32. Equifrequency curve for an MSSW propagating in an FDM structure: initiation of the anomalous Doppler effect.**

## 5.4. Conclusion

The phenomenon of the anomalous Doppler effect observed during the MSBVW propagation in a free ferromagnetic film is theoretically substantiated. Plots of the Doppler shift are constructed for specified parameters. In addition, the possibility of the occurrence of the anomalous Doppler effect during propagation of an MSSW in an FDM structure in a certain range of system parameters is substantiated. All calculations were provided for the yttrium iron garnet and the following system parameters $H = 367$ *Oe*, $4\pi M = 1870$ *G*, and $d = 82$ $\mu m$ in the ferrite-dielectric-metal structure corresponding to the dielectric thickness $t = 0.5d$.

It is found that the anomalous Doppler effect may be observed in these structures in the frequency range *4.2-5 GHz* and $k > 120$ $cm^{-1}$. A demonstration model is constructed that illustrates this effect with the use of equifrequency curves in the frequency range *3-5 GHz*.

# General conclusion

The main obtained results can be concordantly distributed into four parts strictly corresponding to four chapters of the present work. And it was already done in the conclusion of each chapter. Here we will try to systemize the main points of obtained results. For the deeper consideration one can see the described sources or related articles.

As the work was successfully made and the corresponding articles were published, the assigned main check-points declared into the introduction were fulfilled:

**Theoretical description for the high frequency and non-linear waves propagation in thin planar ferromagnetic structures with different compositions is derived**. The basic theoretical research is presented in the 1st Chapter as each further Chapter contains the additional particular study. In total the second-order nonlinear Landau-Lifshitz equation, Maxwell equation in magnetostatic approximation with different boundary conditions were solved here. Additional questions of magnetoelastic and magnetoelectric energy conversion were dicussed in details.

**LF vibrations of the cantilever can be amplified when FMR is excited by HF electromagnetic field near SRT**. This phenomenon was clearly demonstrated theoretically and experimentally. The experiments were provided in 500MHz-4GHz frequency range of the RF generator signal modulated by a square wave, whose frequency was resonant for the mechanical system of the problem. The experimental and theoretical data on FMR and magnetoelastic demodulation in the $TbCo_2$/FeCo nanostructure and $La_{0.7}Sr_{0.3}MnO_3$ thin film deposited on Si and $NdGaO_3$ cantilevers respectively, show that low-frequency vibrations of the cantilever can be amplified when FMR is excited by HF electromagnetic field near SRT. The experimental data also showed the dispersion of magnetic relaxation coefficient in the vicinity of spin reorientation transition. This fact is of interest for the research activities on the magnetic relaxation dispersion calculation. The $TbCo_2$/FeCo nanostructure has one order higher mechanical response in spite of the higher HF attenuation. This is caused by the fact that the $TbCo_2$/FeCo nanostructure has approximately one order higher magnetoelastic coupling factor value than the one for the $La_{0.7}Sr_{0.3}MnO_3$ thin film. The results of calculations are in good agreement with the experimental data of measurements of FMR line and with the data of the optical detection of elastic vibrations of the magnetostrictive cantilever under HF electromagnetic field. The phenomenon under consideration can find applications in the area of MMMSs and MEMSs in general distantly controlled by a HF external electromagnetic field.

**The magnetoelastic demodulation effect can be clearly demonstrated by nonlinear magnetoelectric effect with a piezoelectric inter-layer supplementation**. Nonlinear resonance magnetoelectric effect induced by HF electromagnetic field in thin film composite multiferroic structure TbCo/FeCo-AlN is observed experimentally and described theoretically. The experiments were carried out in the 500 MHz – 2 GHz frequency range. The effect is studied in conditions of spin reorientation transition in the magnetostrictive nanostructure. The results of calculations are in good agreement with the experimental data on magnetic field dependence of LF magnetoelectric voltage and on HF power absorption. The experimental data showed unusual phenomenon of the second ferromagnetic resonance branch disappearing. The unusual disappearing of the FMR line in the saturation phase, where magnetisation is collinear to magnetizing field, is explained by specific geometry of the experiment and strong HF absorption. Nonlinear magnetoelectric effect becomes sufficient in the vicinity of spin reorientation transition. It is shown that conductivity contribution to FMR line width is relatively weak in the magnetostrictive nanostructure. Obtained value of nonlinear magnetoelectric conversion coefficient amounts to $100\ \mu V/mW$. Calculations show for optimal orientation of anisotropy axis increase of the conversion coefficient by one order of magnitude.

We calculated **the dispersion of a surface magnetostatic wave propagating in a film, whose thickness varies linearly, with a periodic structure in the form of parallel etched strips**. The frequency bands set becomes more intensive with the thickness decrease. This phenomenon is of great interesting for new types of HF comb and narrow band filters development. All provided calculations showed a good agreement with provided experiments on the structures with a constant thickness. On the assumption that the wave propagates at a constant frequency, the wave number must increase with decreasing the film thickness. The allowance for the correction calculated using the Wentzel—Kramers—Brillouin method shows that, as a surface magnetostatic wave propagates in a film whose thickness varies linearly, the wave ceases to be surface wave; it takes a volume component radiated deep to the ferromagnetic film. The surface magnetostatic wave amplitude increases as the film thickness decreases and decreases as its thickness increases. This term is in agreement with the law of energy conservation.

Using the Kronig—Penney method, it is shown that, as a surface magnetostatic wave propagating in a film, whose thickness varies linearly, with a periodic structure in the form of parallel etched strips, the spectrum of its energy states becomes more saturated as the film thickness decreases. Possible applications of the effects investigated for designing narrow-band and comb microwave filters were considered. Varying the geometric parameters of the film, the period and the width of etched cavities, a

required transmission characteristic of a ferromagnetic film with such structures can be obtained. In particular, it was shown that varying the parameters of system one can obtain the transmission bands of order of one MHz at the carrier frequency of 3-4 GHz.

The possibility of **the occurrence of the anomalous Doppler effect during propagation of a magnetostatic surface wave in a ferrite-dielectric-metal structure** in a certain range of system parameters is substantiated. It is found that the anomalous Doppler effect for the yttrium iron garnet and the following system parameters $H = 367$ *Oe*, $4\pi M = 1870$ *G*, and $d = 82$ $\mu m$ in the ferrite-dielectric-metal structure corresponding to the dielectric thickness $t = 0.5d$ may be observed in these structures in the frequency range *4.2-5 GHz* and $k > 120$ $cm^{-1}$. The innovative method of equifrequency curves was proposed to demonstrate the conditions of phenomenon observation. A demonstration model is constructed that illustrates this effect with the use of equifrequency curves in the frequency range *3-5 GHz*. The calculations on the anomalous Doppler shift during the propagation of BVMSWs in a free ferromagnetic plate were also presented. The phenomena are of interest for the new structures development in the physical electronics.

Recently investigated high-frequency and non-linear phenomena in thin active ferromagnetic planar structures possessed several unique features that can be promising from perspectives of possible practical applications. In fact between all solved problems there is a strong connection provided by the system geometry and main theoretical basics. This fact can be interesting from a perspective to use considered phenomena under the same technological platform or/and even within the same device. For example, this can be actual if it is necessary to provide MMMS based on the magnetoelastic demodulation with WDM filters allowing magnetostatic approximation within the device accurancy. There are few promising propositions for real practical applications of the anomalous Doppler effect occurrence during the MSSW propagation in FDM structures. Generally it is a quite interesting phenomenon that can be observed with corresponding conditions and it is reasonable to investigate it at least as a part of magnetostatic wave behavior in the considered system geometry.

# Résumé étendu en Français

Les phénomènes à haute fréquence (HF) et non linéaires dans les films minces ferro-magnétiques actifs ont gagné beaucoup d'intérêt depuis la 2ème partie du 20ème siècle principalement en raison des perspectives d'applications pratiques offertes dans le spectre micro-onde. Ils sont utilisés comme composante de base des filtres à multiplexage par répartition en longueur d'onde (WDM), des microsystèmes électromécaniques (MEMS), des actionneurs, etc. Ces phénomènes sont également utilisés pour la richesse des effets dynamiques survenant sous l'influence d'un champ électromagnétique à haute fréquence sur les systèmes ferromagnétiques résonants amortis et pour les recherches fondamentales portant sur l'interaction du champ électromagnétique avec un matériau à fort ordre magnétique.

Un des objectifs les plus prometteurs pour la dynamique magnétique non linéaire est l'exploitation de ces propriétés originales d'intégrer des structures de film minces qui sont déjà des éléments fondamentaux pour les technologies de circuit intégré. Les propriétés principales dues à une précession magnétique non linéaire apparaissent surtout dans les structures aimantées de façon homogène. Si la valeur de la réponse d'un système à une influence externe est importante et que l'on utilise ces effets non linéaires, c'est la dynamique de précession homogène qui est préférée. Dans le présent mémoire, nous nous intéresserons principalement à la dynamique de précession homogène dans les structures de film minces uniformément aimantées et les applications pratiques possibles qui en découlent.

Nous nous focalisons ici sur une sous partie du domaine de la dynamique magnétique HF dans les films actifs minces ferro-magnétiques. Nous considérons l'étude des ondes magnetostatiques (MSWs) se propageant dans un milieu aimanté ainsi que les applications pratiques basées sur les phénomènes apparentés. Les MSWs sont attrayantes grâce à leurs faibles pertes de propagation. Par exemple, à 9 GHz en utilisant des films de grenat de fer et d'yttrium (YIG) de la largeur d'une raie spectrale $\leq 0.3$ Oe, les pertes de propagation sont $\leq 20$ dB/μs. En comparaison, les pertes de propagation d'autres types d'onde acoustique de surface sur niobate de lithium sont à plus de 100 dB/μs dans la même gamme de fréquence. En outre, parce que les dispositifs basés sur les MSW sont planaires, ils sont compatibles avec les circuits hybrides actuellement disponibles et les circuits intégrés à micro-ondes monolithiques (MMICs). De plus, comme les MSWs sont plus lentes que les ondes électromagnétiques et se propagent de deux à quatre ordres de grandeur plus lentement, des composants

compacts peuvent être obtenus avec une largeur de raie spectrale comprise entre 10-500 μm, ce qui permet des techniques simples. Un autre avantage clé de la technologie MSW est une faculté d'adaptation. La réponse en fréquence d'appareils MSW, tels que de les lignes à retard, les filtres et les résonateurs, peut être adaptée dans une certaine plage, en variant la force du champ magnétique avec laquelle on sature le film YIG. Cette particularité est très utile pour les composants de type oscillateur et filtre.

Ces vingt dernières années, il y a eu beaucoup de travaux fait dans ces directions, en particulier sur les propriétés des matériaux, le développement de nouveaux composés (multiferroïques, cristaux photoniques (magnoniques), etc.), l'amélioration de l'efficacité de conversion d'énergie, etc... Ce travail se base sur les résultats obtenus dans ces domaines et s'inscrit dans la direction des thématiques du domaine de recherche actuelle. Son contenu scientifique général se compose en quatre parties différentes précédées d'un chapitre général :

Le chapitre 1 présente les modèles théoriques et les calculs principaux utilisés dans les autres chapitres.

• R**ésonance ferro-magnétique et démodulation magnétoélastique dans les films actifs minces ferro-magnétiques** (Chapitre 2). Ce travail a un grand intérêt pour les applications MEMS (Micro-Electro-Mechanical-Systems) et MMMS (Micro-Magneto-Mechanical-Systems) pour la microélectronique et la radiométrie HF parce qu'il tient compte des derniers progrès de la recherche dans le domaine des nouveaux matériaux nanostructurés contrôlés à distance. Il expose l'exploitation d'effets résonants couplés (la résonance mécanique et la résonance ferro-magnétique (FMR)) et la transition de phase pour gagner en efficacité de conversion d'énergie.

• **Effets magnétoélectriques non-linéaires dans une nanostructure multiferroique TbCo/FeCo-AlN soumise à un champ électromagnétique haute fréquence** (Chapitre 3). Ce chapitre continue logiquement le précédent en utilisant le même système magnetoélastique associé avec une couche piézoélectrique pour mesurer directement l'effet de la démodulation sous forme d'une tension.

• **Propagation des ondes de surface magnétostatiques dans un cristal magnonique unidimensionnel avec épaisseur variable** (Chapitre 4). Ce travail est prometteur pour les applications d'un type nouveau telles que le développement de filtres WDM HF basés sur une structure magnonique dans un film avec une épaisseur variable. Il est aussi basé sur les travaux théoriques et expérimentaux déjà effectués dans les films d'épaisseur constante qui présentent des caractéristiques intéressantes susceptibles d'améliorer les paramètres des filtres.

• **Effet Doppler anomal observé pendant la propagation d'ondes magnétostatiques dans les films ferro-magnétiques et les structures ferrite–diélectrique–métal (FDM)** (Chapitre 5). Cette partie a pour but l'investigation du phénomène connu d'effet Doppler anomal dans de nouvelles structures.

Le travail sur **la résonance ferromagnétique et la démodulation magnétoélastique dans les films minces ferromagnétiques actifs** concerne une partie de l'activité de recherche sur les microsystèmes électromécaniques (MEMS) destinés à être utilisés dans les systèmes d'objets communicant autonomes ou encore "Smartdust". Il est supposé couvrir les parties de contrôle de distance et les efficacités de tels systèmes.

En fait les films uniaxiaux magnétostrictifs avec une transition de réorientation de spin (TRS) artificielle induite par un champ magnétique externe ont un grand intérêt dans la pratique. La sensibilité des microsystèmes magnéto-mécaniques (MMMS) peut augmenter d'environ deux ordres de grandeur au voisinage de la TRS dans de telles nanostructures magnétostrictives multicouches. La zone située à proximité de la TRS présente également un certain nombre de propriétés dynamiques et fortement non linéaires. En particulier, une grande efficacité d'excitation des sous-harmoniques de vibrations élastiques peut être observée près de la TRS. Un effet magnétoélectrique fort a également été obtenu près de la TRS dans un composite TbCo/FeCo sur PZT ainsi que des structures multicouches TbCo/FeCo sur AlN.

La démodulation magnétoélastique d'ondes électromagnétiques peut également devenir efficace dans les nanostructures à magnétostriction géante près de la TRS. Ce phénomène a un intérêt pour le contrôle HF des MMMS. Pour la démodulation des micro-ondes, l'effet de la TRS peut être amplifié en se plaçant non loin de la résonance ferromagnétique (FMR).

Sur la base des phénomènes non-linéaires observés lors de l'investigation de la démodulation magnétoélastique, nous avons étudié **l'effet magnétoélectrique non linéaire** de façon théorique. Pour ce faire, une couche piézoélectrique a été associée à une structure magnétostrictive semblable à la précédente en vue d'accéder directement au signal démodulé sous forme de tension.

L'effet magnétoélectrique peut être considérablement plus efficace dans un composite piézo-électrique/magnétostrictif que dans les matériaux avec des propriétés magnétoélectriques intrinsèques. L'efficacité de la conversion d'énergie magnétoélectrique est essentiellement définie par deux facteurs: la valeur du facteur de couplage électromécanique dans le composant piézo-électrique et la valeur de la magnétostriction de la partie magnétique. Par ailleurs, les films de nitrure d'aluminium (AlN) suscitent

beaucoup d'intérêt dans le domaine de la physique appliquée en raison de la relative simplicité de mise en oeuvre technologique et de la valeur importante du coefficient de couplage électromécanique.

L'effet magnétoélectrique peut être sensiblement amélioré dans une structure composite à proximité de la TRS.

L'efficacité de la conversion d'énergie magnétoélectrique augmente fortement dans les conditions de résonance mécanique (RM) d'une structure composite. Il a été montré que le coefficient magnétoélectrique à la résonance pour les structures multiferroïques minces peut atteindre plus de 700 V / (cm*Oe) pendant la résonance.

L'utilisation conjointe de la FMR, la TRS, la RM, une magnétostriction géante et une valeur importante du coefficient piézo-électrique peut améliorer de façon significative la conversion magnétoélectrique non linéaire dans les structures à films minces. La démodulation HF entraînant une excitation à la résonance de vibrations élastiques a été observée précédemment à proximité de la TRS dans un film magnétostrictif TbCo/FeCo déposé sur un substrat de Silicium.

La formulation du problème de la **propagation des ondes superficielles magnétostatiques dans un cristal magnonique unidimensionnel avec une épaisseur variable** est le résultat du travail intensif dans ce domaine pendant les dernières années à l'Institut Kotel'nikov de Radio-ingénierie et d'électronique de Moscou. Le problème semblait le plus prometteur à propos de l'information sur les types neufs de filtres WDM. Les méthodes qui ont été utilisées pour estimer l'influence de l'épaisseur variable (WKB approximation) et de la structure périodique (le modèle Kronig-Penny) sont assez simples et sont valables pour des petites variations d'épaisseur.

Les films ferromagnétiques présentant des structures périodiques offrent un intérêt particulier en raison de la possibilité de contrôle de leurs caractéristiques par l'application d'un champ magnétique. La combinaison d'une périodicité homogène et d'une épaisseur variable de la structure pourra engendrer de nouvelles propriétés du milieu servant de guide d'ondes et ouvrira de nouveaux domaines d'application des cristaux magnoniques.

Les milieux présentant simultanément des valeurs négatives de la susceptibilité magnétique et de la permittivité présentent un certain nombre de propriétés dynamiques spécifiques. En particulier, **l'effet Doppler anomal** peut être observé dans ces milieux. Cet effet se manifeste par la diminution de la fréquence du signal reçu alors que sa source se déplace vers le récepteur.

Un certain nombre d'études récentes ont été consacrées à l'observation de l''effet Doppler anomal dans des lignes de transmission d'ondes magnétostatiques volumiques inverses. Il a également été étudié

l'effet Doppler anomal observé dans les cristaux photoniques et phononiques, dans lesquels cet effet est causé par l'interaction des ondes acoustiques et électromagnétiques avec le réseau cristallin.

**Le but principal** de ce travail a été le développement d'une base théorique universelle pour les ondes magnétostatiques non-linéaires de second ordre et de l'utiliser pour l'étude de certains problèmes théoriques et expérimentalaux. Pour cela **les objectifs** suivants ont été fixés:

- Le développement d'une base universelle théorique pour les ondes magnétostatiques du second ordre non-linéaires dans les films minces ferromagnétiques;
- Montrer l'augmentation de la conversion de l'énergie dans un film mince soumis à un champ électromagnétique à haute fréquence lorsque le point de FMR est à proximité de la TRS. Montrer la possibilité de visualiser ce phénomène par un effet magnétoélectrique non linéaire.
- Calculer la dispersion d'une onde superficielle magnétostatique dans un film, dont l'épaisseur varie linéairement, avec une structure périodique sous la forme de bandes parallèles gravées, et montrer les applications pratiques possibles de ces structures;
- Démontrer la possibilité de l'apparition de l'effet Doppler anomal lors de la propagation des MSSWs dans une structure de type FDM avec une certaine gamme de paramètres du système;

Ce travail a été soutenu par l'ambassade française à Moscou qui dépend du ministère français des affaires étrangères, la fondation russe de la recherche fondamentale (les subventions n° 09-02-93107-NCNIL_a et 08-02-00785-a) ainsi que le projet ANR NAMAMIS (08-NAN-035-O 01).

# References

[1]. Monosov Ya A, Nelineinyi Ferromagnitnyi Rezonans (Nonlinear Ferromagnetic Resonance) (Moscow: Nauka, 1971)

[2]. L'vov V S Nelineinye Spinovye Volny (Nonlinear Spin Waves) (Moscow: Nauka, 1987)

[3]. Bryant P H, Jeffries C D, Nakamura K, Phys. Rev. A 38 4223 (1988)

[4]. Kandaurova G S, Sviderski A E, Pis'ma Zh. Eksp. Teor. Fiz. 47 410 (1988) [JETP Lett. 47 490 (1988)]

[5]. Kaganov M I, Pustyl'nik N B, Shalaeva T I Usp. Fiz. Nauk 167 191 (1997) [Phys. Usp. 40 181 (1997)]

[6]. D. I. Sementsov, A. M. Shutyi, Uspekhi Fizicheskikh Nauk 177 (8) 831 - 857 (2007)

[7]. Chaplygin Yu A (Ed.) Nanotekhnologii v Elektronike (Nano-technologies in Electronics) (Moscow: Tekhnosfera, 2005)

[8]. Ishak W. S., Proc. IEEE, Vol. 76, No. 2 (1988)

[9]. Bostjan Batagelj, Jurij Tratnik, Luka Naglic, Vitalii Bagan, Yury Ignatov, Maxim Antonenko, “Optical Access Network Migration from GPON to XG-PON”, Proc. of The Third International Conference on Access Networks ACCESS 2012, Venice, Italy (2012)

[10]. E. du Tremolet de Lacheisserie. Magnetostriction, Theory and Applications of Magnetoelasticity. - CRC Press, Boca Raton (USA) (1993)

[11]. Yannick Dusch, Nicolas Tiercelin, Alexey Klimov, Vasyl Rudenko, Yury Ignatov, Sami Hage-Ali, Philippe Pernod, Vladimir Preobrazhensky , J. Appl. Phys. 109, 07A720 (2011)

[12]. Yu. A. Ignatov, A. A. Klimov, S. A. Nikitov, Journal of Communications Technology and Electronics, Volume 55, Number 4, 449-456 (2010)

[13]. A. Klimov, Yu. Ignatov, N. Tiercelin, et al., J. Appl. Phys. 107 (8), 093916 (2010)

[14]. S.L. Vysotsky, S.A. Nikitov, N.N. Novitskii, A.I. Stognii, Yu.A. Filimonov, 2011, published in Zhurnal Tekhnicheskoi Fiziki, Vol. 81, No. 2, pp. 150–152 (2011)

[15]. M. Weiler, A. Brandlmaier, S. Geprags, M. Althammer, M. Opel, C. Bihler, H. Huebl, M. S. Brandt, R. Gross, and S. T. B. Goennenwein, New J. Phys. 11, 013021 (2009)

[16]. S. Platonov, S. Nikitov, Magnetostatic spin waves propogation in two-dimensional wedge magnonic crystal, Book of Abstract European Conference “Physics of magnetism”, Poznan, Poland, June 27- July 1 (2011)

[17]. Yu. A. Ignatov, A. A. Klimov, S. A. Nikitov, V. I. Shcheglov, Physics of the Solid State, Volume 52, Number 10, 2090-2098 (2010)

[18]. Stancil D. D. and Prabhakar A., Spin Waves: Theory and Applications, 2009 (Springer, New York)

[19]. E. Quandt, H. Holleck, Microsystem Technologies 1 178-184 (1995)

[20]. E. Quandt, Journal of alloys and compounds 258 pp. 126-132 (1995)

[21]. N. Tiercelin, P. Pernod, V. Preobrazhensky, H. Le Gall, J. Ben Youssef, P. Mounaix, D. Lippens, Sens. & Actuators 81 pp. 162-165 (2000)

[22]. J. Ben Youssef, N. Tiercelin, F. Petit, H. Le Gall, V. Preobrazhensky, P. Pernod, IEEE Transactions on Magnetics 38 (5) pp. 2817-2819 (2002).

[23]. N. Tiercelin, J.B. Youssef, V. Preobrazhensky, P. Pernod, H.L. Gall, JMMM, 249 519-523 (2002)

[24]. Klimov, N. Tiercelin, V. Preobrazhensky, P. Pernod, IEEE Trans. Mag, Vol 42 (2006) 309093092.

[25]. V. I. Ozhogin and V. Preobrazhensky, JMMM 100 (91) 544 (1988)

[26]. Yu. V. Gulyaev, I. E. Dikstein, V. G. Shavrov, Phys. Usp. 167 p. 7 (1997)

[27]. N. Tiercelin, P. Pernod, V. Preobrazhensky, H. Le Gall, J. Ben Youssef, Ultrasonics 38 pp. 64-66 (2000)

[28]. N. Tiercelin, V. Preobrazhensky, P. Pernod, A. Ostachenko, App. Phys. Lett. 92 p. 062904 (2008)

[29]. N. Tiercelin, A. Talbi, V. Preobrazhensky, P. Pernod, V. Mortet, K. Haenen, A. Soltani, App. Phys. Lett. 93 p. 162902 (2008)

[30]. N. Tiercelin, V. Preobrazhensky, V. Mortet, A. Talbi, A. Soltani, K. Haenen, P. Pernod, JMMM 321 pp. 1803-1807 (2009)

[31]. H. Le Gall, J. Ben Youssef, F. Socha, N. Tiercelin, V. Preobrazhensky, P. Pernod, J. Appl. Phys. V.87 (8) pp. 5783-5785 (2000)

[32]. N. Tiercelin, V. Preobrazhensky, P. Pernod, H. Le Gall, J. Ben Youssef, JMMM 210 pp. 302-308 (2000)

[33]. V. D. Buchel'nikov, N. K. Dan'shin, L. T. Tsymbal, V. G. Shavrov, Phys. Usp. 39 p. 547 (1996)

[34]. L. I. Koroleva, R.V. Demin,, A. M. Balbashov, ZhETF Lett. 65 pp. 474-478 (1997)

[35] E. M. Chudnovsky, D. A. Garanin, and R. Schilling, Phys. Rev.B 72, 094426 (2005)

[36] V. S. Lutovinov, M. Yu. Reizer, JETP 77, 2, 707 (1979).

[37]. R.V. Demin, L. I. Koroleva, A. M. Balbashov, JMMM 177 pp. 871-872 (1998)

[38]. H. Boschker, M. Mathews, E. P. Houwman, H. Nishikava, A. Vailionis, G. Koster, G. Rijners, D. H. A. Blank, Phys. Rev. B 79 p. 214425 (2009)

[39]. G. A Ovsyannikov, A. M. Petrzhik; I. V. Borisenko, A. A. Klimov, Yu. A. Ignatov, V. V. Demidov, S. A. Nikitov, ZhETF 108 pp. 56-64 (2009)

[40]. L.D. Landau and E.M. Lifshits, *Theory of elasticity*, first ed. (Pergamon Press Ltd., London, 1959)

[41]. C. Kittel, Phys. Rev. 110 p. 836 (1956)

[42]. I. Ahieser, V. G. Bar'yahtar, S. V. Peletminskiy, *Spin waves* (Nauka Press, Moscow, 1967)

[43]. J. Torby, *Advanced Dynamics for Engineers* (Holt, Rinehart, and Winston, 1984)

[44]. Belov K P, Zvezdin A K, Kadomtseva A M, Levitin R Z, *Orientatsionnye Perekhody v Redkozemel'nykh Magnetikakh (Orientational Transitions in Rare-Earth Magnetic Materials)*, (Moscow: Nauka) (1979)

[45]. M. Fiebig, J. Phys. D 38, R123 (2005)

[46]. N. A. Spaldin and M. Fiebig, Science 309, 391 (2005)

[47]. M.-A. Dubois, P. Muralt, Appl. Phys. Lett. 74, 3032 (1999)

[48]. C.D. White, G. Piazza, P. J. Stephanou, A. P. Pisano, Sensors & Actuators: A. Physical 134 (1), 239-244 (2007)

[49]. M. I. Bichurin, D. A. Filippov, V. M. Petrov, V. M. Laletsin, N. Paddubnaya, G. Srinivasan, Phys. Rev. B 68, 132408 (2003)

[50]. Henry Greve, Eric Woltermann, Hans-Joachim Quenzer, Bernhard Wagner, and Eckhard Quandt, Appl. Phys. Lett. 96, 182501 (2010)

[51]. Y. K. Fetisov and G. Srinivasan, Appl. Phys. Lett. 87, 103502 (2005); Electron. Lett. 41, p. 1066 (2005)

[52]. A. B. Ustinov, G. Srinivasan, and Yuri K. Fetisov. J. Appl. Phys. 103, p. 063901 (2008).

[53]. N. Benatmane, S. P. Crane, F. Zavaliche, R. Ramesh, and T. W. Clinton, Appl. Phys. Lett. 96, p. 082503 (2010)

[54]. M. I. Bichurin,V. M. Petrov, S. V. Averkin, E. Liverts, J. Appl. Phys. 107, 053905 (2010)

[55]. E. M. Weiler, L. Dreher, C. Heeg, H. Huebl, R. Gross, M. S. Brandt, S.T.B. Groennenwein, Phys. Rev. Lett. 106, 117601 (2011).

[56]. E. du Trémolet de Lacheisserie and J. C. Peuzin, J. Magn. Magn. Mater. 136, p. 189 (1994)

[57]. B. Heinrich, R. Urban, and G. Woltersdorf, J. Appl. Phys. 91, p. 7523 (2002)

[58]. W.P. Mason, *Physical Acoustics and the Properties of Solids* (Princeton, New Jersey, 1958)

[59]. C.M. Lueng, H.L.W. Chan, C. Surya, C.L. Choy, J. Appl. Phys. 88 (9), pp. 5360-5363 (2000)

[60]. T. M. Vasilevskaya and D. I. Sementsov, Phys. Of The Solid State 52, 6, pp. 1210-1216 (2010)

[61]. M. I. Kaganov, JETP Lett. 10, pp. 336-340 (1969)

[62]. J. D. Joannopoulos, S. G. Johnson, J. N. Winn, R. De Meade. Photonic Crystals: Molding the flow of light. Second edition. Princeton University Press, Princeton (2008). 286

[63]. M. S. Kushwaha, P. Halevi, G. Mart´ınez, L. Dobrzynski, B. Djafari-Rouhani. Phys. Rev. B 49, 2313 (1994)

[64]. Sergey A. Nikitov, Roman S. Popov, Ivan V. Lisenkov, Chul Koo Kim. IEEE transactions on ultrasonics, ferroelectrics and frequency control 55, 8 (2008)

[65]. Yu. V. Gulyaev and S. A. Nikitov, Dokl. Akad. Nauk 380 (4-6), 469 (2001) [Dokl. Phys. 46 (10), 687 (2001)

[66]. S. A. Nikitov, Ph. Tailhades, and S. S. Tsai. J. Magn. Magn. Mater. 236, 320 (2001)

[67]. L. Brillouin and M. Parodi, Propagation des ondes dans les milieux periodiques (Dunod, Paris, 1956; Inostran- naya Literatura, Moscow, 1959)

[68]. Yu. V. Gulyaev, S. A. Nikitov, L. V. Zhivotovskii, A. A. Klimov, Ph. Tailhades, L. Presmanes, C. Bon- ningue, C. S. Tsai, S. L. Vysotskii, and Yu. A. Filimonov, Pis'ma Zh. Eksp. Teor. Fiz. 77 (10), 670 (2003) [JETP Lett. 77 (10), 567 (2003)]

[69]. H. Al-Wash, A. Akjouj, B. Djafari-Rouhani, J.O. Vasseur,. L. Dobrzynski, P.A. Deymier. Phys. Rev. B 59, 8709 (1999)

[70]. N. Yu. Grigor'eva and B. A. Kalinikos, Zh. Tekh. Fiz. 79 (8), 110 (2009) [Tech. Phys. 54 (8), 1196 (2009)]

[71]. Ernst Schlomann. J. Appl. Phys. 35, 159 (1964)

[72]. Ernst Schlomann, R. I. Joseph. J. Appl. Phys. 35, 167 (1964)

[73]. A.V. Vashkovsky, E.H. Lock, V.I. Shcheglov, V.I. Zubkov. IEEE Trans. on Magn. 26, 1480 (1990)

[74]. A.V. Vashkovskii, V. I. Zubkov, E. G. Lokk, and V. I. Shcheglov, Radiotekh. Elektron. (Moscow) 38, 818 (1993)

[75]. J. O. Vasseur, L. Dobrzynsky, B. Dijafari-Rouhani, H. Puszkarski. Phys. Rev. B 54, 1043 (1996)

[76]. A.M. Merzlikin, A.P. Vinogradov, A.V. Dorofeenko, M. Inoue, M. Levy, A.B. Granovsky. Physica B: Cond. Matter 394, 277 (2007)

[77]. R. W. Damon, J.R. Eshbach. J. Phys. Chem. Solids 19, 308 (1961)

[78]. V. Vashkovskii, V. I. Zubkov, E. G. Lokk, and V. I. Shcheglov, Pis'ma Zh. Tekh. Fiz. 15 (4), 1 (1989) [Sov. Tech. Phys. Lett. 15 (2), 120 (1989)]

[79]. Mathews J., Walker R.L. Mathematical methods of physics. W.A. Benjamin, New York (1970). 515

[80]. Adams, *Introduction to Optical Waveguides* (Wiley, New York, 1981; Mir, Moscow, 1984)

[81]. A. G. Gurevich and G. A. Melkov, Magnetic Oscillations and Waves (Nauka, Moscow, 1994; CRC, New York, 1996)

[82]. R. de L. Kronig, W. Penney. Proc. Roy. Soc., 130, 499 (1931)

[83]. F. Villa, J. A. Gaspar-Armenta. Opt. Express 12, 2338 (2004)

[84]. J. D. J. Ingle, S. R. Crouch. Spectrochemical Analysis, Prentice Hall, New Jersey (1988). 589 pp.

[85]. D.D. Stancil, B.E. Henty, A.G. Cephi and J.P. Van't Hof, Phys. Rev B 74, 060404(R) (2006)

[86]. V.G. Veselago, USP. Fiz. Nauk 92, 517 (1968) [Sov. Phys. Usp. 10, 509(1968)]

[87]. N. Engheta, A.R. Mikelson and C.H. Papas, IEEE Trans. Antennas Propag. AP-28, 519 (1980)

[88]. A.M. Belyantsev and A.B. Kozyrev, Sov. Phys. Tech. Phys. 47, 1477 (2002)

[89]. N. Seddon and T. Beapark, Science 302, 1537 (2003)

[90]. E.J. Reed, M. Soljacic and J.D. Joannopoulos, Phys. Rev. Lett. 91, 133901 (2003)

[91]. X.Hu, Z. Hang, J. Li, J. Zi and C.T. Chan, Phys. Rev. E 73, 015602(R) (2006)

[92]. A.V. Vashkovskii and E.H. Lokk, Physics-Uspekhi 47, 601 (2004)

[93]. A.V. Vashkovskii and E.H. Lokk, Physics-Uspekhi 49,389 (2006)

[94]. Charles P. Poole, Jr. Electron Spin Resonance. John Wiley & Sons, 1983.

[95]. J.D. Jackson, Classical Electrodynamics, 2nd ed. (Wiley, New York, 1975), p.509

[96]. R.E. De Wames and T. Wolfram, J. Appl. Phys. 41, 987 (1970)

[97]. W.L. Bongianni, J Appl. Phis. 43, 2541 (1972)

[98]. A. I. Lourier, Theory of Elasticity (Nauka, Moscow, 1970)

[99]. Chun Yeol you and Sung-Chul Shina, Appl. Phys. Lett. 69 (9), 1315-1317 (1996)

# APPENDIX A

Linearized Landau-Lifshitz equation **(6)** following from magnetic energy density is **[81]**:

$$\hat{A}(\omega)\vec{m}(t) = \vec{h}(t), \tag{A.1}$$

Where:

$$\hat{A}(\omega) = \begin{pmatrix} i\omega & \Omega_1 & -\gamma H_A \cos(\varphi_A)\sin(\varphi_A) \\ -\Omega_2 & i\omega & 0 \\ 0 & 0 & i\omega \end{pmatrix}, \tag{A.2}$$

$$\begin{cases} \Omega_1 = \gamma(H\sin(\varphi_A) + H_A\cos(2\varphi_A)) - i\alpha(\omega + n\Omega), \\ \Omega_2 = \gamma(H\sin(\varphi_A) + H_A\cos^2(\varphi_A)) - i\alpha(\omega + n\Omega). \end{cases} \tag{A.3}$$

Thus we obtain the magnetic susceptibility tensor for the mode "n" **[60]**:

$$\hat{\chi}_{ij}^{(n)} = \frac{\gamma M_0}{\Omega_1\Omega_2 - (\omega + n\Omega)^2}\begin{pmatrix} \Omega_1 & i(\omega + n\Omega) & 0 \\ -i(\omega + n\Omega) & \Omega_2 & 0 \\ 0 & 0 & 0 \end{pmatrix}, \tag{A.4}$$

Solving the non-linear Landau-Lifshits equation in the second order approximation, we correspondingly obtain the tensor of non-linear susceptibility **[13]**:

$$\hat{\chi}_{ijk}^{(n)} = -4\Theta_{im}\cdot(\varepsilon_{mlj}(\hat{\chi}_{lk}^{(n)})' + \varepsilon_{muv}S^{vv}((\hat{\chi}_{uj}^{(n)})'(\hat{\chi}_{vk}^{(n)})' + (\hat{\chi}_{uj}^{(n)})''(\hat{\chi}_{vk}^{(n)})''))/(\pi\det\hat{\Theta}) \tag{A.5}$$

Here: $S^{ij} = \left[\partial(H_{eff})_j \Big/ \partial m_i\right]_{m=0}$, $\vec{H}_{eff}(\vec{m})$ is the effective magnetic field, $\varepsilon_{ijk}$ is the Levi-Civita symbol; $\chi'_{vl}$ and $\chi''_{vl}$ are real and imaginary components of the HF magnetic susceptibility respectively; $\hat{\Theta} = \hat{A}(\Omega)$ is the operator of the linear Landau-Lifshitz equation (A.2) for low-frequency vibrations which differs from the high-frequency operator by the low frequency $\Omega$ instead of HF $\omega$ (See Appendix D).

# APPENDIX B

Internal magnetic field strength $\vec{h}(x,t)$ inside the conductive film placed to the external HF field $h_{ex}$ can be obtained from the Maxwell equation solution:

$$\vec{h}(x,t)=\begin{pmatrix} 0 & -\frac{\mu_{12}}{\mu_{11}}\frac{\cos(k_\perp x)}{\cos(k_\perp \frac{d_m}{2})} & 0 \\ 0 & \frac{\cos(k_\perp x)}{\cos(k_\perp \frac{d_m}{2})} & 0 \\ 0 & 0 & \frac{\cos(k_{II} x)}{\cos(k_{II} \frac{d_m}{2})} \end{pmatrix}\vec{h}_{ex}e^{i\omega t}=\hat{\vartheta}(x)\vec{h}_{ex}e^{i\omega t}, \qquad \text{(B.1)}$$

Where:

$$\vec{h}_{ex}=\begin{pmatrix} 0 \\ \sin(\varphi_0+\varphi_A) \\ -\cos(\varphi_0+\varphi_A) \end{pmatrix}h_0, \qquad \text{(B.2)}$$

here $h_0$ is the amplitude of the external field,

$$\hat{\mu}(\omega)=1+4\pi\hat{\chi}(\omega), \qquad \text{(B.3)}$$

$$\begin{cases} k_\perp^2=\frac{4\pi i\sigma\omega}{c^2}\mu_\perp(\omega), \\ k_{II}^2=\frac{4\pi i\sigma\omega}{c^2}. \end{cases}, \qquad \text{(B.4)}$$

where σ is the film conductivity, c – light velocity and:

$$\mu_\perp(\omega)=\mu_{22}(\omega)-\frac{\mu_{12}(\omega)\mu_{21}(\omega)}{\mu_{11}(\omega)}, \qquad \text{(B.5)}$$

The magnetic field component interacting with magnetic subsystem is:

$$\vec{h}(x,t)=\begin{pmatrix} 0 & -\frac{\mu_{12}}{\mu_{11}} \\ 0 & 1 \end{pmatrix}\frac{\cos(k_\perp x)}{\cos(k_\perp \frac{d_m}{2})}\vec{h}_0e^{i\omega t}=\hat{\beta}_0\frac{\cos(k_\perp x)}{\cos(k_\perp \frac{d_m}{2})}\vec{h}_0e^{i\omega t}=\hat{\beta}(x)\vec{h}_0e^{i\omega t}, \qquad \text{(B.6)}$$

Where:

$$\vec{h}_0 = \begin{pmatrix} 0 \\ \sin(\varphi_0 + \varphi_A) \end{pmatrix} h_0, \qquad \text{(B.7)}$$

The absorption power was calculated as normal projection of the Pointing vector integrated over the surface of the film:

$$P = \iint_S (\vec{S}_P(x = \frac{d}{2}))d\vec{S}, \qquad \text{(B.8)}$$

Where:

$$\begin{cases} \vec{S}_P(x) = \dfrac{c}{4\pi}[\vec{E}^* \times \vec{H}], \\ \vec{E} = \dfrac{c}{4\pi\sigma} rot(\vec{h}(t)). \end{cases} \qquad \text{(B.9)}$$

As the result the absorption power for condition $|k_\perp d_m| << 1$ is:

$$P = P_\alpha + P_\sigma \approx \frac{\omega}{4\pi} abh_0^2 \frac{d_m}{2} \sin^2(\varphi_A + \varphi_0)(R_\alpha + R_\sigma), \qquad \text{(B.10)}$$

Where:

$$\begin{cases} R_\alpha(\omega) = \operatorname{Im} \mu_\perp(\omega), \\ R_\sigma(\omega) = \dfrac{4\pi\sigma\omega}{3c^2} (\dfrac{d_m}{2})^2 \operatorname{Re}(\mu_\perp^2(\omega)). \end{cases} \qquad \text{(B.11)}$$

The $R_\sigma(\omega)$ describes magnetic contribution of skin effect **[61]**.

The relative influence of conductivity on the HF magnetic damping is described by the ratio:

$$\frac{P_\sigma}{P_\alpha}(\omega) \cong \frac{\pi\sigma\omega}{3c^2} d_m^2 \frac{\operatorname{Re} \mu_\perp^2(\omega)}{\operatorname{Im} \mu_\perp(\omega)} \propto 10^{-2} (\frac{1}{\alpha(\omega)}) \qquad \text{(B.12)}$$

.

In our experimental conditions the influence of conductivity on the HF magnetic damping is quiet small (less than *10%*) as the value of $\alpha(\omega)$ for *TbCo/FeCo* films is usually about *0.1-1* **[13]**.

# APPENDIX C

According to the elasticity theory **[40]** one dimensional displacement $U_n(\xi)$ in flexural modes is:

$$U_n(\xi) = (\cos(\eta_n l) + \cosh(\eta_n l))(\cos(\eta_n \xi) - \cosh(\eta_n \xi)) + (\sin(\eta_n l) - \sinh(\eta_n l))(\sin(\eta_n \xi) - \sinh(\eta_n \xi)) \quad \text{(C.1)}$$

Here $\eta_n = \sqrt[4]{\Omega_n^2 \frac{\mathrm{P}}{c_S^2 I_y}}$, $l$ is the length of sample, $P$ is the sample cross-section, $c_S = \sqrt{\frac{E}{\rho}}$ is the longitudinal sound velocity, E is the Young modulus, ρ is the material density, $I_y$ is momentum of inertia along *Oy* axis.

Thus we have an inhomogeneous distribution of deformations along the ξ-axis of the sample. It generates an inhomogeneity in the distribution of the electric field. The integrals that define magneto-electric voltage are shown below:

$$\iiint_{V_P} x \cdot \frac{\partial^2 U_n}{\partial \xi^2} dV = -ad_{PE} d\eta_n ((\sinh(\eta_n l)\cos(\eta_n l) + \sin(\eta_n l)\cosh(\eta_n l)) \quad \text{(C.2)}$$

$$\iiint_{V_M} x \frac{\partial^2 U_n}{\partial \xi^2} \beta_{jl}(x)\beta^*_{kq}(x)dV = -2a\eta_n ((\sinh(\eta_n l)\cos(\eta_n l) + \sin(\eta_n l)\cosh(\eta_n l))(\beta_0)_{jl}(\beta_0^*)_{kq}\psi_0 \quad \text{(C.3)}$$

where *a* is the width of the structure and:

$$\psi_0 = \frac{1}{\cos(k_\perp \frac{d}{2})\cos(k_\perp^* \frac{d}{2})} \left\{ \cosh((k_\perp)''d)(\frac{1}{2} dd_m + \frac{1}{((k_\perp)'')^2}) - \cos((k_\perp)'d)(\frac{1}{2} dd_m - \frac{1}{((k_\perp)')^2}) \right\} \quad \text{(C.4)}$$

Here:

$$\begin{cases} k_\perp = (k_\perp)' + i(k_\perp)'', \\ k_\perp^* = (k_\perp)' - i(k_\perp)''. \end{cases} \quad \text{(C.5)}$$

# APPENDIX D

Here one can find the main theoretical results on the calculation of the second-order non-linear LF magnetization dynamics caused by HF signal modulated by a square wave.

- **Low-frequency precession**

Thus LF-dynamics of the magnetic moment can be described by the following equation (8):

$$\frac{\partial\vec{\mu}}{\partial t} = -\gamma\left[\vec{\mu}\times\overrightarrow{H_{eff}^{0}}\right] - \gamma\left[\vec{M}\times\frac{\partial(H_{eff}^{0})_j}{\partial M_i}\mu_j(t) + \frac{\partial(H_{eff}^{0})_i}{\partial u_{lj}}\epsilon_{lj}(t) + \frac{\partial(H_{eff}^{0})_i}{\partial H_j}h_j(t)\right] - \\ -\gamma\overline{[\overrightarrow{m\,(t)}\times\overrightarrow{h\,(t)} + ac\;\partial\,(H_{eff}^{0})_j\partial M_i m_j(t)]}^{\tau} - \gamma\overline{\left[\vec{M}\times\frac{\partial^2(H_{eff}^{0})_j}{\partial M_i\partial M_l}m_l(t)m_j(t)\right]}^{\tau}. \tag{D.1}$$

Where: $1/\Omega \gg \tau \gg 1/\omega$. For the nonlinear part of Landau-Lifshits equation we will calculate in real numbers:

$$\vec{m}^{Re}(t) = \frac{\vec{m}(t)+\vec{m}^{*}(t)}{2} = Re\,(\vec{m}(t)). \tag{D.2}$$

Similarly:

$$\vec{h}^{Re}(t) = \frac{\vec{h}(t)+\vec{h}^{*}(t)}{2} = Re\,(\vec{h}(t)). \tag{D.3}$$

Let us notice that

$$\frac{\partial\vec{\mu}}{\gamma\partial\,t} + [\vec{\mu}\times\overrightarrow{H_{eff}^{0}}] + [\vec{M}\times\frac{\partial(H_{eff}^{0})_j}{\partial M_i}\mu_j^{Re}(t) + \frac{\partial(H_{eff}^{0})_i}{\partial H_j}h_j^{Re}(t)] = \hat{\Theta}\vec{\mu}(t), \tag{D.4}$$

Where $\widehat{\Theta} = \hat{A}(\Omega)$ is the operator of the linear Landau–Lifshits equation for LF vibrations, which differs from the high frequency operator by the LF $\Omega$ instead of HF $\omega$. The LF frequency $\Omega$ corresponds to the first resonant frequency of the bulk vibrations.

Then:

$$\widehat{\Theta}\vec{\mu}(t) = -\overline{[\overrightarrow{m^{Re}(t)}\times\overrightarrow{h^{Re}(t)} + \frac{\partial(H_{eff}^{0})_j}{\partial M_i}m_j^{Re}(t)]}^{\tau} - \overline{[\vec{M}\times\frac{\partial^2(H_{eff}^{0})_i}{\partial M_l\partial M_j}m_l^{Re}(t)m_j^{Re}(t)}^{\tau} \tag{D.5}$$

In the tensor formulation:

$$\theta_{lt}\mu_t(t) = -\overline{\epsilon_{lij}m_i^{Re}(t)h^{Re}(t)_j}^{\tau} - \overline{\epsilon_{lkn}[m_k^{Re}(t)\frac{\partial(H_{eff}^0)_j}{\partial M_n}m_j^{Re}(t)]}^{\tau}$$
$$- \overline{\epsilon_{luv}[M_u\frac{\partial^2(H_{eff}^0)_j}{\partial M_{u'}\partial M_v}m_{u'}^{Re}(t)m_j^{Re}(t)]}^{\tau} \quad \text{(D.6)}$$

Where $\vec{m}(t) = \hat{\chi}\vec{h}(t), \mu_t = \mu_t^0 e^{i\Omega t}$.

Let us calculate:

$$\frac{\partial^2(H_{eff}^0)_l}{\partial M_i \partial M_j} = 0. \quad \text{(D.7)}$$

We need to consider only two summands:

$$\overline{[\overrightarrow{m^{Re}(t)}\times\overrightarrow{h^{Re}(t)} + \frac{\partial(H_{eff}^0)_j}{\partial M_i}m_j^{Re}(t)]}^{\tau}. \quad \text{(D.8)}$$

In the homogeneous case we have:

$$\overline{[\overrightarrow{m^{Re}(t)}\times\frac{\partial(H_{eff}^0)_j}{\partial M_i}m_j^{Re}(t)]}^{\tau}. \quad \text{(D.9)}$$

Within the accuracy of a small magnetoelastic term:

$$S_i^j = \frac{\partial(H_{eff}^0)_j}{\partial M_i} \approx \frac{\partial(H_{eff}^0)_i}{\partial M_i} = S^i. \quad \text{(D.10)}$$

Further we will conduct the calculations of the generalized force caused by the nonlinearity of the Landau-Lifshitz equation:

$$f_l = \overline{\epsilon_{lkn}[m_k^{Re}(t)S_n^j m_j^{Re}(t)]}^{\tau} = \epsilon_{lkn}S_n^j\overline{[m_k^{Re}(t)m_j^{Re}(t)]}^{\tau}. \quad \text{(D.11)}$$

$$\begin{cases} m_k^{Re} = \frac{m_k + m_k^*}{2}, \\ m_j^{Re} = \frac{m_j + m_j^*}{2}. \end{cases} \quad \text{(D.12)}$$

Then the expression for the generalized force takes the following form:

$$f_l = \frac{1}{4}\epsilon_{lkn}S_n^j\overline{m_k^*m_j^* + m_km_j + m_k^*m_j + m_km_j^*}^{\tau}. \quad \text{(D.13)}$$

Where HF magnetization precession $m \sim \frac{sin(\frac{\pi n}{2})}{\frac{\pi n}{2}}e^{i\omega t}$. Then one can be shown that:

$$\overline{m_k^*m_j^* + m_km_j}^{\tau} = 0. \quad \text{(D.14)}$$

One can write the expression for the generalized force:

$$f_l = \frac{1}{4}\epsilon_{lkn}S_n^j\overline{m_k^*m_j + m_km_j^*}^{\tau}. \quad \text{(D.15)}$$

Where: $\begin{cases} m_k = \chi_{ks} h_s, \\ m_j = \chi_{jp} h_p. \end{cases}$

Then:

$$f_l = \frac{1}{4} \epsilon_{lkn} S_n^j \overline{(\chi_{ks} h_s)^* \chi_{jp} h_p + \chi_{ks} h_s (\chi_{jp} h_p)^*}^{\tau}. \quad \text{(D.16)}$$

Considering that:

$$(a + ib)\,(c + id)^* + \,(a + ib)^* (c + id) \,= 2\,(ac + bd), \quad \text{(D.17)}$$

And also that :

$$\begin{cases} Re\,[(a + ib)\,(c + id)] \,= ac - bd, \\ Im\,[(a + ib)\,(c + id)] \,= ad + bc. \end{cases} \quad \text{(D.18)}$$

We have:

$$f_l = \frac{1}{2} \epsilon_{lkn} S_n^j \overline{(\chi_{ks} h_s)'(\chi_{jp} h_p)' + (\chi_{ks} h_s)''(\chi_{jp} h_p)''}^{\tau} = \frac{1}{2} \epsilon_{lkn} S_n^j \overline{((\chi_{ks})'(h_s)' - (\chi_{ks})''(h_s)'')}$$

$$\overline{((i_{jp})'(h_p)' - (\chi_{jp})''(h_p)'') + ((\chi_{ks})''(h_s)' + (\chi_{ks})'(h_s)'')((\chi_{jp})''(h_p))' + (\chi_{jp})'(h_p))''}^{\tau} =$$

$$= \frac{1}{2} \epsilon_{lkn} S_n^j \overline{((\chi_{ks})'(\chi_{jp})' + (\chi_{ks})''(\chi_{jp})'')((h_p)'(h_s)' + (h_p)''(h_s)'') + ((\chi_{ks})'(\chi_{jp})'' +}$$

$$\overline{+(\chi_{ks})''(\chi_{jp})'')((h_p)''(h_s)' - (h_p)'(h_s)'')}^{\tau}. \quad \text{(D.19)}$$

One can be shown that the second summand decreases to zero with the randomness of indexes s and p.

Then the generalized force can be written as:

$$f_l = \frac{1}{2} \epsilon_{lkn} S_n^j \overline{((\chi_{ks})'(\chi_{jp})' + (\chi_{ks})''(\chi_{jp})'')((h_p)'(h_s)' + (h_p)''(h_s)'')}^{\tau}. \quad \text{(D.20)}$$

$$f_l = \epsilon_{lkn} S_n^j ((\chi_{ks})'(\chi_{jp})' + (\chi_{ks})''(\chi_{jp})'') \overline{[h_p^{Re}(t) h_s^{Re}(t)]}^{\tau}. \quad \text{(D.21)}$$

Or, using the accepted approach,

$$f_l = \epsilon_{lkn} S^j ((\chi_{ks})'(\chi_{jp})' + (\chi_{ks})''(\chi_{jp})'') \overline{[h_p^{Re}(t) h_s^{Re}(t)]}^{\tau}. \quad \text{(D.22)}$$

Thus, the Landau-Lifshitz equation is:

$$-\widehat{\Theta}\vec{\mu} = \overline{[\overrightarrow{m^{Re}(t)} \times \overrightarrow{h^{Re}(t)} + \frac{\partial (H_{eff}^0)_j}{\partial M_i} m_j^{Re}(t)]}^{\tau}. \quad \text{(D.23)}$$

The expression for the first generalized force can be easily obtained with the assumption:

$$\begin{cases} S_i^j = 1, \\ \chi_{jp} = 1, \\ p \equiv n. \end{cases} \quad \text{(D.24)}$$

Here we have:

$$-\widehat{\Theta}\vec{\mu} = \epsilon_{lkn}(\chi_{ks})'\overline{[h_n^{Re}(t)h_s^{Re}(t)]}^{\tau} + \epsilon_{lkn}S_n^j((\chi_{ks})'(\chi_{jp})' +$$
$$+(\chi_{ks})''(\chi_{jp})'')\overline{[h_p^{Re}(t)h_s^{Re}(t)]}^{\tau}. \quad \text{(D.25)}$$

And as the result:

$$\mu_t(t) = -\tilde{\chi}_{tl}(\Omega)[\epsilon_{lkp}(\chi_{ks})' + \epsilon_{lkn}S_n^j((\chi_{ks})'(\chi_{jp})' +$$
$$+(\chi_{ks})''(\chi_{jp})'')]\overline{[h_p^{Re}(t)h_s^{Re}(t)]}^{\tau}. \quad \text{(D.26)}$$

- **Averaging of high-frequency parameters.**

The spectrum of an external high-frequency magnetic field is:

$$\vec{h}(t) = \vec{h}_0 \sum_{-\infty}^{\infty} \frac{sin\,(\frac{\pi n}{2})}{\pi n/2} e^{i\,(n\Omega+\,\omega)\,t} = \vec{h}_0 \sum_{-\infty}^{\infty} a^{(n)}\, e^{i\,(n\Omega+\,\omega)\,t}. \quad \text{(D.27)}$$

Here $a^{(n)} \in R$.

Then we have:

$$h_i + h_i^* = h_i^0 \sum_{-\infty}^{\infty} a^{(n)}\,(e^{i\,(n\Omega+\,\omega)\,t} + e^{-i\,(n\Omega+\,\omega)\,t}), \quad \text{(D.28)}$$

$$\overline{(h_i + h_i^*)\big(h_j + h_j^*\big)}^{\tau} =$$
$$= h_i^0 h_j^0 \sum_{n=-\infty}^{\infty}\sum_{k=-\infty}^{\infty} \overline{a^n a^k (e^{i\,(n\Omega+\,\omega)\,t} + e^{-i\,(n\Omega+\,\omega)\,t})(e^{i\,(k\Omega+\,\omega)\,t} + e^{-i\,(k\Omega+\,\omega)\,t})}^{\tau} =$$
$$= h_i^0 h_j^0 \sum_{n=-\infty}^{\infty}\sum_{k=-\infty}^{\infty} \overline{a^n a^k (e^{i\,((n+k)\Omega+2\,\omega)\,t} + e^{-i\,(n-k)\Omega t} + e^{i\,((n-k)\Omega t} + e^{-i\,((n+k)\Omega+2\,\omega)\,t})}^{\tau} =$$
$$= h_i^0 h_j^0 \sum_{n=-\infty}^{\infty}\sum_{k=-\infty}^{\infty} a^n\, a^k (e^{-i\,(n-k)\Omega t} + e^{i\,(n-k)\Omega t})$$

. (D.29)

Let us consider the mode $+\Omega$ with the assumption for the possibility for $\Omega$ to accept negative values. Thus, following combinations are possible: $k = n - 1$ and $k = n + 1$.

At the same time one can notice that

$a^n a^{n\pm1} = \frac{sin\,(\pi n/2)\,sin\,(\pi\,(n\pm1)/2)}{(\pi/2)^2 n\,(n\pm1)} \neq 0$ only in the following cases: $n = 0$ $(k = \pm1)$ or $n = \pm1 (k = 0)$.

Then it is possible to obtain the following expression for the corresponding mode:

$$\overline{(h_i + h_i^*)(h_j + h_j^*)} = 4\frac{2}{\pi} h_i^0 h_j^0 e^{i\Omega t}. \quad \text{(D.30)}$$

And we have:

$$\widehat{\Theta}\vec{\mu}_t(t) = -\epsilon_{lkp}(\chi_{ks})' + \epsilon_{lkn}S_n^j((\chi_{ks})'(\chi_{jp})' + (\chi_{ks})''(\chi_{jp})'')\overline{h_p^{Re}(t)h_s^{Re}(t)}^{\tau}, \quad \text{(D.31)}$$

Where $\widehat{\Theta} = \hat{A}(\Omega)$ is the operator of the linear Landau–Lifshitz equation for LF vibrations, which differs from the high frequency operator by the LF Ω instead of HF $\omega$.

Thus, we obtain the final expression for the dependence of low-frequency magnetization precession amplitude on the amplitude of the external alternating high-frequency magnetic field with low frequency modulation:

$$\mu_t^0 = -\frac{4}{\pi}\frac{\Theta_{lt}}{det\ \Theta}(\epsilon_{lkp}(\chi_{ks})' + \epsilon_{lkn}S_n^j((\chi_{ks})'(\chi_{jp})' + (\chi_{ks})''(\chi_{jp})''))h_s^0 h_p^0 = \kappa_{tsp}h_s^0 h_p^0 \tag{D.32}$$

Where: $\kappa_{tsp} = -\frac{4}{\pi}\frac{\Theta_{lt}}{det\ \Theta}(\epsilon_{lkp}(\chi_{ks})' + \epsilon_{lkn}S_n^j((\chi_{ks})'(\chi_{jp})' + (\chi_{ks})''(\chi_{jp})''))$, is the magnetic susceptibility tensor on low frequency modulation.

$\Theta_{lp}$ is the algebraic complement to the corresponding element of the operator $\widehat{\Theta}$.

By turn,

$$det\Theta = \frac{i\,\Omega}{\gamma}(-(\frac{\Omega}{\gamma})^2 - a_{32}a_{23} - a_{31}a_{13}). \tag{D.33}$$

# APPENDIX E

$$\hat{\chi}^{(n)} = \frac{1}{detA}\begin{pmatrix} A_{31}M_y^0 & -A_{31}M_x^0 & -A_{11}M_y^0+A_{21}M_x^0 \\ A_{32}M_y^0 & -A_{32}M_x^0 & -A_{12}M_y^0+A_{22}M_x^0 \\ A_{33}M_y^0 & -A_{33}M_x^0 & -A_{13}M_y^0+A_{23}M_x^0 \end{pmatrix}. \quad \text{(E.1)}$$

Here $A_{ij}$ – an algebraical complement to ij-element of matrix A:

$$\hat{A}(n\Omega+\omega) = \begin{pmatrix} \frac{i(n\Omega+\omega)}{\gamma} & 0 & a_{13} \\ 0 & \frac{i(n\Omega+\omega)}{\gamma} & a_{23} \\ a_{31} & a_{32} & \frac{i(n\Omega+\omega)}{\gamma} \end{pmatrix} \quad \text{(E.2)}$$

The elements of matrix A are:

$$\begin{cases} a_{13} = H + 4\pi M_y^0, \\ a_{31} = -H + \frac{H_A}{M_0} M_y^0, \\ a_{23} = -M_x^0(\frac{H_A}{M_0} + 4\pi), \\ a_{32} = M_x^0 \frac{H_A}{M_0}. \end{cases} \quad \text{(E.3)}$$

**High frequency and nonlinear phenomena in thin active ferromagnetic planar structures**

Recently discovered investigations on the high frequency and nonlinear phenomena in thin active ferromagnetic planar structures showed a great number of new studies and promising practical applications. The magnetoelastic energy conversion can be much more efficient in the vicinity of spin reorientation transition (SRT). The thin active ferromagnetic planar structures provide a lot of unique high frequency features: for instance, the anomalous Doppler effect conditions can be satisfied. The magnon crystals are also an actual area for the further investigation of the domain.

In the present work we derived the theoretical description for the high frequency and non-linear waves propagation in thin planar ferromagnetic structures with different compositions. It was demonstrated experimentally and theoretically that LF vibrations of the cantilever can be amplified when FMR is excited by HF electromagnetic field near SRT. Moreover the magnetoelastic demodulation effect can be supplemented with nonlinear magnetoelectric effect. The possibility of the occurrence of the anomalous Doppler effect during propagation of an MSSW in an FDM structure in a certain range of system parameters is substantiated. The dispersion of a surface magnetostatic wave propagating in a film, whose thickness varies linearly, with a periodic structure in the form of parallel etched strips was calculated. As it was clearly demonstrated these works are of great interest for the new studies and practical applications.

Keywords:
-Magnetoelastic demodulation
-Ferromagnetic resonance
-Nonlinear magnetoelectric effect
-Spin reorientation transition
-Magnon crystals
-Magnetostatic waves
-Anomalous Doppler effect
-Ferrite-dielectric-metal structures

**Phénomènes hyperfréquences et nonlinéaires dans les structures actives ferromagnétiques planaires**

Les récentes découvertes sur les phénomènes hyperfréquences et nonlinéaires dans les structures minces ferromagnétiques actives planaires ont fait émerger un grand nombre de nouvelles études et applications pratiques prometteuses. La conversion de l'énergie magnétoélastique peut être beaucoup plus efficace à proximité de la transition de réorientation de spin (TRS). Les structures minces ferromagnétiques actives planaires fournissent un grand nombre de caractéristiques haute fréquence

uniques : par exemple, les conditions pour l'effet Doppler anomal peuvent être satisfaites. Les cristaux magnoniques représentent également un domaine prometteur pour les futures investigations.

Dans le présent travail nous avons établi la description théorique de la propagation des ondes hyperfréquences et non-linéaires dans les structures minces ferromagnétiques actives planaires de compositions différentes. Il a été démontré expérimentalement et théoriquement que les vibrations basse fréquence d'un cantilever peuvent être amplifiées quand la résonance ferromagnétique est excitée par un champ électromagnétique HF à proximité de la TRS. En outre, l'effet de la démodulation magnétoélastique peut être complété par un effet magnétoélectrique nonlinéaire. La possibilité de l'apparition de l'effet Doppler anomal lors de la propagation d'une onde de surface magnétostatique dans une structure ferrite-diélectrique-métal, dans une certaine plage de paramètres du système, est démontrée. La dispersion d'une onde magnétostatique de surface se propageant dans un film dont l'épaisseur varie linéairement, et possédant une structure périodique sous la forme de bandes parallèles gravées, a été calculée. Comme il a été clairement démontré ces travaux ont un grand intérêt pour de nouvelles études et applications pratiques.

Mots – clés:
- Démodulation magnétoélastique
- Résonance ferromagnétique
- Effet magnétoélectrique non linéaire
- Transition de réorientation de spin
- Cristaux magnoniques
- Ondes magnétostatiques
- Effet Doppler anormal
- Structures ferrite-diélectrique-métal